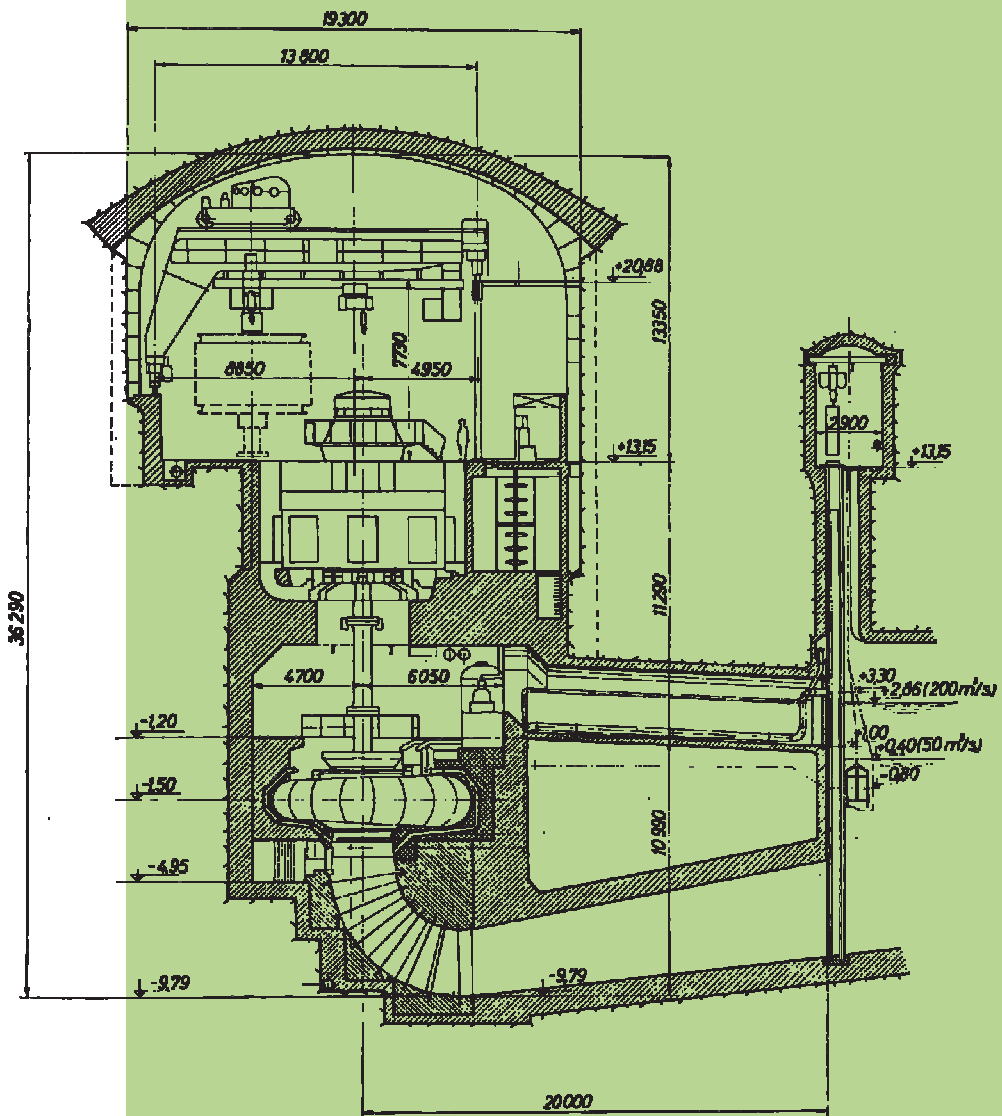


# STROJNIŠKI VESTNIK

## JOURNAL OF MECHANICAL ENGINEERING



cena 3,34 EUR



9 770039 248001

ISSN 0039-2480

## Vsebina - Contents

**Strojniški vestnik - Journal of Mechanical Engineering  
letnik - volume 53, (2007), številka - number 1  
Ljubljana, januar - January 2007  
ISSN 0039-2480**

Izhaja mesečno - Published monthly

### **Uvodnik**

Alujevič A.: Strojniški vestnik v letu 2007

### **Razprave**

- Ozalp, A. A.: Vzporedni vplivi pospeška in površinskega ogrevanja na stisljiv tok: simulacija vesoljske pogonske šobe s srednje veliko površinsko obrabo 3  
Imrak, C. E., Gerdemeli, I.: Določitev tornega količnika v brazdah z napetostno funkcijo  
Bazaras, J., Bazaras, Ž., Sapragonas, J.: Numerično modeliranje notranjih zvokov v železniških vozilih 18  
Ulozas, R. V.: Teoretična in eksperimentalna analiza dinamike mehanizmov Rolomite 26  
Voća, N., Krička, T., Janušić, V.: Optimizacija neprekinjenega postopka sušenja v težnostnih sušilnicah 48

### **Osebne vesti**

- Prešernove nagrade za študente Fakultete za strojništvo v Ljubljani 59  
Doktorati, magisterija in diplome 61

### **Navodila avtorjem**

### **Editorial**

- 2 Alujevič A.: Journal of Mechanical Engineering in Year 2007

### **Papers**

- Ozalp, A. A.: Parallel Effects of Acceleration and Surface Heating on Compressible Flow: Simulation of an Aerospace Propulsion Nozzle with a Medium Amount of Surface Wear 3  
Imrak, C. E., Gerdemeli, I.: Determination of the Friction Coefficient of Groove Forms Using the Stress-Function Method 13  
Bazaras, J., Bazaras, Ž., Sapragonas, J.: Numerical Modelling of the Internal Sound in Railway Rolling Stock 18  
Ulozas, R. V.: A Theoretical and Experimental Investigation of the Dynamics of Rolomite-Type Mechanisms 26  
Voća, N., Krička, T., Janušić, V.: Optimization of the Performance of the Continuous-Drying Process in Gravity Dryers 48

### **Personal Events**

- Students' Prešeren Awards of the Faculty of Mechanical Engineering in Ljubljana 59  
Doctor's, Master's and Diploma Degrees 61

### **63 Instructions for Authors**

## Uvodnik - Editorial

### Strojniški vestnik v letu 2007 - Journal of Mechanical Engineering in Year 2007

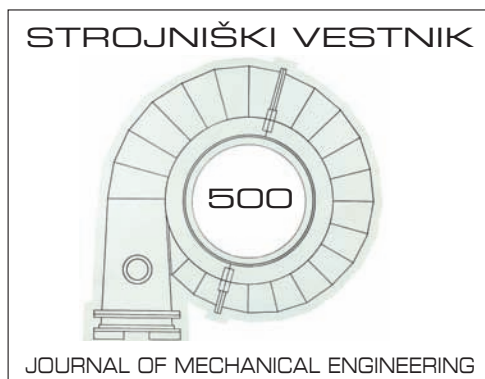
Leto je naokrog in naša Slovenija je vstopila v evroobmočje. Ob tem je Izdajateljski svet Strojniškega vestnika zaradi denarnih težav uporabil "zasilno zavoro" in uvedel prispevno dajatev 20 evrov/stran, to bodo morali poravnati avtorji v objavo sprejetih prispevkov, ki so prispevli v uredništvo po 1.1.2007. Drugače se ne moremo izkopati iz "rdečih številk". Tematske so bile tudi že doslej obremenjenje z "globo" 500.000,00 SIT na zvezek, kolikor nam prispeva tudi Javna agencija za raziskovalno dejavnost Republike Slovenije. Mogoče pa je tudi namesto neposrednega plačila pridobiti sponzorska sredstva za oglase v Strojniškem vestniku. Z anketo smo povprašali nove avtorje, ali sprejemajo to obvezo, in večina nam je odgovorila pritrdilno.

Kot urednik sem sicer žalosten, saj bomo verjetno izgubili nekaj kakovostnih člankov. Nisem član Izdajateljskega sveta Strojniškega vestnika, prav tako tudi nisem zadolžen za finančno pokritje (poslovodni organ sta dekana obeh fakultet), kajti nihče mi ne daje možnosti vpliva na potek prilivov

in odlivov sredstev. Ko mi bo konec 2007 potekel petletni mandat, bom uredniška opravila prepustil svojemu namestniku, ki naj ga izvolijo ali pa izberejo koga, da bo zbiral oglase in bo iz tega prejemal tudi svoje plačilo. Tak podjetniški način utegne izkopati rešitev denarnih problemov Strojniškega vestnika. Meni so bili pred dvema letoma ukinjeni potni stroški.

V letu 2007 Strojniški vestnik za zdaj nima težav z izbiro vsebine. Gradiva iz preteklega leta, ki je že prestalo recenzijski postopek ocenjevanja (1.01 tudi v tujini) se ga je nabralo kar precej, tako da bomo v letošnjem letu poleg "mešanih" objavili naslednja tematska zvezka z izbranimi ter dopolnjenimi prispevki s konferenc TMCE'06 (Tools and Methods of Competitive Engineering) in TMT 2006 (Trends in the Development of Machinery and Associated Technology).

*Urednik  
prof.dr. Andro Alujevič*



Osnutek (p)osebne znamke Pošte Slovenije d.o.o.

# Vzporedni vplivi pospeška in površinskega ogrevanja na stisljiv tok: simulacija vesoljske pogonske šobe s srednje veliko površinsko obrabo

## Parallel Effects of Acceleration and Surface Heating on Compressible Flow: Simulation of an Aerospace Propulsion Nozzle with a Medium Amount of Surface Wear

A. Alper Ozalp  
(Uludag University, Turkey)

*Numerične simulacije vesoljskih pogonskih šob so, zaradi nujnosti sočasnega obravnavanja pospeška toka, stopenj prenosa topote, hravavosti površine, temperaturno odvisnih lastnosti zraka in sprememb gostote tokovnic zaradi stisljivosti toka, zelo zapletene. Da bi zagotovili pregled za večstransko obravnavo toka pogonskih šob, smo razvili nov računski model, ki vključuje osnosimetrično zveznost, vztrajnostne in energijske enačbe. Izvedli smo računske preizkuse z različnimi geometrijskimi oblikami šob in vstopnimi robnimi pogoji ter s skupno obravnavo površinskega topotnega toka in hravavosti. Izračuni so pokazali, da se vstopna moč pogonske šobe in njene izgube povečujejo z večanjem notranjega staticnega tlaka ter zmanjšujejo z zoževalnim kotom šobe in površinskim topotnim tokom. Ugotovili smo, da je razmerje izgub glede na vstopno moč neodvisno od topotnega toka, vendar pa se linearno zmanjšuje s povečanjem zoževalnih krov.*

© 2007 Strojniški vestnik. Vse pravice pridržane.

**(Ključne besede: pogonske šobe, stisljivi tok, pretočni koeficient, izgube moči)**

*Numerical simulations of aerospace propulsion nozzles are very complex due to the necessity to simultaneously handle flow acceleration, momentum heat-transfer rates, surface roughness, temperature-dependent air properties and streamwise density variations due to the compressible character of the flow. To provide an overview for a multitask consideration of the propulsion-nozzle flows, a new computational model that integrates the axi-symmetrical continuity, the momentum and the energy equations has been developed. Numerical experiments were performed with various nozzle geometries, inlet-boundary conditions, with the combined handling of the surface heat flux and roughness conditions. The computations indicated that the input and loss power values of the propulsion nozzle increase with higher inlet stagnation pressures and decrease with higher nozzle convergence half angles and surface heat flux. The ratio of the loss to the input power was found to be independent of the heat flux; however, it decreases linearly with an increase in the convergence half angles.*

© 2007 Journal of Mechanical Engineering. All rights reserved.

**(Keywords: propulsion nozzle, compressible flow, discharge coefficient, power losses)**

## 0 INTRODUCTION

Compressible flows are encountered in a wide variety of engineering applications, e.g., the flow accelerator of environmental control systems in commercial aircraft [1] which supplies fresh air to the passenger cabins of aircraft and the exhaust system of nuclear propulsion engines [2], which generate

energy and thrust. Most aerospace applications are equipped with nozzles such that the overall system performance is significantly influenced by the flow acceleration, the surface heating, the inlet conditions and the wear-based friction. Recent studies have pointed out the considerable influence of high pressures and temperatures on the frictional behaviours of nozzle flows. In spite of the objective, an accurate

prediction in the design-oriented calculations of compressible flows is still a challenging task that is becoming increasingly important.

The main design considerations for compressible-flow applications with nozzles are the flow geometries, the inlet-boundary conditions and the flow heat-transfer characteristics, where the performance predictions are reported by several experimental and numerical investigations. The effect of nozzle-exit over-pressure on vortex formation, with its contribution to nozzle thrust, was experimentally examined by Krueger and Gharib [3]. Significant losses in efficiency, due to heat transfer, especially when the ratio of the inlet stagnation to the back pressure converges to unity was determined by Lear et al. [4], who modelled the dissipative effects of heat transfer on the exit kinetic energy and the nozzle efficiency. Orieux et al. [5] illustrated the steady and transient performance of micro-nozzles for various nozzle geometries, ambient conditions and surface cooling, where the thrust values decreased both with cooling and with a narrower nozzle exit. The heat transfer and gas dynamics structure in a choked nozzle with cooling was experimentally investigated by Back et al. [6]. Instabilities in the propulsion of rockets, due to pressure and temperature fluctuations at the upstream of the rocket nozzle and due to the flow geometry, were numerically considered by Assovskii and Rashkovskii [7]. Bartz [8] handled the heat-transfer phenomena in compressible nozzle flows and considered the Nusselt number as a function of the inlet stagnation pressure and the convergence half angle, and Ahmad [9] correlated the variation of the nozzle discharge coefficients and surface heat-transfer values for various nozzle geometries. A 10° convergence half-angle nozzle with different working fluids and with a wide range of inlet stagnation pressures was experimentally considered by Massier et al. [10], who recorded lower discharge coefficients with a decrease in the inlet stagnation pressure. Paik et al. [11] studied the influence of flow geometry and Reynolds number on the variation of the discharge coefficients for sonic nozzles that are applied to gas flow-rate measurements, and reported higher discharge coefficients with an increase in the mass flow rate. Kim et al. [12] considered the effects of several kinds of gases and turbulence models with a wide range of Reynolds numbers on different sonic nozzle geometries. The combined effects of Reynolds number, area ratio and flow velocity on the critical pressure ratio of sonic

nozzles were investigated by Park et al. [13]. Sato et al. [14] presented recent data on a real-time air-cooled propulsion ramjet engine. Ribault and Friedrich [15] investigated compressible flow behaviour along adiabatic and cooled walls by implementing the turbulent momentum and heat-transport analogies in a code.

Although the available literature is highly concentrated on heating/cooling applications, inlet/exit conditions and the geometrical structures of the nozzles, surface roughness ( $\varepsilon$ ) is becoming of major interest for compressible/incompressible nozzle flows. Gas-solid particle flows in the nozzles together with the high pressures and temperatures within the flow volume are the main sources of augmentations in the surface roughness. Kumar et al. [16] performed an experimental study of nozzle wear due to gas-solid particle flow and determined an increase in the relative roughness ( $\varepsilon/D_{in}$ ) values from 0.006 to 0.052. Bussiere and Mora [17] presented the real-time data of an Ariane 5 rocket-booster nozzle, where the relative roughness increased from a perfect surface finish to 0.012 during a flight that initiates with a launch and ends with the rocket in orbit.

Although the surface roughness and the surface heat flux act simultaneously in real-time systems, the available literature deals with them separately. The combined effects have not yet been considered. To perform a comprehensive computational study, a new mathematical model, capable of implementing both the surface roughness and the surface heat flux ( $Q$ ) conditions for aerospace propulsion nozzles was developed. Choked and un-choked cases were investigated for various convergence half angles ( $\alpha$ ), ratio of inlet stagnation to back pressure ( $\beta = (P_{\infty}/P_b)$ ) and  $Q$  cases, and the proposed method was validated with the previous experimental and numerical reports.

## 1 MODELLING AND COMPUTATION

The overall aim here is to build a predictive model for propulsion-nozzle flows in the presence of surface roughness and constant heat-flux conditions. The model should permit the determination of the necessary design parameters, such as the nozzle geometry and the inlet-boundary conditions for any given performance requirement depending on the applications. Thus, the main requirements are adaptability, simplicity and a short calculation time. The calculations rely on the principles of mass and en-

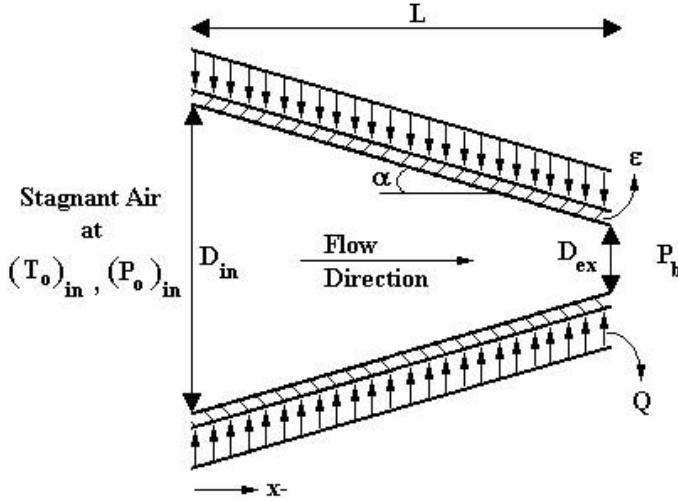


Fig. 1. Schematic outline of the aerospace propulsion nozzle

ergy conservation and on the momentum and state equations applied to the control volume, given in Fig. 1. It is assumed that the stagnation conditions of pressure and temperature in the storage tank, upstream of the nozzle, are homogeneous and, as in many numerical studies [2] to [13], the air velocity, pressure and temperature are considered to be uniform across any section normal to the flow axis. Since air properties, like the specific heat at constant pressure ( $C_p$ ), the kinematic viscosity ( $\nu$ ) and the Prandtl number ( $Pr$ ), are substantially dependent on temperature ( $T$ ) [18], they are characterized by 6<sup>th</sup>-order polynomials with an uncertainty of less than 0.02%, and the temperature dependency is indicated by the superscript T throughout the formulation.

As the study is focused on flows with friction and heat transfer, the stagnation pressure ( $P_o$ ) and stagnation temperature ( $T_o$ ) values will also vary in the flow direction with the variation in the Mach number ( $M$ ). Thus, the conventional equations (Eqs. 1 and 2) for compressible, isentropic and one-dimensional flows are applicable only with the simultaneous handling of the momentum and energy equations.

$$\frac{(P_o)_i}{P_i} = \left(1 + \frac{\gamma-1}{2} M_i^2\right)^{\frac{\gamma}{\gamma-1}} \quad (1)$$

$$\frac{(T_o)_i}{T_i} = 1 + \frac{\gamma-1}{2} M_i^2 \quad (2)$$

$$m = \rho_i U_i A_i \quad (3)$$

$$U_i = M_i \sqrt{\gamma R T_i} \quad (4)$$

$$\rho_i = \frac{P_i}{R T_i} \quad (5)$$

$$(Re_D)_n = \frac{U_n D_n}{\nu_n} \quad (6)$$

The nodal values (subscript i) of the mass flow rate ( $m$ ) the air velocity ( $U$ ) and the density ( $\rho$ ) can be calculated using Eqs. 3 to 5, where the mass flow rate, the most significant consideration from a numerical point of view, is kept constant in the flow direction. On the other hand, the diameter ( $D$ ), based the Reynolds number (Eq. 6), is assigned to each differential cell with the mean cellular values of  $U$ ,  $D$  and  $\nu$ . The friction coefficient ( $f$ ) is a function of both  $Re_D$  and  $\varepsilon$  (Eq. 7), and the cell-based (subscript n) shear stress ( $\tau$ ) and friction force ( $F_f$ ) can be expressed with Eqs. 8 to 9.

$$\frac{1}{\sqrt{f_n}} = -3.6 \log \left[ \frac{6.9}{(Re_D)_n} + \left( \frac{\varepsilon / D_n}{3.7} \right)^{1.11} \right] \quad (7)$$

$$\tau_n = \frac{f_n \rho_n (U_n)^2}{2} \quad (8)$$

$$(F_f)_n = \tau_n \pi D_n \Delta x_n \quad (9)$$

The one-dimensional momentum (Eq. 10) and energy equations (Eq. 11) are applied to each differential cell in the nozzle, where the nodal properties, such as  $P$ ,  $U$  and  $C_p$ , are interrelated with the contributions of cellular variants like  $F_f$  and the impulse ( $I$ ). Eq. 11 represents the conservation of mechanical and thermal energy by the implementation of a cell-based surface flux and the frictional loss term.

$$P_i A_i + m U_i = P_{i+1} A_{i+1} + m U_{i+1} + (F_f)_n + I_n \quad (10)$$

$$(C_p^T)_i T_i + \frac{U_i^2}{2} + \frac{Q(A_s)_n}{m} = (C_p^T)_{i+1} T_{i+1} + \frac{U_{i+1}^2}{2} + \frac{(F_f)_n U_n}{m} \quad (11)$$

Vargas and Bejan [1] evaluated heat-transfer data in their mathematical model for a compressible nozzle flow, where the Mach number was in the range

0.50 to 0.85, with the empirical correlation of Eq. 12. In the current study the Mach numbers are within 0.05 to 1.0, similar to the subsonic data of [1], and Eq. 12 is applied with the cell-based values of  $f$ ,  $Pr$  and  $Re_D$ . Moreover, the combined effects of  $\varepsilon$  and  $Q$  on the mass flow rate are investigated through the non-dimensional discharge coefficient ( $C_d$ ) of Eq. 13, which compares the real mass flow rate with that of the isentropic case.

$$(Nu_D)_n = \frac{\left(\frac{f_n}{2}\right)\left[\left(Re_D\right)_n - 10^3\right]Pr_n^T}{1 + 12.7\left(\frac{f_n}{2}\right)^{0.5}\left[\left(Pr_n^T\right)^{2/3} - 1\right]} \quad (12)$$

$$C_d = \frac{m_{real}}{m_{isen}} \quad (13)$$

For the one-dimensional, compressible marching procedure, forward difference discretization is applied in the flow direction, as defined by Chapra and Canale [19]. Since the continuity, momentum and energy equations are to be solved, the geometric domain is divided into  $n$  sequential cells, having an equal width equal to  $\Delta x$ . The fineness of the computational grids was examined to ensure that the obtained solutions were independent of the grid employed. Initial runs indicated that with more than 1000 cells the results showed no sign of change with the grid density. Therefore, to provide more reasonable predictions computations were performed with  $n=1000$ . Flow parameters, like  $U$ ,  $P$ ,  $T$ ,  $\rho$  and stagna-

tion data ( $P_o$ ,  $T_o$ ), were calculated at the nodes of these cells, which are numbered from  $i=1$  to  $n+1$ , whereas  $\tau$ ,  $I$ ,  $Re_D$  and  $Nu_D$  were evaluated on a cell basis using the mean values of nodal inlet and exit data of each cell.

As shown in Fig. 2, by disregarding the surface roughness and heat transfer, the flow of the solution logic first handles the problem as an isentropic type, which is manipulated as described by Laney [20]. The  $M_{in}$  value of the isentropic approach is the initial guess of the iterative solution procedure of the non-isentropic nozzle flow. The non-isentropic approach governs the complete equation set described above; however, if the solution scheme encounters singularities, like  $M_i > 1$ ,  $M_{ex} = 1$  &  $P_{ex} < P_b$  or  $M_{ex} < 1$  &  $P_{ex} \neq P_b$ ,  $M_{in}$  is modified using a direct Monte Carlo simulation, similar to that explained by Wu and Tseng [21]. The convergence criteria for the mass flow rate throughout the flow volume is of the order of 0.01%, and successive non-isentropic runs were performed until  $M_{ex}$  was in the range 0.99 to 1.0 for the choked nozzle, and the shift of  $P_{ex}$  from the back pressure is less than  $P_b \cdot 10^{-4}$  for the un-choked case.

## 2 RESULTS AND DISCUSSION

Computations were performed with ratios of the inlet stagnation to the back pressure ( $\beta = (P_o)_{in}/P_b$ ) equal to 1.01, 1.25, 1.50, 1.75 and 2.00, covering both

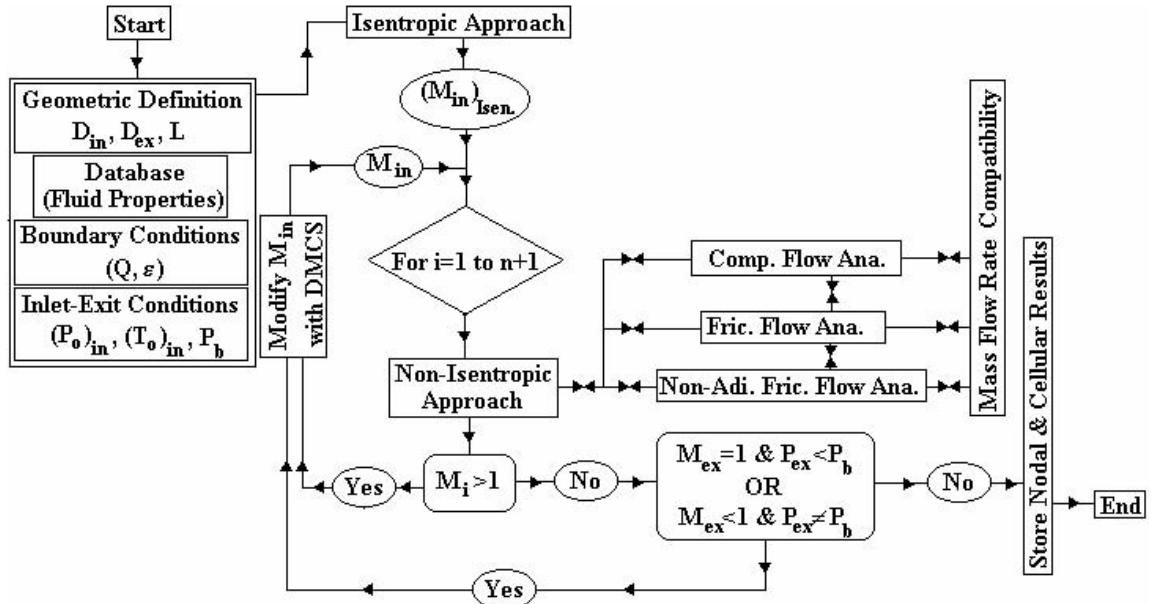
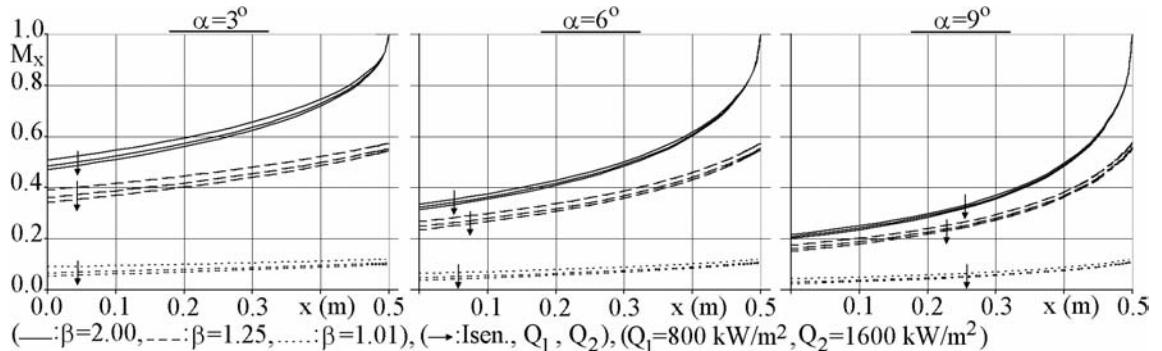


Fig. 2. Computational solution method for non-adiabatic and frictional compressible nozzle flow

Fig. 3. Streamwise variation of the Mach number with various  $\alpha$ ,  $\beta$  and  $Q$  conditions

the un-choked and choked flow cases. To build a comprehensive overview and to include the most frequent geometrical structures, analyses were conducted at nozzle-convergence half angles ( $\alpha$ ) from  $3^\circ$  to  $9^\circ$ . The medium value of 0.0125, which is similar to the experimental data of Kumar et al. [16] and Bussiere and Mora [17], was selected for the non-dimensional surface roughness ( $\varepsilon/D_{in}$ ) of the nozzle wall, and the effects of constant surface heat flux were evaluated by imposing three distinct values of  $Q=800, 1200$  and  $1600 \text{ kW/m}^2$ . The results of various design and boundary-condition cases are discussed through streamwise variations of the Mach number, non-dimensional pressure values, flow and surface temperature data and the Nusselt number. Moreover, the influences of the  $\alpha$ ,  $\beta$  and  $Q$  conditions on the discharge coefficient and the input and loss power values are presented for a comparison.

Streamwise Mach-number variations are given in Fig. 3 for various  $\alpha$ ,  $\beta$  and  $Q$  cases. Fig. 3 suggests that flows with a lower  $\beta$  result in a lower  $M_{in}$  and  $M_{ex}$  for all the nozzle-convergence half angles ( $\alpha=3^\circ$  to  $9^\circ$ ). When compared with the  $\beta=2.00$  pattern,  $\beta=1.25$  caused a decrease of 22.8% and 27.2% in  $M_{in}$  for the isentropic and  $Q=1600 \text{ kW/m}^2$  cases in the  $\alpha=3^\circ$  nozzle, whereas the similar ratios for  $\beta=1.01$  are 82.3% and 88.5%. On the other hand, for the  $\alpha=9^\circ$  nozzle, the decreased amounts in  $M_{in}$  for  $\beta=1.25$  were 18.9% and 24.8%, and for  $\beta=1.01$  they were 80.2% and 85.6% for the isentropic and  $Q=1600 \text{ kW/m}^2$  cases, respectively. These proportions suggest that the decreased amounts are more apparent for lower  $\alpha$  and less for the sharp convergent case ( $\alpha=9^\circ$ ). In the exit plane the  $M_{ex}$  values are identical and equal to 1, being independent of  $M_{in}$ , for the  $\beta=2.00$  case, which corresponds to a choking condition for the complete  $\alpha$  range. However, as  $\beta$  is lowered, the nozzles run in the un-choked condition with

accompanied decreases in  $M_{ex}$ . The variations in  $M_{ex}$ , when compared with the above discussions about  $M_{in}$ , are small and kept in the range 2 to 4% for the complete  $\alpha$ ,  $Q$  and  $\beta$  set. Fig. 3 further implies that the application of a surface heat flux produces lower  $M$  values throughout the nozzle, regardless of the level of  $\beta$  and  $\alpha$ . These findings are similar to those of Lear et al.'s [4] numerical and Sato et al.'s [14] experimental determinations. Application of the constant-surface-temperature condition on the nozzle wall [4] caused flow velocities, and thus  $M$ , to decrease, whereas the cooling of the nozzle surface [14], which is the opposite operation to that studied here, resulted in higher mass flow rates. For the  $\alpha=3^\circ$  nozzle, the heat flux of  $Q=1600 \text{ kW/m}^2$  results in a decrease in  $M_{in}$  by 7.3%, 12.5% and 40% for  $\beta$  equal to 2, 1.25 and 1.01, respectively. On the other hand, the same flux constitutes a lower  $M_{in}$  by 6.9%, 11.6% and 36.5% for  $\alpha=9^\circ$  in the same  $\beta$  range. These proportions suggest that the effect of the heat flux on the  $M$  pattern is more apparent with a lower  $\alpha$ .

In compressible flows, static pressure ( $P$ ) variation is a major consideration since in the case that the inlet stagnation ( $P_o$ ) values attain significant levels, the nozzle walls will be obliged to face pressure forces that may be at the wear or crack limit of the nozzle material. In fact the conventional theory (Eq. 1) implies that the extreme  $P$  value can be as high as  $P_o$ , which can be controlled at the nozzle inlet. However, the missing part of the theory is the probability of an augmentation in  $P_o$  in the flow direction within the nozzle. Fig. 4 displays the streamwise variation of  $P$ , that is non-dimensionalized by the inlet stagnation value of  $(P_o)_{in}$ . For the complete  $\alpha$  range, higher  $\beta$  cases resulted in lower  $P$  values at the inlet, which can be attributed to the corresponding higher mass flow rates and inlet Mach numbers, as described in Fig. 3.

On the other hand, with an increase in the surface heat flux, the  $P$  values, throughout the flow volume, also increased, which was accompanied by a decrease in the Mach numbers (Fig. 3), and the variations in the static pressures and the Mach numbers were more distinguishable for the nozzles with low convergence half angles ( $\alpha=3^\circ$ ). For the  $\alpha=3^\circ$  case, Fig. 4 further indicates that the pressure values continuously decrease in the streamwise direction if the ratio of the inlet stagnation to the back pressure ( $\beta$ ) is kept above 1.25, which is similar to the reports of Kim et al. [12]. This fact keeps the static pressure values below the stagnation value, which in return eliminates the probability of system damage. However, for the lowest  $\beta$  of 1.01, the static pressure values remain around the inlet stagnation value, which is remarkable from the point of view of momentum transfer. In the cases with higher convergence half angles ( $\alpha=6$  to  $9^\circ$ ) the local static pressure values exceed the inlet stagnation value by up to 6.3%, particularly for the scenario of  $\alpha=9^\circ, \beta=1.01$ . Simultaneous handling of the momentum and energy equations (Eqs. 10 and 11) suggests that the frictional behaviour of the compressible flow decreases the stagnation pressure in the flow direction; however, the application of the surface heat flux produces the opposite effect on the stagnation pressure. The curves of Fig. 4 indicate that the impact of  $Q$  on  $P_o$  increases in cases with higher  $\alpha$ , where the mass flow rates are comparably smaller. The energy transferred through the nozzle walls is absorbed by the flow, in greater amounts per unit mass for  $\alpha$  of 6 to  $9^\circ$  with  $\beta=1.01$ , and stored in stagnation pressure form. As a consequence, increased static pressure values may cause damage to the nozzle structure; moreover, they may also increase the wear rates. The following decrease in  $P$  values for  $x>0.3$  m ( $\alpha=9^\circ$ ) is due to the higher acceleration rates of the flowing air, which can also be seen in Fig. 3.

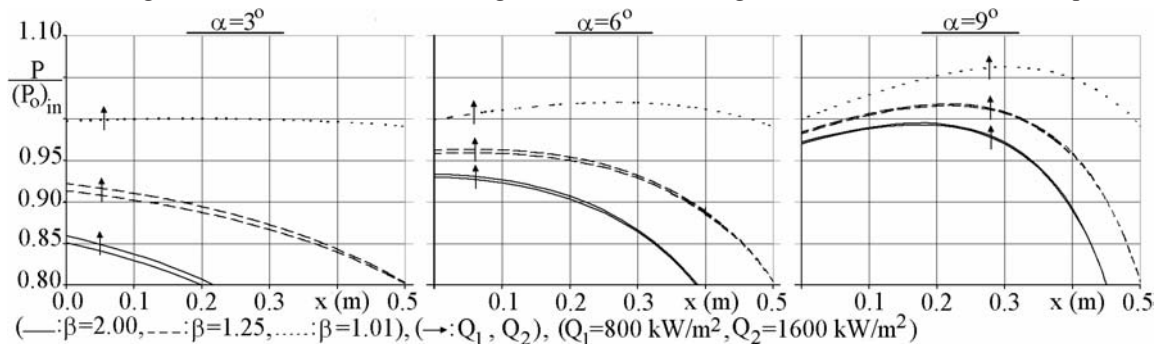
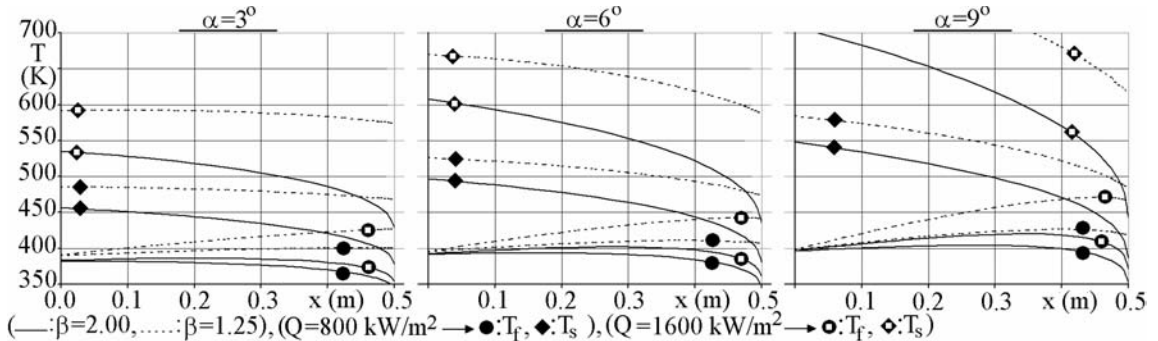
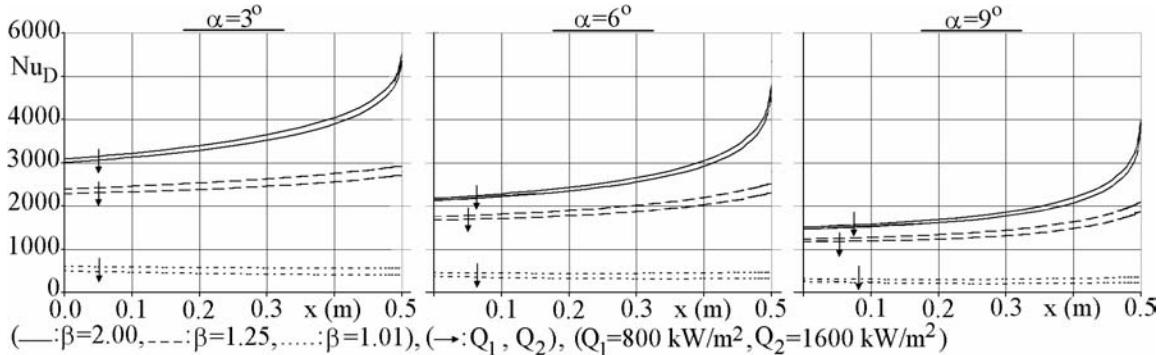


Fig. 4. Streamwise variation of non-dimensional pressure with various  $\alpha$ ,  $\beta$  and  $Q$  conditions

The streamwise variations of the fluid ( $T_f$ ) and surface ( $T_s$ ) temperatures are presented in Fig. 5. As a consequence of the applied surface heat flux, the  $T_s$  values are above  $T_f$  for the complete  $\alpha$  and  $\beta$  ranges and also throughout the flow volume. On the other hand, as the  $T_s$  values decrease in the streamwise direction, the opposite is true for  $T_f$  in all cases. The decrease rates of  $T_s$  become more significant towards the nozzle exit, especially for  $x>0.45$  m, where the highest flow acceleration is determined for all the nozzles. Lower  $\beta$  and higher  $\alpha$  indicates lower mass flow rates, which constitutes higher  $T_s$  and  $T_f$ , especially at the nozzle inlet. The durability of the nozzle material is directly related to the  $T_s$ , and the computations suggest the upstream nozzle sections should be carefully considered. On the other hand, surface wear is connected with  $T_f$ , and the vital regions appear towards the downstream regions of the nozzle, specifically at the exit plane.

Fig. 6 presents the streamwise variations of surface heat-transfer rates for various convergence-half-angle and pressure-ratio cases, with the application of constant surface heat-flux values of 800 and 1600 kW/m<sup>2</sup>. The Nusselt numbers ( $Nu_D$ ) were observed to increase in the flow direction for the complete set of investigated systems; however,  $\alpha$  and  $Q$  appeared to cause the  $Nu_D$  to decrease in both the choked ( $\beta=2.00$ ) and un-choked ( $\beta<2.00$ ) cases. This outcome is highly dependent on the fact that narrower nozzles and higher heat-flux values contributed to lower mass flow rate values (Fig. 3), and thus  $M$  and  $U$ , which also decrease the amount of heat swept from the nozzle wall. On the other hand, the ratio of the exit to inlet Nusselt numbers  $\lambda=(Nu_D)_{ex}/(Nu_D)_{in}$  increases with  $\beta$  and  $\alpha$ , whereas it decreases with  $Q$ . Bartz [8] also reported increased  $\lambda$  ratio with higher  $\alpha$  and  $\beta$ ; moreover, the typical report of Ahmad [9] for a nozzle with  $\alpha=45^\circ$  is  $\lambda=3.9$ . The most significant ratio, evaluated in the present

Fig. 5. Streamwise variation of flow and surface temperature with various  $\alpha$ ,  $\beta$  and  $Q$  conditionsFig. 6. Streamwise variation of Nusselt number with various  $\alpha$ ,  $\beta$  and  $Q$  conditions

paper for the choking case of  $\alpha=9^\circ$ , is  $\lambda=2.70$ , and this is higher than the corresponding report of Back et al. [6] ( $\lambda=1.61$ ) for the nozzle with  $\alpha=15^\circ$ . Fig. 6 further suggests that the application of different heat-flux values causes  $Nu_D$  to vary both at the inlet and exit planes of the nozzle. The most significant variations are recorded for the  $\beta$  case of 1.01 for the complete  $\alpha$  set, where these intervals are  $\pm 9.4\%$  (inlet) and  $\pm 19.8\%$  (exit) for  $\alpha=3^\circ$  and  $\pm 11.8\%$  (inlet) and  $\pm 28.1\%$  (exit) for the  $\alpha=9^\circ$  case. These values additionally imply that the effect of the wall's heat flux on surface heat-transfer rates becomes more significant in higher  $\alpha$  cases, and thus in tasks with lower mass flow rates.

The combined effects of  $\alpha$ ,  $Re_D$  and  $Q$  conditions on the discharge coefficient is given in Fig. 7a for the choked case of  $\beta=2.00$ . It can be seen from Fig. 7a that the isentropic values are not only in agreement with the ISO 9300 (Paik et al. [11]) standardized correlation of  $C_d=f((Re_D)_{ex})$  for choked nozzles but also with the experimental reports of Massier et al. [10] and Kim et al. [12]. A higher  $\alpha$  produced a lower exit  $Re_D$ , where the lower  $Re_D$  and higher  $Q$  are accompanied by reduced values of  $C_d$  and point to lower mass flow rates, which show parallelism with

the Mach-number variations of Fig. 3 and are similar to the reports of Paik et al. [11].

$$C_d = 0.2636 + 4.6279 \cdot 10^{-2} \ln(Re_D)_{ex} \quad (14)$$

$$C_d = \left[ 1.0106 + 0.0074(\ln \alpha)^2 \right]^{-1} \quad (15)$$

The adiabatic ( $Q=0$ ) correlations (Eqs. 14 and 15) of Ahmad [9] produce higher  $C_d$  values for the present  $\alpha$  and  $Re_D$  intervals; the gap is the outcome of the applied heat flux values; however, the gap decreases with lower  $\alpha$  and with higher  $(Re_D)_{ex}$  values. The numerical results show, particularly for the  $Q=1600 \text{ kW/m}^2$  case, that the nozzles of  $\alpha=3^\circ$ ,  $6^\circ$ ,  $9^\circ$  result in  $C_d$  values of 0.935, 0.933 and 0.93 respectively, where Kim et al. [12] also reported a lower  $C_d$  with higher convergence half angles.

The input power ( $\Psi$ ) necessary to form the compressible flow within the nozzle and the amount of power loss ( $\Psi_{loss}$ ) are the main considerations from the point of view of the energy requirements to run the propulsion nozzles. Fig. 7(b) demonstrates that both  $\Psi$  and  $\Psi_{loss}$  increase with higher  $\beta$  and lower  $\alpha$ , which indicates that the amount of air directed towards the nozzle is the characteristic design parameter. Increasing the surface heat flux from 800 to 1600  $\text{kW/m}^2$  caused a decrease in  $\Psi$  by 2.7% for all  $\alpha$

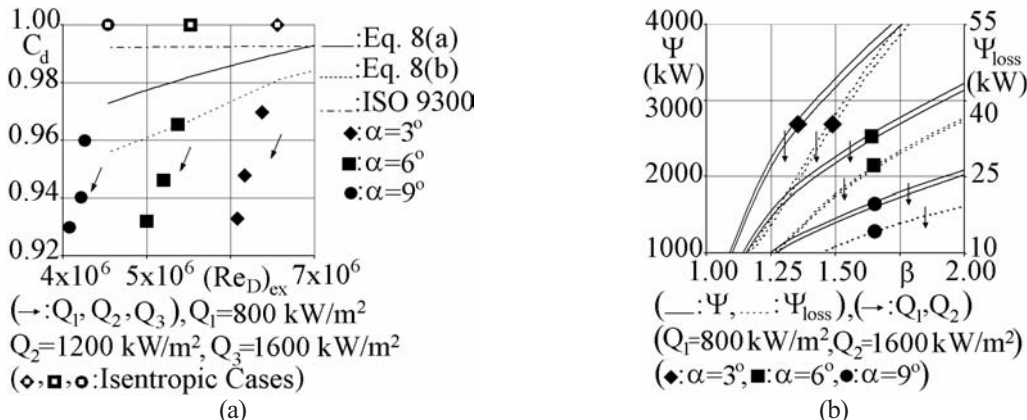


Fig. 7. Variation of (a) discharge coefficient for the choked flow and (b) input and loss power values with various  $\alpha$ ,  $\beta$  and  $Q$  conditions

values with  $\beta=2.00$ , where this influence is slightly lower than the  $C_d$  gap among the identical cases shown in Fig. 7a. However, the effect of  $Q$  on  $\Psi_{loss}$  definitely varies with  $\alpha$ ; as the decrease rate for  $\alpha=3^\circ$  is 2.9% the corresponding values for  $\alpha=6^\circ$  and  $\alpha=9^\circ$  are 1.4% and 0.8%, respectively. Since the main source of  $\Psi_{loss}$  is  $F_f$  (Eq. 9), Fig. 7b further suggests that  $Q$  also has an opposite effect on  $F_f$  which is in agreement with the reports of Ribault and Friedrich [15], who determined higher friction-coefficient values (Eq. 7) with surface cooling. Lastly, the  $\Psi_{loss}/\Psi$  ratio is dependent on both  $\alpha$  and  $\beta$  and appears to be independent of  $Q$ : for  $\beta=1.01$  the ratio is equal to 0.03% for the complete  $\alpha$  set, whereas for  $\beta=2.00$  the ratio exhibits a linear style and has values of 1.3%, 1.1% and 0.9% for  $\alpha$  of  $3^\circ$ ,  $6^\circ$  and  $9^\circ$ , respectively.

### 3 CONCLUSION

A computational method for an investigation of compressible flow and heat-transfer characteristics in aerospace propulsion nozzles was developed. The model is capable of handling various flow geometries and inlet-boundary conditions, together with the simultaneous application of surface heating and roughness conditions. The main conclusions from the numerical experiments can be summarized as follows:

- Surface heating produces lower inlet Mach numbers but higher inlet non-dimensional pressure values; moreover, the effect of  $Q$  on both of the values is more apparent in flows with lower acceleration.
- The heat flux, especially in cases with high acceleration, directly increases the stagnation pressure and causes augmented static pressure values, which is remarkable from the point of view of surface wear and system damage, specifically for the nozzle section of 0.25 to 0.40 m. Moreover, the point of maximum shifts downstream in the flows with lower  $\beta$  and a reduced mass flow rate.
- The Nusselt numbers decrease with lower inlet stagnation pressures and with higher convergence half angles and heat-flux conditions; moreover, the effect of surface heat flux on the Nusselt numbers is more apparent in un-choked flows.
- The maximum values of  $T_s$  are recorded in the downstream nozzle sections, which is the very important for the nozzle material; and the decrease rates of  $T_s$  become significant towards the nozzle exit, especially for  $x>0.45$  m, where the highest flow acceleration is determined for all the nozzle geometries.
- The augmentation of  $T_f$  in the flow direction is accompanied by the energy-transfer mechanism and also with the contribution of a lower  $T_s$ , and labels the exit-plane neighbourhood as vital from the point of view of wear.

### 4 NOMENCLATURE

$A$	cross-sectional area, $\text{m}^2$	$F_f$	frictional force, N
$C_d$	discharge coefficient	$I$	thrust, N
$C_p$	specific heat at constant pressure, $\text{J/kgK}$	$L$	nozzle length, m
$D$	nozzle diameter, mm	$m$	mass flow rate, $\text{kg/s}$
$f$	skin friction factor	$M$	Mach number

$Nu_D$	Nusselt number	$\nu$	kinematic viscosity, m <sup>2</sup> /s
$P$	pressure, Pa	$\rho$	density, kg/m <sup>3</sup>
$Pr$	Prandtl number	$\tau$	shear stress, Pa
$Q$	surface heat flux, W/m <sup>2</sup>	$\Psi$	power, kW
$R$	gas constant, J/kgK		
$Re_D$	Reynolds number		
$T$	temperature, K		
$U$	air velocity, m/s		
$x$	streamwise direction, m		
<b>Greek Letters</b>			
$\alpha$	convergence half angle, deg		
$\beta$	ratio of the inlet stagnation to the back pressure		
$\varepsilon$	surface roughness, mm		
$\gamma$	specific heat ratio		
<b>Subscripts</b>			
b, o	back, stagnation		
D	diameter		
ex, in	exit, inlet		
i, n	node, cell number		
loss	loss power		
s	heat-transfer surface		
<b>Superscripts</b>			
T	temperature dependency		
—	cellular average		

## 5 REFERENCES

- [1] Vargas, J.V.C., A. Bejan (2001) Thermodynamic optimization of finned crossflow heat exchangers for aircraft environmental control systems. *Int J Heat Fluid Flow* 22(2001), pp. 657-665.
- [2] Kammash, T., T. Godfroy (1997) An open cycle gas core fusion rocket for space exploration. *Acta Astronautica* 41(1997), pp. 229-237.
- [3] Krueger, P.S., M. Gharib (2003) The significance of vortex ring formation to the impulse and thrust of a starting jet. *Physics of Fluids* 15(2003), pp. 1271-1281.
- [4] Lear, W.E., S.A. Sherif, J.R. Langford (1997) Efficiency and gas dynamics analysis of two-phase mixtures in supersonic nozzles with inter-phase heat transfer and slip. *Acta Astronautica* 40(1997), pp. 701-706.
- [5] Orieux, S., C. Rossi, D. Esteve (2002) Compact model based on a lumped parameter approach for the prediction of solid propellant micro-rocket performance. *Sensors and Actuators A-Physical* 101(2002), pp. 383-391.
- [6] Back, L.H., P.F. Massier, R.F. Cuffel (1996) Some observations on reduction of turbulent boundary-layer heat transfer in nozzle. *AIAA Journal* 4(1996), pp. 2226-2229.
- [7] Assovskii, I.G., S.A. Rashkovskii (2001) Low-frequency instability of solid rocket motors: Influence of the Mach effect and charge geometry. *Combustion, Explosion and Shock Waves* 37(2001), pp. 321-330.
- [8] Bartz, D.R. (1957) A simple equation for rapid estimation of rocket nozzle convective heat transfer coefficients. *Jet Propulsion* 27(1957), pp. 49-51.
- [9] Ahmad, R.A. (2001) Discharge coefficients and heat transfer for axisymmetric supersonic nozzles. *Heat Transfer Engineering* 22(2001), pp. 40-61.
- [10] Massier, P.F., L.H. Back, M.B. Noel, F. Saheli (1970) Viscous effects on the flow coefficient for supersonic nozzle. *AIAA Journal* 8(1970), pp. 605-607.
- [11] Paik, J.S., K.A. Park, J.T. Park (2000) Inter-laboratory comparison of sonic nozzles at KRISS. *Flow Measurement and Instrumentation* 11(2000), pp. 339-344.
- [12] Kim, H.D., J.H. Kim, K.A. Park, T. Setoguchi, S. Matsuo (2003) Computational study of the gas flow through a critical nozzle. *Proc Instn Mech Engrs Part C: J Mech Eng Sci* 217(2003), pp. 1179-1189.
- [13] Park, K.A., Y.M. Choi, H.M. Choi, T.S. Cha, B.H. Yoon (2001) The evaluation of critical pressure ratios of sonic nozzles at low Reynolds numbers. *Flow Measurement and Instrumentation* 12(2001), pp. 37-41.
- [14] Sato, T., N. Tanatusgu, Y. Naruo, T. Kashiwagi, J. Omi, J. Tomike, T. Nishino (2000) Development study on ATREX engine. *Acta Astronautica* 47(2000), pp. 799-808.
- [15] Ribault, C.L., R. Friedrich (1997) Investigation of transport equations for turbulent heat fluxes in compressible flows. *Int J Heat Mass Trans* 40(1997), pp. 2721-2738.

- [16] Kumar, R., A.P. Verma, G.K. Lal (1983) Nozzle wear during the flow of a gas-particle mixture. *Wear* 91(1983), pp. 33-43.
- [17] Bussiere, M., B. Mora (1994) Ariane 5 booster nozzle: components description and dimensioning. *Acta Astronautica* 34(1994), pp. 83-89.
- [18] Incropera, F.P., D.P. De Witt (1990) Fundamentals of heat and mass transfer. *John Wiley & Sons*, New York.
- [19] Chapra, S.C., R.P. Canale (1990) Numerical methods for engineers. *McGraw Hill*, Singapore.
- [20] Laney, C.B. (1998) Computational gasdynamics. *Cambridge University Press*, Cambridge.
- [21] Wu, J.S., K.C. Tseng (2001) Analysis of micro-scale gas flows with pressure boundaries using direct simulation Monte Carlo method. *Computers and Fluids* 30(2001), pp. 711-735.

Author's Address: Prof. Dr. A. Alper Ozalp  
Uludag University  
Department of Mechanical Eng.  
16059 Gorukle, Bursa, Turkey  
aozalp@uludag.edu.tr

Prejeto: 27.4.2005  
Received:

Sprejeto: 25.10.2006  
Accepted:

Odperto za diskusijo: 1 leto  
Open for discussion: 1 year

# Določitev tornega količnika v brazdah z napetostno funkcijo

## Determination of the Friction Coefficient of Groove Forms Using the Stress-Function Method

C. Erdem Imrak - Ismail Gerdemeli  
(Istanbul Technical University, Turkey)

*Največja sila trenja, ki lahko nastane v brazdah, je funkcija dejanskega tornega količnika med vryo in brazdo. Torni količnik je predstavljen na različne načina za vsako vrsto oblike brazde. V prispevku je prikazan obrazec za porazdelitev tlaka na stični površini okrogle in/ali brazde v obliki črke U. Z metodo napetostne funkcije smo določili tudi torni količnik brazd.*

© 2007 Strojniški vestnik. Vse pravice pridržane.

**(Ključne besede: žleb na obodu koluta, torni količnik, napetostne funkcije)**

*The maximum traction that can be developed in sheave grooves is a function of the actual coefficient of friction between the rope and the groove. The coefficient of friction is presented in different ways for every type of groove form. In this paper an expression for the pressure distribution on the contact surface of round and/or U-shaped grooves is obtained, and the friction coefficient of the groove forms is determined by the stress-function method.*

© 2007 Journal of Mechanical Engineering. All rights reserved.

**(Keywords: rope groove, friction coefficient, stress function method)**

### 0 INTRODUCTION

Driving sheaves are widely employed to transmit power to the ropes that drive elevators, cable cars, funiculars, etc. The groove form favourably increases the effective coefficient of friction between the rope and the groove at the expense of increasing the pressure and wear on the groove surface. The trade off between the traction produced and the pressure causing the abrasion of the groove may be best explained by the concept of shape factors for the coefficient of friction of U-shaped grooves. During normal operations sheave and drum grooves are under constant pressure.

The groove form affects the magnitude of the tractive force on the driving sheaves for power transmission. The contact area between the rope and the groove is smaller with U-shaped grooves than with round grooves since the rope loses contact with the groove where the undercut is machined. Thus an undercut groove provides a tighter grip-

ping action due to an increased groove pressure, and its traction capability is greater than that of a round groove. However, a round groove has a longer rope life and a lower level of noise because of the lower groove pressure at high speeds. When the problem of insufficient traction arises with a round groove it should be noted that it can be overcome by increasing the angle of wrap, by changing the groove form to a U-shaped groove with an appropriate shape or by using a material with a higher coefficient of friction [1].

The U-shaped groove sheave, found predominantly in older installations, is the sheave of choice for optimum rope life. Its large size, when compared with the drive sheave diameters in newer installations, in combination with its supportive grooves minimizes the amount of abrasion and fatigue. The support given to the rope by the groove is illustrated in Fig.1. The groove cradles the rope, resulting in low groove pressures that allow the wires and strands to move about freely while the rope is

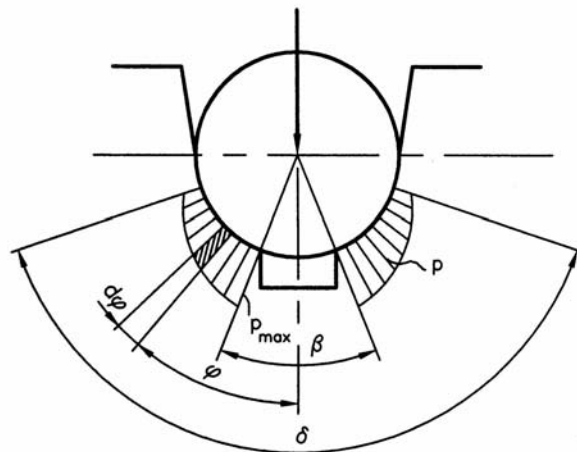


Fig.1. The U-shaped groove form

operating. Also important to the U-shaped groove's success in achieving excellent rope life is the relative diameter of the sheave required to maintain traction. In general, an undercut U groove, a modern type of groove, increases the traction by increasing the groove pressures. The beauty of these groove types is that the diameter of the sheave utilizing this modern groove design can be reduced.

The maximum traction that can be developed in the sheave grooves is a function of the effective coefficient of friction between the rope and the groove and the angle of contact that the rope makes with the circumference of the sheave (known as the angle of wrap). The groove form can favourably increase the effective coefficient of friction between the rope and the groove since the radial force due to the rope tension produces greater normal and frictional forces acting along the area of contact given by the shape of the groove [2].

Airy introduced his stress function as a device for solving certain problems in linear elastostatics for homogenous isotropic bodies. There are many published studies on the Airy stress function applied to solid mechanics ([3] to [10]). In this paper, to obtain the pressure distribution on the contact surface of undercut grooves, the Airy stress-function method was used. The effects of the groove geometry and the angle of wrap on the traction were investigated and tabulated with the ratio of the forces for different angle values by Imrak and Ozkirim [1].

In this paper the application of the Airy stress-function method for determining the shape factors for the coefficient of friction for both round and undercut grooves is presented. The effect of the changes in the groove angle and the undercut-

ting angle on the coefficient of friction and the traction are also studied.

## 1 BASIC EQUATIONS

Due to the existence of axial symmetry related to the geometry and specific pressure distribution along the boundary of a U-shaped groove it is preferable to employ polar coordinates rather than the Cartesian system and to assume that the stress condition is one of plane stress. The geometry and the loading of an undercut groove are illustrated in Fig. 1. The angle of the outer normal lines of the contact area  $\delta$  may have a maximum value  $180^\circ$ ; the angle of the undercutting  $\beta$  must not be greater than  $105^\circ$ , as shown in Fig. 1.

Due to the normal force and the symmetrical loading in the traction drive, only the plane stress is employed. In the plane-stress state the following relations are valid as long as the mass forces are negligible. By plugging in the equations associated with Airy's stress function into the equilibrium condition we can illustrate that the functions do indeed satisfy the equilibrium. The Airy function is chosen so as to satisfy the equilibrium equations automatically. The equation of compatibility, which means that the body must be physically pieced together in terms of Airy's stress function, is [11]:

$$\nabla^2 \phi = \left( \frac{\partial^2}{\partial r^2} + \frac{1}{r^2} \frac{\partial^2}{\partial \varphi^2} + \frac{1}{r} \frac{\partial}{\partial r} \right) \left( \frac{\partial^2 \phi}{\partial r^2} + \frac{1}{r^2} \frac{\partial^2 \phi}{\partial \varphi^2} + \frac{1}{r} \frac{\partial \phi}{\partial r} \right) = 0 \quad (1)$$

where  $\nabla^2$  is the Laplace operator. The Airy stress function is developed and used to solve classic two-dimensional problems fundamental to stress analysis. The Airy stress-function approach works best

for problems where a solid is subjected to prescribed tractions on its boundary, rather than prescribed displacements [8].

Using symmetrical straining we obtain  $\partial/\partial r = d/dr$ . Therefore, Eq.(1) becomes:

$$\left( \frac{d^2}{dr^2} + \frac{1}{r} \frac{d}{dr} \right) \left( \frac{d^2\phi}{dr^2} + \frac{1}{r} \frac{d\phi}{dr} \right) = 0 \quad (2)$$

Thus, the solution reduces to finding a solution of the differential equation of compatibility that satisfies the boundary conditions of the problem.

To obtain a solution of these two equations, one can write an arbitrary function  $\phi = \phi(r, \varphi)$ . This arbitrary function is called the Airy stress function [12]. In the case of plane stress and in the event that the body forces are negligible the differential equations of equilibrium in polar coordinates are as follows:

$$\sigma_r = \frac{\partial^2\phi}{\partial r^2} \quad \sigma_\varphi = \frac{\partial^2\phi}{\partial r^2} \quad \tau = -\frac{\partial^2\phi}{\partial r \partial \varphi} \quad (3)$$

and the boundary conditions are  $\sigma_r = p$ ,  $\sigma_\varphi = 0$ , and  $\tau = 0$ .  $dt = r \sin d\varphi \approx r d\varphi$  with respect to the radial derivative. If the second derivative is evaluated in the tangential direction, we advance in the  $r$  direction by  $dr$ , then the angular change is  $d\varphi$ . In the case of plane stress and in the event that the body forces are negligible the differential equations of equilibrium in polar coordinates are as follows [11]:

$$\begin{aligned} \frac{\partial \sigma_r}{\partial r} + \frac{1}{r} \frac{\partial \tau}{\partial \varphi} + \frac{\sigma_r - \sigma_\varphi}{r} &= 0 \\ \frac{1}{r} \frac{\partial \sigma_\varphi}{\partial \varphi} + \frac{\partial \tau}{\partial r} + \frac{2\tau}{r} &= 0 \end{aligned} \quad (4)$$

The usual method for solving these equations is by introducing a single new function  $\phi = \phi(r, \varphi)$ , commonly known as Airy's stress function, which satisfies Eqs. (4) and is related to the stresses as follows:

$$\begin{aligned} \sigma_r &= \frac{1}{r^2} \frac{\partial^2\phi}{\partial \varphi^2} + \frac{1}{r} \frac{\partial\phi}{\partial r} \quad \sigma_\varphi = \frac{\partial^2\phi}{\partial r^2} \\ \tau &= -\frac{\partial}{\partial r} \left( \frac{1}{r} \frac{\partial\phi}{\partial \varphi} \right) = \frac{1}{r^2} \frac{\partial\phi}{\partial \varphi} - \frac{1}{r} \frac{\partial^2\phi}{\partial r \partial \varphi} \end{aligned} \quad (5)$$

One can assume the stress function  $\phi(r, \varphi) = CF_r r \varphi \sin \varphi$ , where  $F_r$  denotes the radial force, the distribution  $C$  is a constant,  $r$  is the radius of the rope and  $\varphi$  is the angle. It can be easily verified that the stress function satisfies the equation of compatibility. Thus, it represents the true stress function. For equilibrium, the stress distribution obtained from Eqs.(5) is:

$$\sigma_r = \frac{1}{r^2} \frac{\partial^2\phi}{\partial \varphi^2} + \frac{1}{r} \frac{\partial\phi}{\partial r} = \frac{2CF_r}{r} \cos \varphi \quad \sigma_\varphi = \frac{\partial^2\phi}{\partial r^2} = 0$$

$$\tau = -\frac{\partial}{\partial r} \left( \frac{1}{r} \frac{\partial\phi}{\partial \varphi} \right) = \frac{1}{r^2} \frac{\partial\phi}{\partial \varphi} - \frac{1}{r} \frac{\partial^2\phi}{\partial r \partial \varphi} = 0 \quad (6)$$

The radial force distribution  $F_r$  per unit length along the circumference of the sheave, induced by the tangential rope tension  $S$ , is:

$$F_r = \frac{dN (= Sd\varphi)}{\frac{D}{2} d\varphi} = \frac{2S}{D} \quad (7)$$

where  $D$  is the pitch diameter of the sheave. The boundary conditions along the area of contact, for  $r = d/2$ , in the radial plane at an angle of  $\alpha$  are expressed by:

$$-dN = -F_r \frac{D}{2} d\alpha = 2 \int_{\beta/2}^{\delta/2} \sigma_r \cos \varphi dA \quad (8)$$

where  $dA$  represents an infinitesimal contact area with the dimensions  $(D/2)d\alpha$  along the arc of the wrap of the rope on the sheave and  $(d/2)d\varphi$  in the radial plane of the sheave, where  $d$  is the rope diameter, hence  $dA = d D d\varphi d\alpha/4$ .

Substituting  $dA$  and Eq.(6) into Eq. (8), we obtain:

$$-F_r \frac{D}{2} d\alpha = 2D d\alpha C \eta \int_{\beta/2}^{\delta/2} \cos^2 \varphi d\varphi \quad (9)$$

and then Eq.(9) reduces to:

$$C \int_{\beta/2}^{\delta/2} \cos^2 \varphi d\varphi = -\frac{1}{4} \quad (10)$$

The constant  $C$  can now be determined by integrating Eq.(10) and solving it for  $C$  so as to fulfil the last of the boundary conditions:

$$C = \frac{-1}{\delta - \beta + \sin \delta - \sin \beta} \quad (11)$$

By putting Eq.(11) and Eq. (6) into Eq. (7), the field of stress existing in the radial plane within the sheave at an angle of  $\alpha$  becomes:

$$p = |\sigma_r| = \frac{8S \cos \varphi}{Dd(\delta - \beta + \sin \delta - \sin \beta)} \quad (12)$$

where  $S$  is the rope tension at the point on the arc of the rope with an angle  $\alpha$ .

## 2 SHAPE FACTOR FOR THE FRICTION COEFFICIENT

The drive traction force is initiated by the friction between the ropes and the sheave grooves in traction. The maximum traction that can be developed in the sheave groove is a function of the

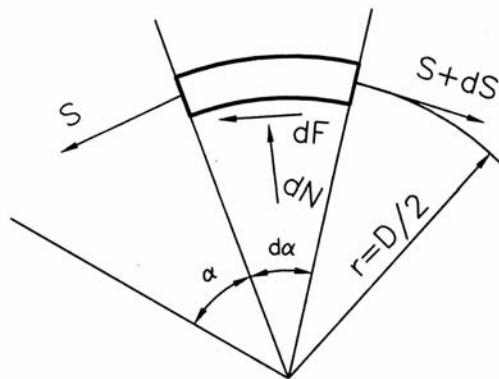


Fig.2. The free body diagram of an indefinitely small element of the rope

coefficient of friction between the rope and the groove and the angle of contact that the rope makes with the circumference of the sheave.

The groove form favourably increases the actual coefficient of friction between the rope and the sheave. Considering the equilibrium condition of an indefinitely small element of the rope shown in Fig.2 when the rope is about to slide, the elementary tangential friction force  $dF$  developed by the radial force  $dN$  can be obtained as follows:

$$dF = 2 \int_0^{\delta/2} \mu_a p dA \quad (13).$$

Substituting  $dA$ , Eq. (12) and into Eq. (13), we obtain:

$$\mu_{eff} S d\alpha = \frac{4\mu_a S}{(\delta - \beta + \sin \delta - \sin \beta)} \int_{\beta/2}^{\delta/2} \cos \varphi d\varphi d\alpha \quad (14).$$

After the rearrangement and integration the final expression becomes:

$$\mu_{eff} = 4 \mu_a \frac{\sin \frac{\delta}{2} - \sin \frac{\beta}{2}}{(\delta - \beta + \sin \delta - \sin \beta)} \quad (15).$$

The shape factor for the coefficient of friction can be defined as:

$$a = 4 \frac{\sin \frac{\delta}{2} - \sin \frac{\beta}{2}}{(\delta - \beta + \sin \delta - \sin \beta)} \quad (16).$$

The shape factors for the coefficient of friction are plotted in Fig. 3. The figure shows how it changes with the changes in the angle of the outer normal lines of the contact area,  $\delta$  and the angle of undercutting,  $\beta$ . The shape factor for the coefficient of friction gets its maximum value, i.e.,  $a = 4/\pi$ , when the angle  $\delta$  becomes  $180^\circ$  and the groove is round.

### 3 CONCLUSIONS

The groove form favourably increases the effective coefficient of friction between the rope and the groove since the radial force due to the rope

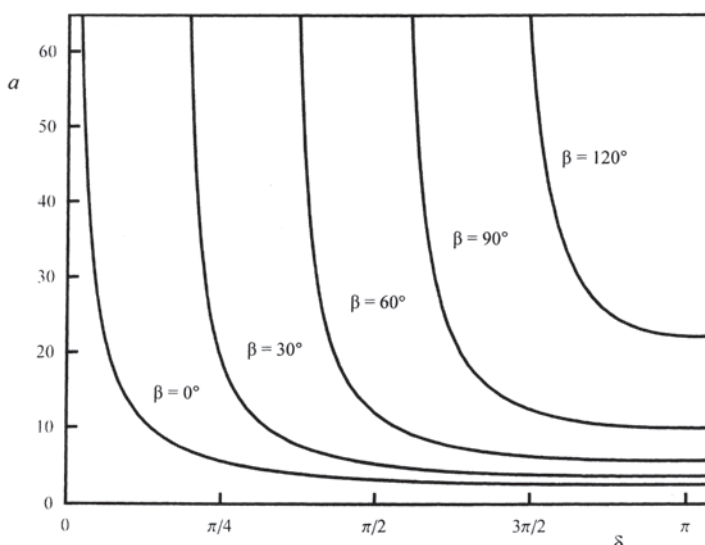


Fig.3. The shape factor for the coefficient of friction

tension produces greater normal and frictional forces acting along the area of contact given by the shape of the groove. Therefore, this work introduces the concept of shape factors for the coefficient of friction for U-shaped grooves and also derives it by means of the Airy stress-function method.

From a careful analysis it can easily be seen that when the angle of the groove decreases the traction improves, but also so does the specific pressure and resultant wear of both the grooves and the ropes. The round groove gives lower traction but a longer rope life, lower specific pressure and lower degree of noise than the undercut. When it is essential to use round grooves the traction capability can still be improved by using non-metallic groove liners with a high coefficient of friction. It is also advisable that the angle of the undercutting should be under 90°, and must not be greater than 105° whenever undercut grooves are in use.

#### 4 SYMBOLS

$a$	shape factor for the coefficient of friction
$A$	contact area
$d$	rope diameter
$D$	pitch diameter of the sheave
$F$	tangential friction force
$F_r$	radial force distribution
$N$	radial force
$S$	rope tension
$\alpha$	angle of wrap
$\beta$	angle of undercutting
$\phi$	Airy's stress function
$\delta$	angle of the outer normal lines of the contact area
$\mu_{eff}$	effective coefficient of friction
$\mu_a$	coefficient of friction

#### 5 REFERENCES

- [1] Imrak, C.E., Ozkirim, M. (2002) Calculating the pressure distribution in undercut grooves: stress-function solution. *Proceedings of the 12<sup>th</sup> International Congress on Vertical Transportation Technologies*, Milan, 141-150.
- [2] Janovsky, L. (1999) Elevator mechanical design 3<sup>rd</sup> edition. *Elevator World*, New York.
- [3] Jesson, D.E., Cottingham, W.N. (1986) Investigation of beam theory using the Airy stress function coupled with analytic function theory. *Journal of Engineering Mathematics*, 20(1), 73-79.
- [4] Bourgois, R.A. (1973) Application of the generalized Airy stress function to problems on elastic vibrations of hollow cylinders. *Journal of Applied Mechanics*, ASME, 40(4), 1140-1141.
- [5] Yen, C.F. (1987) New membrane element based on Airy's stress function, *Journal Institusi Jurutera Malaysia*, 41, 18-25.
- [6] Tarantino, A.M. (1996) Thin hyperelastic sheets of compressible material: Field equations, Airy stress function and an application in fracture mechanics. *Journal of Elasticity*, 44(1), 37-59.
- [7] Gdoutos, E.E. (1982) Stress function interface and boundary conditions in anisotropic materials, *Journal of Applied Mechanics*, ASME, 49(4), 787-791.
- [8] Frank, F.C. (1978) Airy functions in the air: an easy way with stress problems, *Phys. Educ.*, 13, 258-263.
- [9] Hasegawa, H. (1987) On the strain functions and complex stress functions in the two dimensional theory of elasticity, *Nippon Kikai Gakkai Ronbunshu*, A Hen, 53(488), 816-819.
- [10] Fosdick, R. (2003) Generalized Airy stress function, *Meccanica*, 38(5), 571-578.
- [11] Ugural, A.C., Fenster, S.K. (1987) Advanced strength and applied elasticity, *Prentice Hall*, New Jersey.
- [12] Timoshenko, S., Goodier, J.N. (1985) Theory of elasticity, *McGraw-Hill*, New York.

Authors' Addresses: Doc.Dr. C.Erdem Imrak

Dr. Ismail Gerdemeli

Istanbul Technical University

Faculty of Mechanical Eng.

Gümüşsuyu

TR-34437 Istanbul, Turkey

imrak@itu.edu.tr

gerdemeli@itu.edu.tr

Prejeto:  
Received: 9.3.2006

Sprejeto:  
Accepted: 22.6.2006

Odpri za diskusijo: 1 leto  
Open for discussion: 1 year

# Numerično modeliranje notranjih zvokov v železniških vozilih

## Numerical Modelling of the Internal Sound in Railway Rolling Stock

Jonas Bazaras - Žilvinas Bazaras - Jonas Sapragonas  
(Kaunas University of Technology, Lithuania)

*V prispevku je predstavljena analiza zvoka v železniških vozilih. S tehničnim razvojem železniških vozil se povečuje tudi hitrost vlakov, zato se povečuje tudi jakost zvoka, ki pri tem nastane. Hrup je ena izmed škodljivih posledic transporta. Ker je v bivalnih okoljih raven zvoka eden izmed pomembnejših pokazateljev bivalnega ugodja, se povečuje pozornost namenjena raziskavam poteka zvoka. V prispevku so predstavljeni zvoki, ki ga povzročajo prevozna sredstva, njegovo širjenje in njegovo sprememjanje v notranjih prostorih vozil ter različni viri zvoka pri železniškem transportu. Obravnavani so tehnični, organizacijski in administrativni ukrepi za zmanjšanje nastanka zvoka. Prav tako pa so prikazani tudi škodljivi vplivi zvoka na zdravje ljudi. Za raziskavo smo izbrali dve vrsti ruskih lokomotiv M62 in TEP60. Z uporabo programske opreme ANSYS/Multiphysics smo simulirali zvok motorjev z različno močjo. Rezultate preračunov zvoka smo nato primerjali z dovoljenimi vrednostmi.*

© 2007 Strojniški vestnik. Vse pravice pridržane.

**(Ključne besede:** železniška vozila, generiranje zvoka, numerično modeliranje, parametri dušenja)

*The paper presents an analysis of the sound in railway rolling stock. The speeds of trains tend to increase as railway rolling stock improves technically and becomes more sophisticated; however, the sound generated is intensified too. Noise is one of the harmful consequences of transport. As the sound level in domestic surroundings is one of the most important human-comfort indices, increasing attention is being devoted to an investigation of sound processes. The sound generated by transport vehicles, its distribution, and its variation in internal transport-vehicle spaces, and various sound sources in railway transport are considered in the paper. Engineering, organizational and administrative sound-reducing measures are discussed. The harmful effects of sound on human health are discussed as well. Two types of Russian production locomotives - the M62 and the TEP60 - were selected for this research. Using ANSYS/Multiphysics software the acoustic sound of the different power units in the engine sector was simulated. The results of the sound calculations were compared with the acceptable levels.*

© 2007 Journal of Mechanical Engineering. All rights reserved.

**(Keywords:** railway rolling stock, sound analysis, numerical modelling, damping parameters)

## 0 INTRODUCTION

Noise pollution is an increasing nuisance in the EU Member States. The EU Commission, in an attempt to pursue measures against sound problems, has in recent years intensified its activities relating to sound abatement. If sound limits are exceeded for railways, several major factors are considered: the condition of the rail and the wheels, the type of train, etc. But it is certainly also a question of the specific prediction method used. These prediction methods differ in many ways in various parts of Europe.

Noise transmission in locomotives can be difficult to study due to the complexity of the locomotive's structure, and the difficulties in characterizing the excitation or describing the response. Earlier work [1] has shown that structural vibration transmission can be predicted fairly accurately using a statistical energy analysis.

At high frequencies the engine's sound can be a problem in locomotives. Fan sound, combustion events, power-train vibration, road-wheel sound and aerodynamic sound can also input power to the vehicle structure at frequencies above 250 Hz. At

these frequencies a statistical energy analysis can be used to study the transmission of sound ([1] to [6]).

The objective of the paper was to analyse the internal sound pollution in existing locomotives in Lithuania today. The speed of the trains is not high, and at low speeds the locomotive sound is the dominating source. We have chosen two types of locomotives – the freight locomotive M62 and the passenger locomotive TEP60. In this paper we present the results of modelling the internal sound of these locomotives.

## 1 THEORETICAL ANALYSIS

A functional scheme of the existing harmful factors affecting human health in railway transport is presented in Fig. 1.

The standards define the sound level of the rolling stock. The sound of the rolling stock is limited by requisition No 692 of the Minister of Health of the Lithuanian Republic. The equivalent sound levels in railway-transport working places are defined in this requisition (Table 1) ([7] and [8]).

The sound sources in a locomotive are grouped into three categories:

- I – the sound arising from the motion devices – shoes, axle boxes with roller bearings, brake levers, traction engines, traction reducers and axle wheels.
- II – the sound inside the control cabin. This is the sound caused by the speedo meter, the engine driver's crane, the whistle and the watchfulness signal.

Table 1. *Equivalent sound levels in the railway-transport working place [7]*

<i>Object</i>	<i>Equivalent noise level, dB</i>
Cabins of the operators of steam and diesel locomotives	80
Cabins of the operators of suburban electric locomotives	75
Rooms of personnel in the wagons of long-distance communication trains	60
Service rooms in electric stations, cooling sections	60
Service rooms in luggage and post wagons	70
Relaxation rooms in luggage and post wagons	60
Service rooms in the restaurant wagons	70

III – the sound inside the machine section. The main sources of sound in the machine section are the diesel power aggregate, the sound caused by ventilators, the reducers of the auxiliary aggregates, the main electricity generator, the double machine aggregate, the breaking compressor, the turbo compressor and the exhaust system for the combustion products.

The axle-wheel sound is caused by the interaction between the rail irregularities and the bandage rolling on the rail head surface as well as by the sliding of the wheel along the rail in longitudinal and lateral directions. The vibrations of the bandage and the wheel centre can cause a wideband spectrum sound level up to 120 dB. The axle-wheel sound may be drowned out by the gear sound when movement speeds are low and loads are large.

The rolling sound largely depends on the speed of the rolling stock. Normally, the sound pressure rate increases by 9 dB with a doubling of the speed. However, this wheel-based sound may be different with regard to the type of rolling stock. The irregularities of the interacting surfaces agitate the vibrations of the wheel and rail under the influence of the masses inherent in the movement. The vibra-

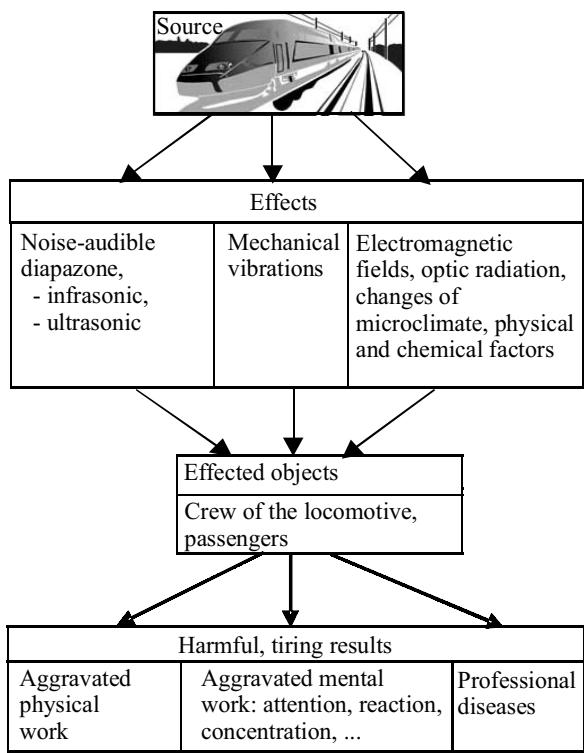


Fig. 1 Scheme of factors harmful to human health

tions of different amplitudes are agitated in the wheel and rail, depending on the properties of the materials and the geometries of the rail and the wheel. The motions of these surfaces cause the vibrations of the air, thus inducing the ambient air sound.

The sound in railway-transport facilities is measured using the procedure established in the following standards:

ISO 1996/1-1982 "Acoustics – measurement and sound description in ambience. Part I. The main parameters and measurement methods";

ISO 1996/2-1987 "Acoustics – measurement and sound description in ambience. Part II. Collection of data relevant to land usage";

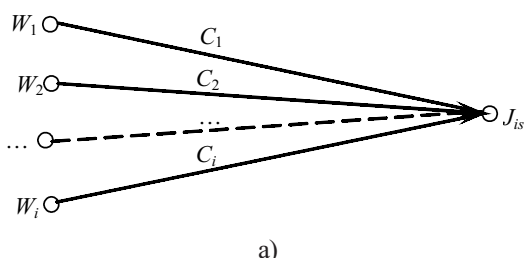
ISO 1996/3-1987 "Acoustics – measurement and sound description in ambience. Part III. Application of sound limitation".

The general diagram can be conveniently represented by signal graphs, as shown in Fig. 2. The joints in the graph represent variable energy flows (sources), and the arcs represent the sound-energy-transmitting channels defined by the reduction indices of the sound-energy intensity ([9] to [11]).

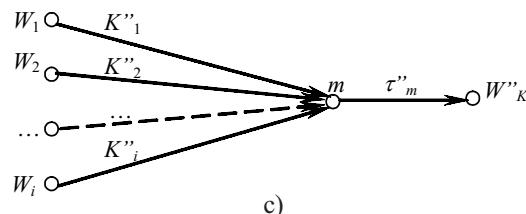
Referring to the signal graph represented in Fig. 2 a sound power flow  $J_{is}$  in the analysed direction of the sound field of the rolling stock is written as follows:

$$J_{is} = W_1 C_1 + W_2 C_2 + \dots + W_k C_k = \sum_{i=1}^{i=k} W_i C_i \quad (1)$$

The value of the intensity rate  $L_{is}$  is equal to the sound pressure rate expressed in dB, as follows:



a)



c)

$$L_{is} = 10 \lg \frac{J_{is}}{J_0} = 10 \lg \sum_{i=1}^{i=k} W_i C_i \leq [L_{is}] \quad (2)$$

where  $W_1, W_2, \dots, W_k$  are the sound capacities of the sound sources;  $C_1, C_2, \dots, C_k$  are the indices involving intensity reduction with the increase of the distance from the sound sources;  $J_0$  is the limiting value of the sound intensity,  $J_0 = 10^{-12} \text{ W/m}^2$ ;  $[L_{is}]$  is the rate of permissible external sound.

Two methods for determining the sound energy in the rolling-stock cabin are used (Fig. 2 b and c): from each source via all the elements of the cabin, or from all sources via each element of the cabin. For the first calculation method the sound energy in the cabin is expressed as follows:

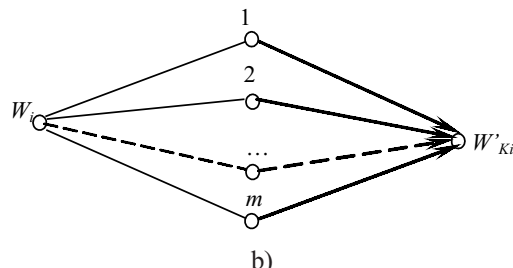
$$W'_{Ki} = W_i (K'_1 \tau'_1 + K'_2 \tau'_2 + \dots + K'_m \tau'_m) = W_i \sum_{i=1}^{i=m} K'_i \tau'_i \quad (3).$$

For the second method of calculation the expression is:

$$W''_{km} = (W_1 K''_1 + W_2 K''_2 + \dots + W_k K''_k) \tau''_m = \tau''_m \sum_{i=1}^{i=k} W_i K''_i \quad (4),$$

where  $K'_1, K'_2, \dots$  and  $K''_1, K''_2, \dots$  are the indices evaluating the transfer of sound energy to the surfaces of the relevant partitions;  $\tau'_1, \tau'_2, \dots$  and  $\tau''_1, \tau''_2, \dots$  are the indices evaluating the transfer of sound energy through the relevant partitions.

The number of signal graphs in the diagram being calculated is defined by the number of sound sources being evaluated, as well as by the number of elements that are homogeneous according to the sound permeability for all the surfaces of the cabin.



b)

Fig. 2 Signal graphs: a) graph for external sound calculations; b) and c) evaluation of the internal sound inside the cabin of the locomotive

The calculations are carried out according to the corrected and octave sound capacity values by evaluating the relevant values of the transfer indices  $\tau$  – the sound permeability through partitions. Evaluating the total sound intensity in the cabin gives:

$$J_k = \frac{\sum W_k}{\bar{\alpha} S_\Sigma} \quad (5),$$

where  $\sum W_k$  is the total sound energy of the cabin, calculated using the following formula

$$\sum W_k = \sum_{i=1}^i W'_{ki} = \sum_{i=1}^m W'_{km} \quad (6),$$

where  $\bar{\alpha}$  is the average sound-absorption coefficient in the cabin and the body;  $S_\Sigma$  is the area of the internal surface of the cabin and the body.

The sound rate (sound-pressure ratio) in the cabin of the rolling-stock is calculated using the formula:

$$L_K = 10 \lg \sum \left/ \left( \bar{\alpha} S_\Sigma J_0 \right) \right. \leq [L_K] \quad (7),$$

where  $[L_K]$  is the allowed sound rate in the cabin.

The transmission indices  $C_i$ , which evaluate the reduction of the sound intensity with the increase of the distance from the point of the sound source, are determined using the relationship:

$$C_i = \frac{1}{\Omega r_i^2} \quad (8),$$

where  $r_i$  is the distance of the  $i$ -th sound source from the field-sound source point of the rolling-stock cabin under consideration;  $\Omega = 4\pi$  for spherical sound radiation, and  $\Omega = 2\pi$  for semi-spherical sound radiation (semi-spherical sound radiation will be for  $H \leq r_i/3$ , here  $H$  is the agreed point-source height above the railroad surface).

The transmission indices  $K_i$  in Equations (3) and (4) are calculated using the formula:

$$K_i = \frac{S_i}{\Omega r_i^2} \quad (9),$$

where  $S_i$  is the surface area of the partition.

The index of the sound-energy transmission through the partitions (sound permeability coefficients) is calculated as:

$$\tau_i = 10^{-0.1 R_i} \quad (10),$$

where  $R_i$  is the sound isolation of the partition.

The presented acoustic-calculation model of a rolling-stock cabin allows an evaluation of the struc-

tural solutions and, in the case of an emergency, taking extra measures in the process of rolling-stock design.

## 2 METHODS OF EVALUATION

### 2.1 Complex evaluation of the impact of sound on the environment

For the modelling of the internal sound in the locomotive we used ANSYS software to create a 2D model of the internal space of the locomotive body. The geometry of the model consists of four different parts:

1. the internal space of the front control cabin;
2. the internal space of the back control cabin;
3. communicating tambours to the internal space of the machine section;
4. the internal space of the machine sector, which, for convenience, when forming the finite-elements grid, was divided into four areas

In the ANSYS/Multiphysics software the problems of acoustics are solved on the basis of a harmonic response analysis by providing the harmonic pressure agitation (sinus type) at some points of fluid structure and obtaining the pressure distribution in the fluid. By changing the agitation frequency, a variable sound distribution in the interval of different frequencies is obtained.

The stages of the harmonic acoustic analysis are as follows:

1. Formation of the model
2. Identification of the boundary conditions and the acoustic loads as well as a solution of the finite-element model
3. Review of the results

### 2.2 Limit conditions of the model and loads

When designing the calculation diagram for the front locomotive a planar structure of finite elements was used. The whole structure was described by FLUID29 2D finite elements designed for a specified acoustic analysis. These acoustic elements have the following degrees of freedom: displacements UX, UY and pressure PRES. For the acoustic FLUID29 finite elements the following characteristics of the material need to be specified: the air density, DENS; the sound velocity in the air, SONC; and the damping index, MU. Also, the real constant is to be indicated, i.e., the sound pressure value taken as an audible limit  $-p_0 = 2 \cdot 10^{-5}$  Pa. During the creation of the

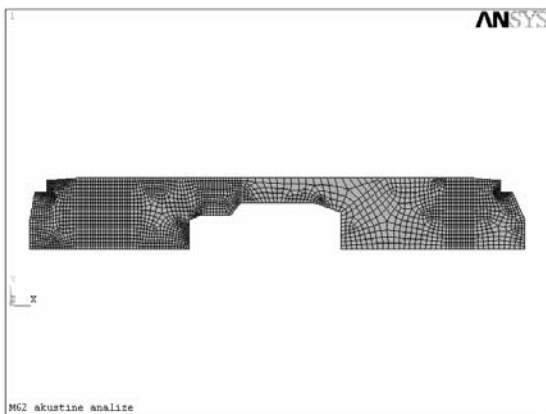


Fig. 3. Finite-element grid of the M62 locomotive

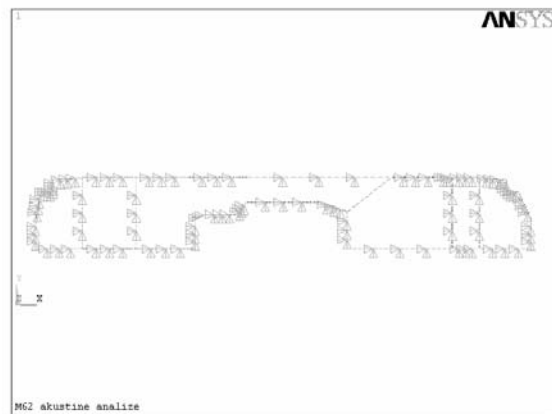


Fig. 4. Boundary conditions of the M62 locomotive model

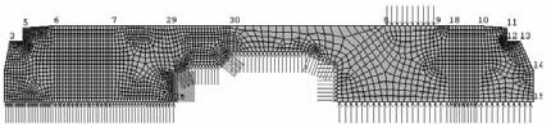


Fig. 5. Excitation places of the fluid in the M62 locomotive model



Fig. 6. Acoustic loads of the M62 locomotive

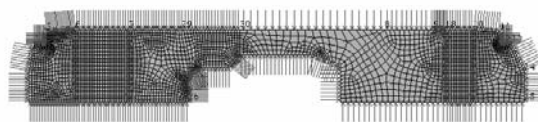


Fig. 7. Energy-damping surfaces of the M62 locomotive model

finite elements' grid (Fig. 3) and the tightening of the body walls, ceilings and floor junctions as well as in the interior body-space linear displacements (Fig. 4), the interaction surfaces of the fluid and a solid structure are indicated.

These surfaces are the floor surface of the locomotive (loaded by outside sound, caused by the rolling of the axle-wheels) as well as the agreed surfaces of the diesel engine and the fan (Fig. 5). On the surfaces of the model, the interaction between the vi-

brating structures and fluid particles occurs. Also, the acoustic load, i.e., the harmoniously varying pressure (Fig. 6), corresponding to the sound pressure levels, existing on these surfaces and represented in Table 2, is also indicated on these surfaces ([7] to [11]).

### 2.3 The solution of the model formed

Depending on the sound frequency, the isolation materials as well as the interior elements' damping characteristics vary as shown in Table 3. Therefore, the calculations were performed by varying both the agitation frequency in terms of the internal geometric frequencies of the octave bands and by accordingly changing the damping coefficients of the parameters defining the sound-energy damping surfaces of the model.

### 2.4 Boundary conditions of the model, conditions of loading and the solution

By forming the grid of finite elements, and restricting the linear displacements in the junctions

Table 2. Noise pressure at various locations of the M62 locomotive [7]

Surface	Noise level dB	Pressure Pa
<i>Floor of vehicle, when speed v is km/h:</i>		
30	90	0.632
60	97	1.420
90	103	2.830
120	111	7.100
<i>Engine</i>	120	20
<i>Fan</i>	104	3.17

Table 3. Noise pressure at various places in the TEP60 locomotive [7]

Surface	Noise level dB	Pressure Pa
Floor of the vehicle, when speed $v$ , km/h:		
$\leq 120$	96	1.260
$120 \leq v \leq 160$	105	3.560
Engine	120	20
Ventilator	109	5.64

of the body walls, ceilings and floors as well as in the internal space of the body, by indicating the interaction surfaces of the fluid and solid structure and by marking the damping surfaces, the model of the finite elements of the passenger locomotive, shown in Fig. 7, is obtained. The variations of the damping parameters and the loads are presented in Tables 3 and 4.

The calculations were carried out when changing the agitation frequency and damping parameters in an order analogous to the one presented in Table 4.

One of the essential indices of human comfort is the level of sound in the working and domestic environment. The permissible sound level in thermal trucks, according to OSZhD recommendations, is the following ([10] to [12]):

- long-term sound,  $N_{80} = 80$  dB,
- interrupted sound,  $N_{85} = 85$  dB.

### 3 RESULTS

The sound levels in the control cabins of the M62 and TEP60 locomotives are not the same when driving at the maximum allowed speed of 120 km/h

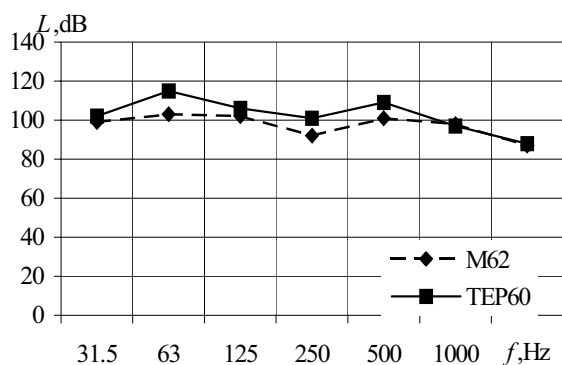


Fig. 8. Comparison of the sound levels in the cabins of the M62 and TEP60 locomotives when the velocity is 120 km/h

Table 4. Noise damping parameters [8]

Frequency Hz	Engine room	Cabin
31.5	0.04	0.17
63	0.04	0.17
125	0.04	0.17
250	0.04	0.26
500	0.04	0.64
1000	0.04	0.89
2000	0.04	0.75
4000	0.04	0.78

due to the difference in power (for the TEP60,  $N_e = 2237$  kW; for the M62,  $N_e = 1421$  kW) (Fig. 8). The internal sound in the cabins of these locomotives exceeds the permissible values.

Fig. 9 shows the change of the sound level  $L$  in the cabin of the M62 locomotive when the sound of the riding wheels increases. The sound increase in the cabin is the result of the increasing velocity of the train.

In Fig. 10 the change of the sound inside the body of the M62 locomotive is presented in the sound frequency range 125 to 1000 Hz. In the machine section, where the damping of sound waves is minimal, the maximum sound pressure is formed, and it reached 122 dB. Such a working environment is harmful to human health. Even a short time spent in such an environment can cause damage to the ear. The sound spreading from the machine sector and the external sound coming into the cabin are damped by the wall, floor and ceiling sound isolation.

### 4 CONCLUSIONS

1. The sound in the high-frequency range of the rolling stock used in Lithuania exceeds the leg-

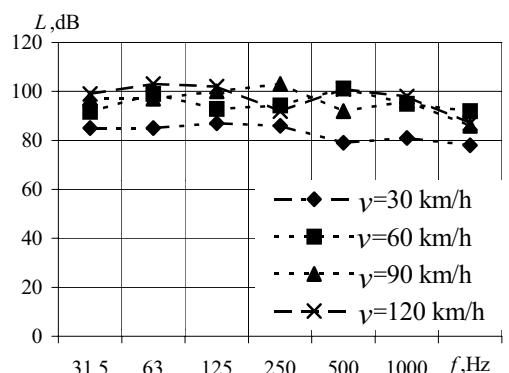


Fig. 9. Change of sound level in the cabin of the M62 locomotive driving at 30 to 120 km/h

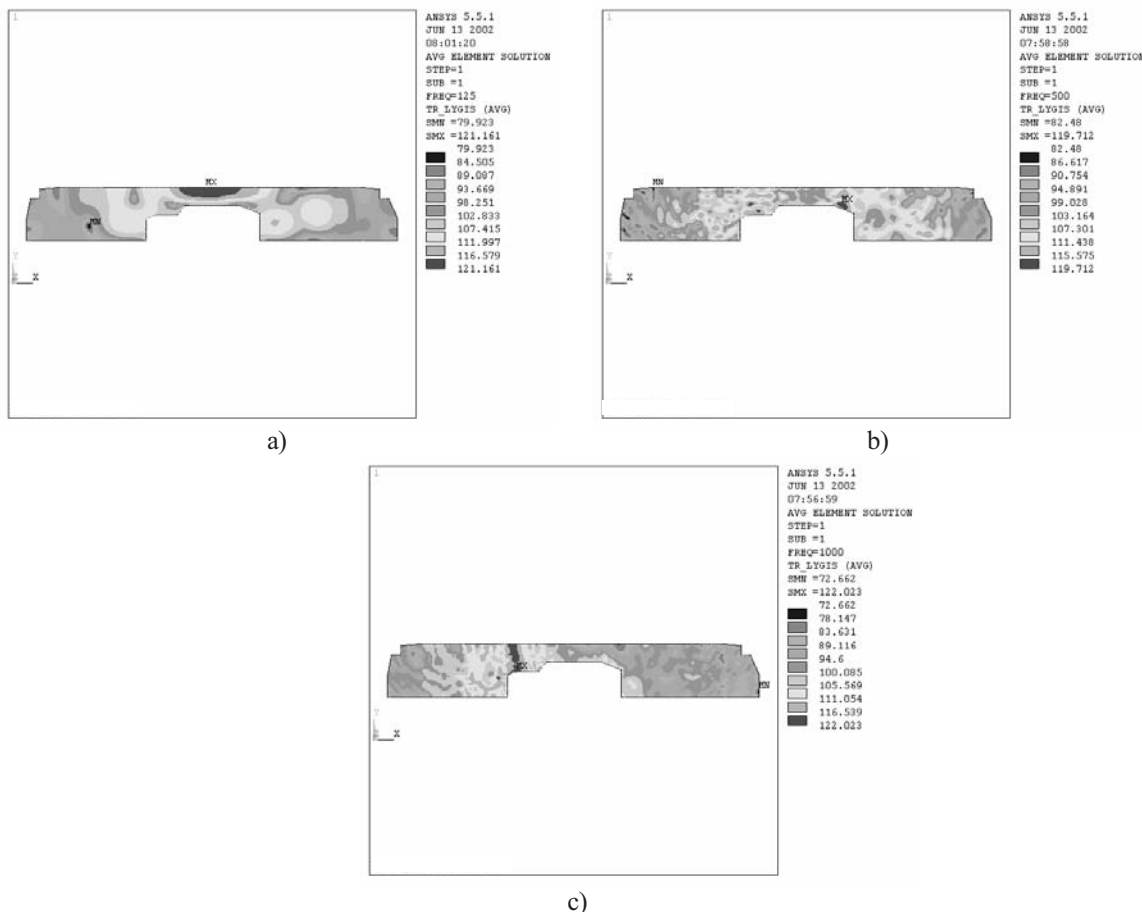


Fig. 10. Change of the sound level [db], when the excitation frequency is: a) 125 Hz; b) 500 Hz; c) 1000 Hz

islated levels by 5 to 25 dB. The main sources of sound pollution, such as the main and additional power aggregates, the road-wheel interaction, the braking equipment, and the sound-isolation equipment, have a mechanical character.

2. The highest sound level in the control cabin of the TEP60 passenger locomotive is 106 dB; in the M62 locomotive it is 106 dB, in the machine section of the TEP60 locomotive it is 120 dB, and in the M60 locomotive it is 125 dB in the 31.5 to 250 Hz range of sound frequencies.

## 5 REFERENCES

- [1] Steel J. A. (1998) A study of engine sound transmission using statistical energy analysis. *J. of Automobile Engineering*, vol.212, part D , 205-213.
- [2] Wunderli J. M. (2005) A measurement procedure for the sound emission of railway sources including source separation. *J. Rail and Rapid Transit*, vol.219, part F, 125-137.
- [3] Bazaras Ž., Leonavičius M. (2005) Simulating the lateral vibrations of passenger wagons. *Strojniški vestnik*, vol.51, No6/05, 346-355.
- [4] A study of European priorities and strategies for railway noise abatement (2002) *Final Report*.
- [5] Gelezinkeliu bendradarbiavimo organizacija OSZD (2001) Gelezinkeliu transporto keliamo triuksmo poveikio aplinkai vertinimo rekomendacijos, Vilnius.
- [6] Baušys R. (1999) Quality assessed solutions in acoustic analysis . *J. Mechanika* Nr.1(16) 1999, 39-43.
- [7] Справочник по электроподвижному составу, тепловозам и дизель-поездам. Под общ. ред. А. И. Тищенко. Т.2. *Транспорт*, Москва (1976)

- [8] Акустика: Справочник (1989) А. П. Ефимов, А. В. Никонов, М. А. Сапожков, В. И. Шоров; Под ред. М. А. Сапожкова. *Радио и связь*. Москва,. – 336 с.
- [9] Koo D.H., Kim J.C., Yoo W.H., Park T.W. (2002) An experimental study of the effect of low-sound wheels in reducing sound and vibration. *Transportation Research Part D* 7, 429-439.
- [10] Bazaras Ž., Ramanauskas M., Ilgakojis P. (2002) Triukšmo modeliavimas lokomotyve. Tarptautinės konferencijos „Transporto priemonės-2002“ pranesimumedziaga. *Technologija* Kaunas, Lithuania.
- [11] Thompson D.J., Jones C.J.C. (2000) A review of the modelling of wheel/rail sound generation *J.Sound Vibration.*, vol.231(3), 519-536.
- [12] Hardy A.E.J. (1999) Noise from railway bridges. *J. Rail and Rapid Transit.* ISSN 0954-4097, 1999, vol.213, part. F, 161-172.
- [13] Hardy A.E.J. (1999) Noise from railway bridges . *J. Rail and Rapid Transit*, vol. 213, part F, 173-180.
- [14] Cervello S., Donzella G., Pola A., Scepi M. (2001) *J. Rail and Rapid Transit.* ISSN 0954-4097, vol. 215, part F, 179-192.

Authors' Address:

Mag. Jonas Bazaras  
Prof. Dr. Žilvinas Bazaras  
Prof. Dr. Jonas Sapragonas  
Department of Transport Engineering  
Kaunas University of Technology  
Kestucio str. 27  
LT-44025 Kaunas-4, Lithuania  
jonasB1@one.lt  
zilvinas.bazaras@ktu.lt  
jonas.sapragonas@ktu.lt

Prejeto:  
Received: 4.1.2006

Sprejeto:  
Accepted: 22.6.2006

Odperto za diskusijo: 1 leto  
Open for discussion: 1 year

# Teoretična in eksperimentalna analiza dinamike mehanizmov Rolomite

## A Theoretical and Experimental Investigation of the Dynamics of Rolomite-Type Mechanisms

Ričardas Viktoras Ulozas  
(Šiauliai University, Lithuania)

*Prispevek najprej poroča o teoretični raziskavi dinamičnega modela valja in jermena pri mehanizmu tipa Rolomite (RTM). Dinamični model valja in jermena mehanizma RTM je opisan z diferencialnimi enačbami ter analiziran na dva načina, tj. v primeru, ko na sistem ne vpliva vibracijsko vzbujanje, in v primeru, ko le-to vpliva na sistem. Ugotovili smo, da je mogoče s parametri vibracijskega vzbujanja spremenjati parametre nezdrsnega območja. To nas je vodilo do predpostavke, da je v dejanskih mehanizmih tipa Rolomite mogoče vplivati na trenje med strukturnimi elementi mehanizma RTM.*

*Eksperimentalni del raziskave dinamike mehanizma tipa Rolomite z vibračnimi elementi je bil izveden v treh smereh: kot analiza dinamičnih pojavov v mehanizmu valja in jermena, kot analiza postopkov obvladovanja trenja med elementi mehanizma RTM in kot analiza dinamičnih pojavov v vibramotorjih Rolomite. Povečanje amplitude električne napetosti, zmanjšanje sile obremenitve gibkega jermena, in zmanjšanje kota, pod katerim gibki jermen ovija valj, povzročijo povečanje amplitude vibracij valjev. Mehanizem RTM z vrtečima se in vibračima valjema ima v primerjavi z vibračima valjema drugačnega tipa boljšo ležajno zmogljivost in je precej bolj občutljiv. Največjo sinhronost vrtenja rotorjev zagotavlja vibramotor Rolomite, ki se sestoji iz dveh rotorjev in piezoelektričnega pretvornika vibracij, ki hkrati vrти oba rotorja. Ta vibramotor primerjamo z vibramotorjem Rolomite z dvema rotorjema in piezo električnim pretvornikom vibracij, ki vrти le enega od rotorjev.*

© 2007 Strojniški vestnik. Vse pravice pridržane.

**(Ključne besede: Rolomite mehanizmi, zdrsavanje, vibracije, dinamični modeli)**

*This paper looks at theoretical research of the dynamic model of the "roller-band" system of the Rolomite-type mechanism (RTM). The dynamic model of the "roller-band" system of the RTM is described by differential equations and is investigated in two ways, i.e., when the system is not influenced by the excitation of vibrations, and when it is influenced by them. We have established that with the parameters of excitation of vibration it is possible to operate the parameters of a non-slipping zone. This allows us to assume that in a real Rolomite-type mechanism it is possible to operate on the friction between the structural elements of the RTM.*

*Experimental research on the dynamics of the Rolomite-type mechanism with vibrating elements was done in three directions: research on the dynamic processes running in the RTM roller-band system; research on the processes of friction-control between the elements of the RTM; and research on the dynamic processes running in the Rolomite vibromotors. The increase of the supply-voltage amplitude, the decrease of the force-load magnitude of the flexible band, and the decrease of the angle of the wrapping of the roller by the flexible band cause an increase in the amplitude of the roller vibrations. An RTM with rotating vibrating rollers, compared with the vibrating rollers of the other type, has a better bearing capacity and is much more sensitive. The highest synchronicity of rotation of the rotors is provided by a Rolomite vibromotor with two rotors and a piezoelectric converter of vibrations that simultaneously rotates both rotors. This is compared with the Rolomite vibromotor with two rotors and a piezoelectric converter of vibrations, which rotates only one rotor.*

© 2007 Journal of Mechanical Engineering. All rights reserved.

**(Keywords: Rolomite type mechanisms, slipping, vibrations, dynamic models)**

## 0UVOD

Donald F. Wilkes je izumil kotalni mehanizem tipa Rolomite (RTM) v letu 1967 ([1] in [2]).

Pri mehanizmu RTM se valja brez trenja kotalita po jermenu, vendar pa avtorji [3] tudi navajajo, da valja pri določenih parametrih mehanizma zdrsneta, čeprav ne podajo nikakršne teoretične podlage za ta pojav. V viru [4] sta navedeni dve vrsti zdrsa mehanizma RTM (geometrični in vzmetni zdrs).

Raziskovalci so predlagali, da bi trenje zmanjšali z uporabo vibracij [5]. Ena izmed metod za zmanjšanje trenja temelji na rabi usmerjevalnih vibracij, ki jih dovajamo stičnim telesom.

Če se vibracijska amplituda vibrajočih elementov med stičnima telesoma povečuje, se pojavi plast vibracij (FV). Mehanizem nastanka plasti vibracij je temeljito opisan v viru [6], zato tu ne bo podrobno opisan.

Najpogosteje uporabljeni sestavnvi deli vibrajočih elementov mehanizma RTM so piezoelektrični pretvorniki, tj. piezo keramični elementi. Pri mnogih konstrukcijah mehanizma RTM le-ti tvorijo dele valjev, ki imajo osi pritrjene na nepremično osnovo. Okrov mehanizma RTM se giblje premočrtno pod vplivom zunanjih sil ali sil, ki jih ustvarja kinematično delovanje valjev in jermenja. Pri takšnem mehanizmu valja opravljata funkcijo vibracijske podpore (VS) ali vibramotorja (VM) [7].

Ko načrtujemo precizni mehanizem RTM z nadzorovanim trenjem za določitev ali krmiljenje napetosti gibkega jermenja kakor tudi natančni mehanizem vlečnega jermenja z vibramotorjem Rolomite (RVM), moramo teoretično in eksperimentalno raziskati dinamične pojave, ki potekajo v mehanizmu RTM in vibramotorju.

Vibramotorje lahko v mehanizmu RTM uporabimo kot vibracijsko podporo usmerjevalnemu gibanju, mehanizmu vlečnega jermenja, črevesni črpalki, mikro vpenjalni čeljusti, idr.

Namen teoretične raziskave je razkritje razmer, v katerih se valja in jermen mehanizma RTM gibljejo sinhrono in brez zdrsov, saj je poznavanje teh razmer bistvenega pomena pri oblikovanju natančnega mehanizma. Drugi namen raziskave pa je analiza mehanizma RTM, ki je izpostavljen vplivu vibracij.

Namen eksperimentalnega dela raziskave je seznanitev z dinamičnimi pojavi v mehanizmu valjev in jermenja, analiza možnosti krmiljenja trenja

## 0INTRODUCTION

Donald F. Wilkes invented the Rolomite-type mechanism (RTM) in 1967 ([1] and [2]).

In the RTM the rollers are rolling on the band without friction; however, the authors of [3] specify that the rollers slip for certain parameters of the mechanism, although they do not provide any theoretical substantiation for this. In [4] two variants of slipping in the Rolomite-type mechanism (geometric and springy slipping) are defined.

Researchers have suggested that the friction could be decreased using vibrations [5]. One of the methods to reduce friction is to provide directional vibrations to the contact bodies.

If the vibrational amplitude of the vibrating elements is increasing between the interacting bodies a film of vibrations (FV) occurs. The mechanism of the FV's formation is comprehensively described in [6], thus we will not describe it in detail here.

The most frequently used constituent parts of the RTM's vibrating elements are piezoelectric converters i.e., piezoceramic elements. In many RTM constructions they form part of the rollers that have their axes fixed to the immobile base. The casing of the RTM under external forces or forces arising in the kinematic roller-band pair performs a rectilinear movement. The rollers of such an RTM perform the functions of vibrosupport (VS) or vibromotors (VM) [7].

When designing precision Rolomite mechanisms with controlled friction for positioning or regulating the tension of the flexible band, as well as precision band-pulling mechanisms with a Rolomite vibromotor (RVM), the dynamic processes taking place in the RTM and RVM have to be explored both theoretically and experimentally.

Vibromotors may be used in a RTM as the vibrosupport of the directional movement, band-pulling mechanisms, peristaltic pumps, micro-manipulator grips, etc.

The purpose of theoretical research is to reveal the conditions under which the bodies of the roller-band of an RTM are moving synchronically without slipping, because their detection is the most important problem in the design of precision mechanisms. The other purpose is to investigate the RTM that is influenced by vibrations.

The purpose of experimental research is to explore the dynamic processes in the RTM roller-band system; to explore the possibilities of control-

mehanizma RTM ter analiza dinamičnih pojavov v vibramotorjih.

Predmeti eksperimentiranja so izvirni mehanizmi RTM, pri katerih sta valja vzbujena z visokofrekvenčnim vibriranjem, ter vibromotor, čigar delovanje je utemeljeno na visokofrekvenčnih diagonalnih udarcih piezokeramične plošče ob vrteči se rotor.

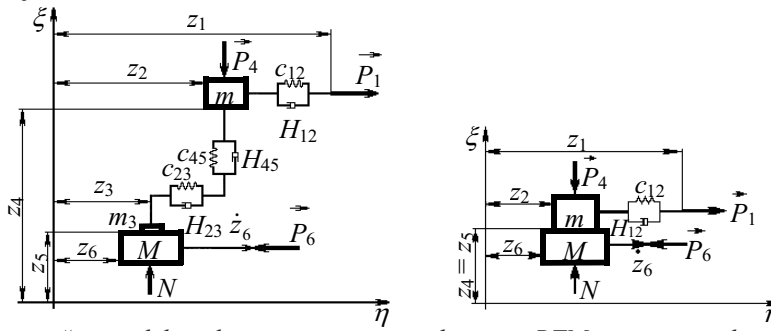
## 1 DINAMIČNI MODELI VALJEV IN JERMENA PRI MEHANIZMU RTM

Dinamični modeli sklopa valjev in jermenja pri mehanizmu RTM v primeru deformiranih in nedeformiranih stikov med telesi (sl. 1) so opisani z diferencialnimi enačbami in analizirani.

Slika 1 kaže, da so  $z_i$  ( $i = 1$  do  $6$ ) pomiki elementov (v pravokotni in strižni smeri),  $\vec{P}_i$  je vlečna sila,  $\vec{P}_6$  je sila odpore gibaju,  $\vec{P}_4$  je sila, ki pritiska maso  $m$  ob maso  $M$  (in povzroča pravokotno tlačno silo  $N$ ).

Jermen opišemo z dvojicami parametrov. V sredini stičnega predela med valjem in jermenom je zgoščena masa jermenja  $m$ , preostali del jermenja pa je v vzdolžni smeri spremenjen v elastični element  $c_{12}$  in razsipni element  $H_{12}$ , ki sta povezana vzporedno. Masa jermenja  $m$  je zbrana vzdolž površine valja. Valj je izražen kot telo z maso  $M$ .

Medsebojno delovanje jermenja in valja je prikazano s prej omenjeno zgoščenje mase  $m$  ter s primerno povezavo elastičnih elementov  $c_{23}, c_{45}$  in razsipnih elementov  $H_{23}, H_{45}$ , ti omogočajo deformacije jermenja, ki se dotika valja v strižni in pravokotni smeri. Zgoščena masa se deloma nanaša na maso  $m$  in deloma na maso  $m_3$ , ki je zbrana neposredno na površini valja in pridobljena s telesom, ki ima maso  $M$ .



Sl. 1. Dinamična modela valja in jermenja pri mehanizmu RTM v primeru stika med telesoma:  
a – deformirani stik, b – nedeformirani stik

Fig. 1. Dynamic models of the roller-band system of the RTM in the case of a contact between bodies:  
a – deformed, b – non-deformed

ling the friction of the Rolamite mechanisms; and to explore the dynamic processes in Rolamite vibromotors.

The objects of the experiments are the original RTM, where the rollers are induced by high-frequency vibration, and the RVM, where the functioning is based on high-frequency diagonal hits by the piezoceramic plate onto the rotor that is rotating.

## 1 DYNAMIC MODELS OF THE ROLLER-BAND SYSTEM OF AN RTM

Dynamic models of the roller-band system of an RTM in the cases of deformed and non-deformed contact between the bodies (Fig. 1) were described by differential equations and investigated.

It is shown in Fig. 1 that  $z_i$  ( $i = 1$  to  $6$ ) are the displacements of the elements (in the normal and tangential directions),  $\vec{P}_1$  is the pulling force,  $\vec{P}_6$  is the force of the resistance to movement,  $\vec{P}_4$  is the force that is pressing the mass  $m$  to mass  $M$  (causing the normal pressing force  $N$ ).

The band is represented by coupled parameters. In the center of the contact zone between the roller and the band is concentrated the band's reduced mass  $m$ , the remaining piece of the band in a longitudinal direction is changed to the elastic element  $c_{12}$  and the dissipative element  $H_{12}$ , connected in parallel. The mass of the band  $m$  is concentrated along the roller's surface. The roller is expressed as a body with the mass  $M$ .

The interaction of a band with a roller is shown by means of the above-mentioned reduced mass  $m$ , and connecting in appropriate way the elastic  $c_{23}, c_{45}$  and dissipative  $H_{23}, H_{45}$  elements, which allow deformations of the band contacting the roller in the tangential and normal directions. The part of the reduced mass of the band relates to the mass  $m$

Deformacija stika med jermenom in obema valjema je mogoča zaradi elastičnih in razsipnih elementov  $c_{23}$ ,  $c_{45}$ ,  $H_{23}$ ,  $H_{45}$  ter tudi zaradi mase  $m_3$ .

Analiziran je primer nepreklenjenega gibanja mas  $m$  in  $M$  v pravokotni smeri.

Poenostavljeni dinamični model natančnega mehanizma valja in jermenoma, kakršnega poznamo pri sistemu RTM, je opisan z diferencialnimi enačbami in analiziran.

V skladu s sliko 1a imajo diferencialne enačbe gibanja naslednje izraze:

$$\begin{aligned} H_{12}(\dot{z}_1 - \dot{z}_2) + c_{12}(z_1 - z_2) &= P_1 \\ m\ddot{z}_2 - H_{12}(\dot{z}_1 - \dot{z}_2) - c_{12}(z_1 - z_2) + H_{23}(\dot{z}_2 - \dot{z}_3) + c_{23}(z_2 - z_3) &= 0 \\ m_3\ddot{z}_3 - H_{23}(\dot{z}_2 - \dot{z}_3) - c_{23}(z_2 - z_3) + [H_{45}(\dot{z}_4 - \dot{z}_5) + c_{45}(z_4 - z_5)]f_0 \cdot sign(\dot{z}_3 - \dot{z}_6) + f(\dot{z}_3 - \dot{z}_6) &= 0 \\ M\ddot{z}_6 - [H_{45}(\dot{z}_4 - \dot{z}_5) + c_{45}(z_4 - z_5)]f_0 \cdot sign(\dot{z}_3 - \dot{z}_6) - f(\dot{z}_3 - \dot{z}_6) &= -P_6 \\ m\ddot{z}_4 + H_{45}(\dot{z}_4 - \dot{z}_5) + c_{45}(z_4 - z_5) &= -P_4 \end{aligned} \quad (1)$$

V skladu s sliko 1b imajo diferencialne enačbe gibanja naslednje izraze:

$$\begin{aligned} H_{12}(\dot{z}_1 - \dot{z}_2) + c_{12}(z_1 - z_2) &= P_1 \\ m\ddot{z}_2 - H_{12}(\dot{z}_1 - \dot{z}_2) - c_{12}(z_1 - z_2) + Nf_0 \cdot sign(\dot{z}_2 - \dot{z}_6) + f(\dot{z}_2 - \dot{z}_6) &= 0 \\ M\ddot{z}_6 - Nf_0 \cdot sign(\dot{z}_2 - \dot{z}_6) - f(\dot{z}_2 - \dot{z}_6) &= -P_6 \\ m\ddot{z}_5 + P_4 &= N \end{aligned} \quad (2)$$

$H_{12}, H_{23}, H_{45}$  - koeficienti viskoznega dušenja;  
 $c_{12}, c_{23}, c_{45}$  - koeficienti togosti;  
 $f_0$  - koeficient suhega trenja;  
 $f$  - koeficient mokrega trenja.

Včasih je koeficient mokrega trenja  $f$  sorazmeren vrednosti pravokotne reakcije, tj.:

and the part to mass  $m_3$ , concentrated directly to the surface of a roller adopted by the way of a body with mass of  $M$ . The deformed contact between a band on both rollers is allowed by the elastic and dissipative elements  $c_{23}$ ,  $c_{45}$ ,  $H_{23}$ ,  $H_{45}$  and also by mass  $m_3$ .

An example of the continuous movement of the masses  $m$  and  $M$  in the normal direction is analyzed.

The simplified dynamic model of a precision roller-band mechanism such as the RTM roller-band system was described by differential equations and investigated.

The differential equations of movement, in accordance with Fig.1 a, have these expressions:

The differential equations of movement, in accordance with Fig.1 b, have the following expressions:

$H_{12}, H_{23}, H_{45}$  - viscous damping coefficients;  
 $c_{12}, c_{23}, c_{45}$  - coefficients of stiffness;  
 $f_0$  - coefficient of dry friction;  
 $f$  - coefficient of wet friction.

Sometimes the coefficient of wet friction,  $f$ , is proportional to the value of the normal reaction, i.e.:

$$f = f_1 N_{45} \quad (3),$$

$f_1$  - koeficient mokrega trenja.

$f_1$  - coefficient of wet friction.

$$N_{45} = H_{45}(\dot{z}_4 - \dot{z}_5) + c_{45}(z_4 - z_5) \quad (4).$$

V primeru zunanjega vzbujanja:

For external excitation:

$$\begin{aligned} P_1 &= A_1 + B_1 \dot{z}_1 + D_1 \sin(\omega t + \alpha_1) \\ P_4 &= A_4 + B_4 \dot{z}_4 + D_4 \sin(\omega t + \alpha_4) \\ P_6 &= A_6 + B_6 \dot{z}_6 + D_6 \sin(\omega t + \alpha_6) \\ z_5 &= D_5 \sin(\omega t + \alpha_5) \\ \cdot &= \frac{d}{dt} \end{aligned} \quad (5).$$

$A_1, A_4, A_6$  komponente nespremenljivih sil;  
 $B_1, B_4, B_6$  stalnice, ki določajo linearno razmerje med silami in ustreznimi hitrostmi;  
 $D_1, D_4, D_6$  amplitudo komponent harmoničnih sil;  
 $\omega$  kotna frekvenc;a;  
 $\alpha_1, \alpha_4, \alpha_6, \alpha_5$  faze.

$A_1, A_4, A_6$  constant force components;  
 $B_1, B_4, B_6$  constants defining the linear relationship between the forces and the appropriate velocities;  
 $D_1, D_4, D_6$  amplitudes of the harmonic force components;  
 $\omega$  angular frequency;  
 $\alpha_1, \alpha_4, \alpha_6, \alpha_5$  phases.

Da bi ocenili delovanje sistema, moramo upoštevati osnovne značilke, na primer delo ali moč, gonalne sile, silo koristnega upora itn.

Glede na sliko 1 je delo gonilnih sil opisano kot:

$$A_m = \int_0^{H_z} P_l dz_1 = \int_0^T P_l \dot{z}_1 dt \quad (6)$$

$T$  - čas integracije;

$H_z$  - značilna razdalja opravljena v času  $T$ .

Dejansko delo je podano z naslednjim izrazom:

$$A_u = \int_0^{H_z} P_6 dz_6 = \int_0^T P_6 \dot{z}_6 dt \quad (7)$$

Izkoristek je podan z naslednjim izrazom:

$$\eta = \frac{A_u}{A_m} = \frac{\int_0^T P_6 \dot{z}_6 dt}{\int_0^T P_l \dot{z}_1 dt} \quad (8)$$

Nepravilnost hitrosti gibanja je podana z naslednjim izrazom:

$$\vartheta_z = \frac{\dot{z}_{\max} - \dot{z}_{\min}}{\bar{z}} \quad (9)$$

$$\bar{z} = \frac{\dot{z}_{\max} + \dot{z}_{\min}}{2} \quad (10)$$

Z vnosom nove spremenljivke dobimo naslednje:

$$x_i = \frac{z_i}{l} \quad (i=1,\dots,6); \quad p = \sqrt{\frac{c_{12}}{m}}; \quad \tau = pt; \quad ' = \frac{d}{dt}; \quad v = \frac{\omega}{p}; \quad 2h_{rs} = \frac{H_{rs}}{pm} \quad (rs=12,23,45); \quad N' = \frac{N}{p^2 ml}; \quad \mu = \frac{M}{m}; \quad \mu_3 = \frac{m_3}{m};$$

$$F_j = \frac{P_j}{p^2 ml} = \frac{P_j}{c_{12} l} \quad (j=1,4,6); \quad a_j = \frac{A_j}{c_{12} l}; \quad b_j = \frac{B_j}{pm}; \quad d_j = \frac{D_j}{c_{12} l}; \quad d_s = \frac{D_s}{l}; \quad \delta_{23} = \frac{c_{23}}{c_{12}}; \quad \delta_{45} = \frac{c_{45}}{c_{12}}$$

$l$  - dolžina jermenja;

$p$  in  $\tau$  sta novi spremenljivki.

Če upoštevamo novo spremenljivko (11), diferencialne enačbe gibanja (1) sprememimo takole:

$$2h_{12}(x'_1 - x'_2) + (x_1 - x_2) = F_1,$$

$$x''_2 - 2h_{12}(x'_1 - x'_2) - (x_1 - x_2) + 2h_{23}(x'_2 - x'_3) + \delta_{23}(x_2 - x_3) = 0$$

$$\mu_3 x''_3 - 2h_{23}(x'_2 - x'_3) - \delta_{23}(x_2 - x_3) + [2h_{45}(x'_4 - x'_5) + \delta_{45}(x_4 - x_5)] \cdot [f_0 \operatorname{sign}(x'_3 - x'_6)] + f(x'_3 - x'_6) = 0 \quad (12),$$

$$\mu x''_6 - [2h_{45}(x'_4 - x'_5) + \delta_{45}(x_4 - x_5)] f_0 \cdot \operatorname{sign}(x'_3 - x'_6) - f(x'_3 - x'_6) = -F_6$$

$$x''_4 + 2h_{45}(x'_4 - x'_5) + \delta_{45}(x_4 - x_5) = -F_4$$

$h_{12}, h_{23}, h_{45}$  so koeficienti dušenja

Če upoštevamo novo spremenljivko (11), diferencialne enačbe gibanja (2) sprememimo takole:

$h_{12}, h_{23}, h_{45}$  - coefficients of damping.

Considering the new variable (11), the differential equations of movement (2) are converted to the type:

$$2h_{12}(x'_1 - x'_2) + (x_1 - x_2) = F_1$$

$$x''_2 - 2h_{12}(x'_1 - x'_2) - (x_1 - x_2) + N' f_0 \operatorname{sign}(x'_2 - x'_6) + f(x'_2 - x'_6) = 0 \quad (13).$$

$$\mu x''_6 - N' f_0 \operatorname{sign}(x'_2 - x'_6) - f(x'_2 - x'_6) = -F_6$$

$$x''_5 + F_4 = N'$$

Nato enačbo (3) sprememimo:

Furthermore, Equation (3) is converted to the type:

$$f = f_1 [2h_{45}(x'_4 - x'_5) + \delta_{45}(x_4 - x_5)] \quad (14).$$

Zunanje vzbujanje (5) v neparametričnem izrazu vodi v naslednje:

The external excitation (5) in the non-parametric expression leads to:

$$\begin{aligned}
 F_1 &= a_1 + b_1 x'_1 + d_1 \sin(\nu\tau + \alpha_1) \\
 F_4 &= a_4 + b_4 x'_4 + d_4 \sin(\nu\tau + \alpha_4) \\
 F_6 &= a_6 + b_6 x'_6 + d_6 \sin(\nu\tau + \alpha_6) \\
 x_5 &= d_5 \sin(\nu\tau + \alpha_5)
 \end{aligned} \tag{15},$$

kjer je  $\nu = \omega/p$ .

Izkoristek je podan z naslednjim izrazom:

here  $\nu = \omega/p$ .

The efficiency is given by the expression:

$$\eta = \frac{A_u}{A_m} = \frac{\int_0^T F_6 x'_6 d\tau}{\int_0^T F_1 x'_1 d\tau} \tag{16}.$$

Nepravilnost hitrosti gibanja je podana takole:

The irregularity of the motion's velocity is given by the expression:

$$\delta x'_s = \frac{x'_{s\max} - x'_{s\min}}{\bar{x}'_s} \quad (s = 1, 2, 6) \tag{17},$$

$$\bar{x}'_s = \frac{x'_{s\max} + x'_{s\min}}{2} \tag{18}.$$

## 2 ANALIZA DINAMIČNIH POJAVOV V DELOVANJU SKLOPA VALJEV IN JERMENA PRI MEHANIZMU RTM, KADAR NANJE NE VPLIVA VIBRACIJSKO VZBUJANJE

Namen te raziskave je definiranje dela, ki ga opravi sklop valjev in jermena pri mehanizmu RTM v odsočnosti vibracijskega vzbujanja.

Raziskava je opravljena na nezdrsnem območju (NZ) upoštevajoč parametre mehanizma. Nezdrsnost je okoliščina, v kateri se telesa raziskovanega mehanizma pomikajo skupaj brez zdrsovanja, tj.  $x'_1 = x'_2 = x'_6$  (sl. 2 do 7):

$$d_1 = d_4 = d_5 = d_6 = 0 \tag{19},$$

kakor se to dogaja v obravnavanem primeru. Raziskava analizira dinamične pojave, ki potekajo v mehanizmu valjev in jermena v sistemu natančnega valja, tj. v jermenskem mehanizmu z nedeformirajočim stikom med telesi.

Značaj dinamičnih pojavov v mehanizmu valjev in jermena z deformirajočim stikom med telesi v enakomerinem gibanju je analogen pojavom, ki so v primeru nedeformirajočega stika. Iz krivulj diagrama zato lahko določimo razmerja med enakomernim gibanjem in njegovimi parametri. Pod vsakim diagramom so v oklepaju prikazani parametri sistema z deformirajočim stikom med telesi.

Glede na sliko 2 pri definirani vrednosti  $a_4$  hitrosti  $x'_1$ ,  $x'_2$  in  $x'_6$  proučevanih teles postanejo istovetne, kar pomeni, da telesa ne zdrsijo v tolikšni meri, da bi se znatno povečal koeficient suhega trenja

## 2 THE ANALYSIS OF DYNAMIC PROCESSES OCCURRING IN THE "ROLLER-BAND" SYSTEM OF THE RTM, NOT INFLUENCED BY THE EXCITATION OF VIBRATIONS

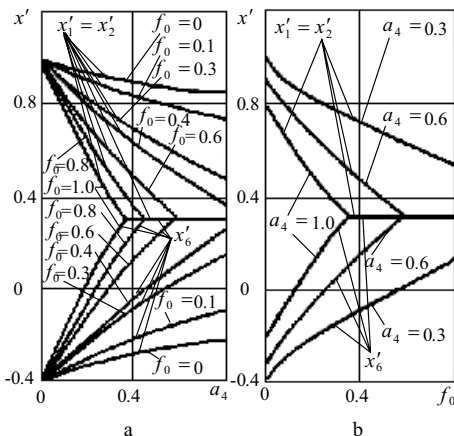
The purpose of the research is to define the work of the "roller-band" system of the RTM in the absence of vibrating excitation.

It is presented in the research of a non-slipping zone of bodies (NZ), depending on the parameters of the system. The non-slipping zone is understood as the condition when the bodies of the investigated system are moving together without slipping, i.e.,  $x'_1 = x'_2 = x'_6$  (Figs. 2 to 7):

as in the considered case. It is presented as research of the dynamic processes occurring in the "roller-band" system of a precision roller, i.e., band mechanisms with a non-deforming contact between the bodies.

The character of the dynamic processes occurring in the "roller-band" system with a deforming contact between the bodies in steady motion is analogous to the processes occurring in this system with a non-deforming contact. Furthermore, from the graphical curves we can determine the relations of steady motion with its parameters. In brackets, under the figures, the parameters of the system with a deforming contact between the bodies are indicated.

According to Fig. 2, at a defined value  $a_4$ , the velocities  $x'_1$ ,  $x'_2$  and  $x'_6$  of the investigated bodies become identical, i.e., the bodies do not slip between themselves at a sufficient increase of the coefficient of



Sl. 2. Grafa kažeta odvisnost hitrosti teles sistema pri enakomernem gibanju od parametrov gibanja

Fig. 2. Graphs showing the dependence of the velocity of bodies of a system in steady motion on the parameters of motion

$$\begin{aligned} a_1 &= 0,5; a_6 = -0,2; b_1 = b_6 = -0,5; 2h_{12} = 0,2; \\ \mu &= 1,0; f_1 = 0,1 (2h_{23} = 2h_{45} = 2,0; \delta_{23} = \delta_{45} = 10; \\ \mu_3 &= 0,01; b_4 = -0,5) \end{aligned}$$

$f_0$  (sl. 2 a). Spoznali bomo, da večja ko je vrednost  $a_4$  pri  $f_0 = \text{konst.}$ , hitreje nastane nezdrsno območje med telesi (sl. 2 b). To pokaže tudi slika 3.

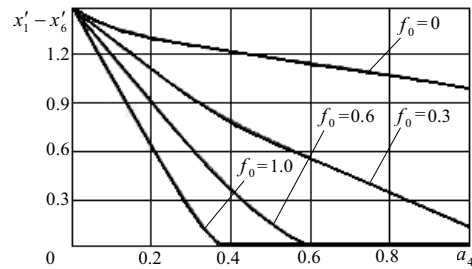
Tako je, pri definirani vrednosti  $f_0$ , zvečanje vrednosti  $a_4$  pomembno le, dokler se približuje vrednosti NZ. Ko pa to vrednost doseže, izgubi pomen, saj se telesa zdaj začnejo gibati z enakimi hitrostmi (sl. 2 in 3).

S povečanjem  $a_4$ , pri koeficientu suhega trenja  $f_0 = \text{konst.}$ , NZ postane definirana vrednost  $a_4$  ne glede na koeficient viskoznega trenja  $f_1$  (sl. 4 a). Pri dani vrednosti  $a_4$  povečana vrednost  $f_1$  povzroči le rahlo zmanjšanje hitrosti  $x'_1$  (krivulje odvisnosti v diagramu postanejo bolj izbočene) (sl. 5 b); vendar pa NZ, pri dani vrednosti  $f_0$ , postane definirana vrednost  $a_4$ , hitrosti  $x'_1, x'_2, x'_6$  pa se izenačijo (sl. 4 a in b).

Pri definirani vrednosti  $a_4$  se hitrosti  $x'_1, x'_2, x'_6$  obravnavanih teles izenačijo, hkrati pa se zmanjša vrednost  $a_1$ , kar pomeni, da manjša ko je vrednost  $a_1$ , večje je nezdrsno gibanje med telesi (sl. 5 a). Pri  $a_1 = \text{konst.}$  se zdrsovjanje teles zmanjša ob povečanju  $a_4$  (sl. 5 b). Krivulje odvisnosti na sliki 5 se ostro prelomijo ob vstopu v NZ.

Če je  $a_6 = \text{konst.}$  in se vrednost  $a_4$  zveča, se poveča hitrost nastanka pojava NZ. Če je  $a_4 = \text{konst.}$ , se navor nezdrsnosti med telesi pojavi ob povečanju  $a_6$  do svoje določene vrednosti (sl. 6 a in b).

V času povečevanja  $a_6$  se povečajo tudi hitrosti  $x'_1 = x'_2 = x'_6$  (Sl. 6 a); kljub temu je pojav NZ



Sl. 3. Graf kaže odvisnost hitrosti zdrsovjanja med telesi sistema pri enakomernem gibanju od parametrov gibanja

Fig. 3. The graph showing the dependence of the velocity of slipping between bodies of a system in steady motion on the parameters of motion  
 $a_1 = 0,5; a_6 = -0,2; b_1 = b_6 = -0,5; 2h_{12} = 0,2;$   
 $\mu = 1,0; f_1 = 0,1 (2h_{23} = 2h_{45} = 2,0; \delta_{23} = \delta_{45} = 10;$   
 $\mu_3 = 0,01; b_4 = -0,5)$

dry friction,  $f_0$  (Fig. 2 a). It will be clear that the greater the value  $a_4$  at  $f_0 = \text{const.}$ , the faster it makes a non-slipping zone of the bodies (Fig. 2 b). Fig. 3 also shows this.

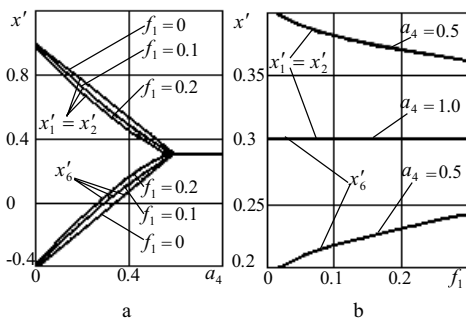
Furthermore, at a defined value,  $f_0$ , the increasing value of  $a_4$  is meaningful only up to NZ. After reaching this value it loses sense, as the bodies start to move with an identical velocity (Fig. 2 and 3).

With increasing  $a_4$  at the coefficient of dry friction  $f_0 = \text{const.}$ , NZ becomes a definite value  $a_4$ , irrespective of the coefficient of viscous friction,  $f_1$  (Fig. 4 a). The increasing  $f_1$  resulted only in a minor decrease of the velocities  $x'_1$  at a given data  $a_4$  (the dependence curves in the figure have a more convex character) (Fig. 5 b); however, NZ at a given data  $f_0$  becomes a defined value  $a_4$ , and the velocities  $x'_1, x'_2, x'_6$  become equal (Fig. 4 a and b).

At a defined value  $a_4$  the velocities  $x'_1, x'_2, x'_6$  of the investigated bodies level off, with a decreasing of value  $a_1$ , i.e., the smaller is  $a_1$ , the faster the non-slipping movement between the bodies comes (Fig. 5 a). At  $a_1 = \text{const}$  the slipping of the bodies decreases with an increase of  $a_4$  (Fig. 5 b). The curves of dependences in Fig. 5 break sharply when going into NZ.

If  $a_6 = \text{const}$  and value  $a_4$  increases, NZ becomes faster. If  $a_4 = \text{const}$ , the moment of non-slipping between the bodies comes with an increase of  $a_6$  up to its definite value (Fig. 6 a and b).

During the increase of  $a_6$  the velocities of bodies  $x'_1 = x'_2 = x'_6$  are increased (Fig. 6 a); however,



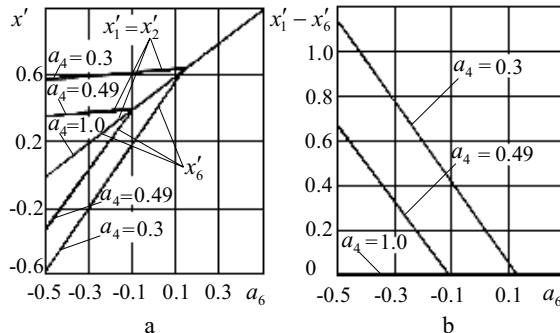
Sl. 4. Grafa kažeta odvisnost hitrosti teles sistema pri enakomernem gibanju od parametrov gibanja  
Fig. 4. Graphs of the dependence of the velocity of the bodies of a system in steady motion on the parameters of motion

$$\begin{aligned} a_1 &= 0,5; a_6 = -0,2; b_1 = b_6 = -0,5; 2h_{12} = 0,2; \\ \mu &= 1,0; f_0 = 0,6 (2h_{23} = 2h_{45} = 2,0; \delta_{23} = \delta_{45} = 10; \\ \mu_3 &= 0,01; b_4 = -0,5) \end{aligned}$$

mogoč, in sicer pri zmanjšani vrednosti  $a_4$  (Sl. 7 a). Če je  $a_4 = \text{konst.}$ , NZ nastane ob povečanju  $f_0$ , v nasprotnem primeru pa, ko je  $f_0 = \text{konst.}$ , NZ nastane ob povečanju  $a_4$  (Sl. 7 b).

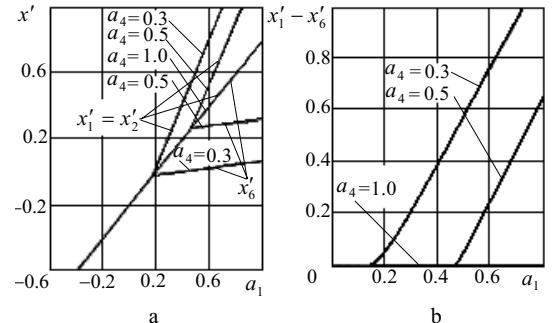
Glede na sliko 7 povečanje  $a_4$  in  $a_6$  povzroči nezdrsno območje med telesi. Pri definirani vrednosti  $a_6$  naraščanje vrednosti  $a_4$  po vstopu teles v območje NZ nima več pomena, ker se telesa zdaj gibljejo z enakimi hitrostmi. Na spodnjih slikah je območje NZ šrafirano.

Poudariti je treba, da je  $f_0 a_4 = \text{konst.}$



Sl. 6. Grafa kažeta odvisnost hitrosti teles sistema pri enakomernem gibanju od parametrov gibanja  
Fig. 6. Graphs of the dependence of the velocity of the bodies of a system in steady motion on the parameters of motion

$$\begin{aligned} b_1 &= b_6 = -0,5; 2h_{12} = 0,2; f_0 = 0,6; f_1 = 0,1 \\ (2h_{23} &= 2h_{45} = 2,0; \delta_{23} = \delta_{45} = 10; \mu_3 = 0,01; b_4 = -0,5; \\ a_1 &= 0,5) \end{aligned}$$



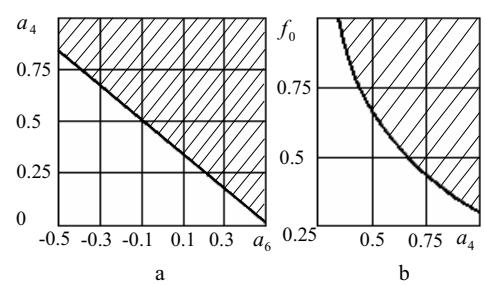
Sl. 5. Grafa kažeta odvisnost hitrosti teles sistema pri enakomernem gibanju od parametrov gibanja  
Fig. 5. Graphs of the dependence of the velocity of the bodies of a system in steady motion on the parameters of motion

$$\begin{aligned} b_1 &= b_6 = -0,5; 2h_{12} = 0,2; f_0 = 0,6; f_1 = 0,1; a_6 = -0,2 \\ (2h_{23} &= 2h_{45} = 2,0; \delta_{23} = \delta_{45} = 10; \mu_3 = 0,01; b_4 = -0,5) \end{aligned}$$

the coming of NZ is possible, and at a smaller value of  $a_4$  (Fig. 7 a). At  $a_4 = \text{const}$  NZ comes with increasing  $f_0$  and, in contrast, at  $f_0 = \text{const}$  with increasing  $a_4$ , we achieve NZ (Fig. 7 b).

According to Fig. 7, the increasing  $a_4$  and  $a_6$  resulted in a non-slipping between the bodies. At a defined value  $a_6$  the increasing value of  $a_4$  after the arrival of the bodies in NZ has no sense, because they are moving with identical velocities. NZ is hatched.

It is necessary to point out that  $f_0 a_4 = \text{const.}$



Sl. 7. Področja obstoja menjavajočih se enakomernih rezimov gibanja teles, odvisnih od parametrov gibanja  
Fig. 7. The areas of existence of varying steady regimes of motion of a system of bodies depending on its parameters

$$\begin{aligned} a_1 &= 0,5; b_1 = b_6 = -0,5; f_1 = 0,1; 2h_{12} = 0,2 \\ (2h_{23} &= 2h_{45} = 2,0; \delta_{23} = \delta_{45} = 10; \mu_3 = 0,01; b_4 = -0,5; \\ a_1 - f_0 &= 0,6; b_1 - a_6 = -0,2) \end{aligned}$$

### 3 ANALIZA DINAMIČNIH POJAVOV V DELOVANJU SKLOPA VALJEV IN JERMENA, KADAR NANJE VPLIVA VIBRACIJSKO VZBUJANJE

Namen te raziskave je definiranje razmer pri delu, ki ga opravi sklop valjev in jermen, kar omogoči nadzor nad pojavom NZ med telesi sistema z vibracijskim vzbujanjem.

Analiziramo delovanje sklopa valjev in jermen pri mehanizmu RTM, na katerega vplivamo z vibriranjem, tj. z ustvarjanjem naslednjega pogoja:  $d_1, d_2, d_3, d_4 \neq 0$ .

Da bi zagotovili pojav NZ, moramo povečati  $f_0$  (pri tem je  $v = \text{konst.}$ ), kar omogoči zmanjšanje vrednosti  $a_4$ , povečanje vrednosti  $v$  (pri čemer je  $f_0 = \text{konst.}$ ) pa povzroči neznatno zmanjšanje vrednosti  $a_4$  (sl. 8 a).

Če na sistem ne vplivamo z vibracijami, kar pomeni, da je  $d_4 = 0$ , NZ, in je  $f_0 = \text{konst.}$ , ima  $a_4$  manjši pomen kakor sicer (sl. 8 a in b).

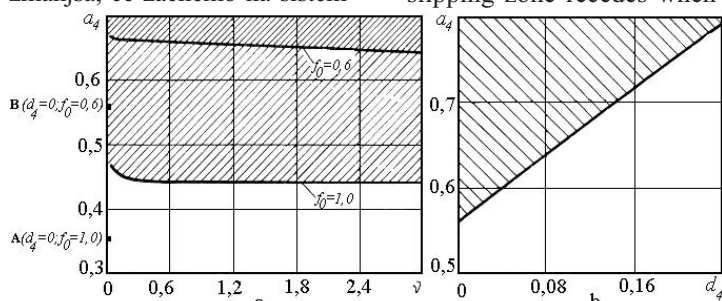
Slednje lahko razložimo z zmanjšanjem sile trenja v primeru, ko vibracije delujejo na sistem in nastane območje NZ, ki ima povečane vrednosti  $a_4$ . Večja ko je amplituda vzbujajočih vibracij  $d_4$ , večja mora biti vrednost  $a_4$ , kar je potrebno za zagotovitev območja NZ (sl. 8 b).

Vrednost povprečne hitrosti  $\bar{x}_1'$  se zveča, medtem ko se vrednost  $\bar{x}_6'$  zmanjša s povečanjem amplitude vibracijskega vzbujanja  $d_5$ ; koeficient izkoristka  $\eta$  se tako strmo zmanjša (sl. 9).

Dogajanje lahko razložimo z zmanjšanjem sile trenja med telesi, zaradi česar se poveča zdrsno območje, posledično pa se zniža vrednost  $h$ .

Pri dejanski konstrukciji mehanizma RTM lahko moč sile trenja nadziramo z uporabo vibracij (sl. 10).

Kakor je razvidno iz dosedanja raziskave, se nezdrsnobno območje zmanjša, če začnemo na sistem



Sl. 8. Polja gibanja teles v različnih razmerah, odvisnih od parametrov vibracijskega vzbujanja

Fig. 8. Fields of movements of bodies in different types of conditions, depending on the parameters of the exciting vibrations

$$a_1 = 0,5; a_6 = -0,2; b_1 = b_6 = -0,5; f_1 = 0,1; x_1' = x_2' = x_6' = 0,3; a) d_4 = 0,1; b) f_0 = 0,6; v/2\pi = 0,5.$$

### 3 THE ANALYSIS OF THE DYNAMIC PROCESSES OCCURRING IN THE "ROLLER-BAND" SYSTEM, INFLUENCED BY THE EXCITATION OF VIBRATIONS

The purpose of the research is to define the conditions of work of the "roller-band" system, ensuring an opportunity to control the NZ between bodies of the system by the excitation of vibrations.

The case is investigated for the "roller-band" system of RTM when it is influenced by vibrations, i.e.,  $d_1, d_2, d_3, d_4 \neq 0$ .

To ensure NZ, it needs to increase  $f_0$  (having  $v=\text{const.}$ ), which ensures the decrease of  $a_4$ , and the increase of  $v$  (having  $f_0=\text{const.}$ ) ensures the non-considerable decrease of  $a_4$  (Fig. 8 a).

If the system is not influenced by vibrations, i.e.,  $d_4=0$ , NZ, when the meanings of  $f_0=\text{const.}$  it will appear to have fewer meanings of  $a_4$  (Fig. 8 a and b).

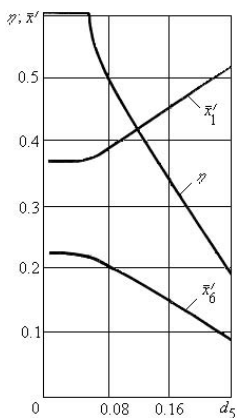
This can be explained by the friction force decreases in the case of vibrations influencing the system and NZ is reached, having greater meanings of  $a_4$ . The greater the amplitude of the exciting vibrations  $d_4$ , the greater must be the meaning of  $a_4$ ; which is necessary to ensure NZ (Fig. 8 b).

The value of the average velocity  $\bar{x}_1'$  increases, and  $\bar{x}_6'$  decreases with the increase of the amplitude of the vibrating excitations  $d_5$ ; the coefficient of efficiency,  $\eta$ , thus sharply decreases (Fig. 9).

It is explained in such a way that the force of friction between the bodies of the system decreases, owing to which the slipping zone of the bodies is increased, and consequently the value of  $\eta$  decreases.

In the real construction of an RTM we can control the magnitude of the friction force with the vibrations (Fig. 10).

As can be seen from this material, the non-slipping zone recedes when the influence of the



Sl. 9. Prikaz odvisnosti povprečnih hitrosti gibanja teles in izkoristka od parametrov vibracijskega vzbujanja, ko je  $f_0 = 1,0$

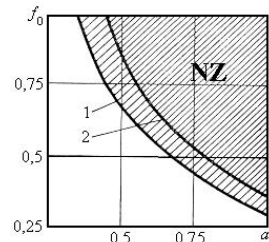
Fig. 9. The diagram of the dependence of the average velocities of the movement of the bodies and the efficiency on the parameters of the vibrating excitation at  $f_0 = 1,0$

vplivati z vibracijami. To pomeni, da je v dejanskem sistemu mogoče nadzirati zdrsovanje med elementi mehanizma RTM, tj. nadzirati navor odpornosti za gibanje. To je pomembno, kadar oblikujemo konstrukcije RTM, saj lahko tako zagotovimo boljšo kakovost in natančnost ter ustvarimo bolj natančne dinamične značilke.

#### 4 ANALIZA DINAMIČNIH POJAVOV MEHANIZMA RTM

Meritve vibracij v mehanizmu RTM so težavna naloga, toda ne le zaradi majhne amplitude vibracij v valjih, ampak predvsem zaradi dejstva, da poleg vibracij zabeležimo tudi njihove številne medsebojne vplive. Ti nastanejo zaradi vibriranja podstavka in geometrične nenatančnosti izdelave posameznih delov mehanizma; ti vplivi se najpogosteje pojavljajo naključno.

Veliko pozornosti namenjamo razvoju metod meritev vibracij in izločevanju vplivov. Metode stične raziskave so omejene, ker vplivi pogosto popačijo rezultate beleženja in tako znatno vplivajo na izid poizkusa. Precej obetavne pa so nestične optične metode meritev, ki v polni meri izpolnjujejo zahteve poizkusov, tj. potrebe po nestičnih, zelo natančnih meritvah in veliki ločljivosti. Te metode so bile uporabljeni v analizi značilk vibriranja v valjih mehanizma RTM.



Sl. 10. Teoretična raziskava poenostavljenega dinamičnega modela RTM z valjema in jermenom

Fig. 10. Theoretical investigation of the simplified dynamic model of RTM "roller-band" system

$$\begin{aligned} a_1 &= 0,5; a_6 = -0,2; b_1 = b_6 = -0,5; f_1 = 0,1; \\ x_1' &= x_2' = x_6' = 0,3; 2h_{12} = 0,2; 2h_{23} = 2h_{45} = 2,0; \\ \delta_{23} &= \delta_{45} = 10; \mu = 1,0, \mu_3 = 0,01; \end{aligned}$$

Sistem: 1 – vibriranje ni aktivirano ( $d_4 = 0$ );  
2 – vibriranje je aktivirano ( $d_4 = 0,1$ ;  $v/2\pi = 0,1$ ), NZ je šrafirano

The system: 1 - vibrations do not influence ( $d_4 = 0$ ), 2 - vibrations influence ( $d_4 = 0,1$ ;  $v/2\pi = 0,1$ ), NZ is hatched

system by vibrations starts. This means that in a real system it can be possible to control the slipping-by between the elements of the RTM, i.e., control of the moment of resistance to motion. This is important when designing the constructions of the RTM, which ensures higher quality and precision and more precise dynamic characteristics.

#### 4 RESEARCH OF THE DYNAMIC PROCESSES RUNNING IN THE RTM ROLLER-BAND SYSTEM

The measurement of vibrations in Rolamite-type mechanisms is quite a complicated task, not only because of the small amplitude of vibrations in the rollers, but mainly because of the fact that along with vibrations there is plenty of interference registered. This arises because of the vibration of the base, the geometrical imprecision of the produced parts, and most often the interference is random.

Much attention is paid to the development of the methods of measuring the vibrations and the separation of interference. The methods of contact research are limited, because the interference quite often distorts the results of the registration and significantly influences the results of the experiment. Quite promising are the non-contact optical methods of measurement, which fully meet the demands of the experiment, i.e. non-contact, high-precision measurements, high dimensional resolution. These methods were used in the research of the characteristics of vibration in the RTM rollers.

Raziskana sta bila dva tipa vibrirajočih valjev mehanizma RTM (sl. 11).

Ko elektrode piezokeramičnega obroča pritrjenega valja št. 1 (Sl. 11 a), ki je ovit z gibkim jermenom, sprejmejo visokofrekvenčni električni signal, valj začne vibrirati. Dejansko področje stika med gibkim jermenom, ki ovija valj 1, in piezokeramičnim obročem 2, ki obdaja elastični torni obroč 3, se zmanjša in pojavi se plast vibracij. Valj 1 je namenjen zmanjšanju trenja v napravah, ki vključujejo mehanizem RTM. Os valja 1 je čvrsto pritrjena na osovo, tako da se valja mehanizma RTM ne kotalita po gibkem jermenu, ampak drsita.

Eksperimentalni valj št. 2 (sl. 11 b) je namenjen zmanjšanju trenja v napravah, ki vključujejo mehanizem RTM. Toda valja takšnega mehanizma se kotalita po gibkem jermenu.

Valj (sl. 11 b) je sestavljen iz osi 1, ki je čvrsto pritrjena na osovo, ter iz piezokeramičnega obročastega elementa, ki je montiran na os. Na notranjo stran piezokeramičnega obroča 2 je pritrjen elastični torni obroč 3, ki je v stiku z osjo 1; z zunanje strani pa je obroč 2 prekrit s togim obročastim pokrovom, ki je čvrsto pritrjen na obroč in je v stiku z ovijajočim gibkim jermenom. Vibracije valja med montiranim obročnim piezokeramičnim elementom, elastičnim tornim obročem 3 in pritrjeno togo osjo 1 ustvarjajo tlačeno plinasto plast (PGF).

Raziskali smo vibracije valjev v prečni smeri ter v primerih obremenitve in neobremenitve (sl. 12).

V primeru obremenitve je valj ovit z gibkim jermenom pod kotom od  $\pi/4$  do  $3/2 \pi$ . En konec jermenja je pritrjen na togo osovo, utež pa je pritrjena na drugi konec jermenja. Kakor je očitno iz izvedenega preizkusa, se amplituda in

Two types of RTM vibrating rollers were explored (Fig. 11).

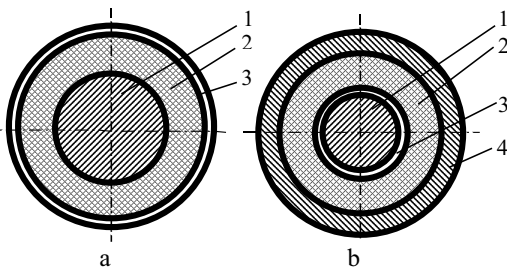
When the electrodes of the piezoceramic ring of the fixed RTM roller No 1 (Fig. 11 a) wrapped by a flexible band receive a high-frequency electric signal, the roller starts to vibrate. The actual area of the contact zone between the flexible band wrapping the roller 1 and the piezoceramic ring 2 wrapping the elastic frictional ring 3 reduces and the film of vibrations occurs. The roller 1 is intended to reduce the friction in devices containing an RTM. The axis of the roller 1 is fixedly attached to the base, and the rollers of the RTM do not roll on the flexible band, but slip.

The experimental roller No 2 (Fig. 11 b) is intended to reduce the friction in devices containing an RTM. But the rollers of such an RTM roll on the flexible band.

The roller (Fig. 11 b) consists of an axis 1, fixedly attached to the base, and of an assembled piezoceramic ring element that is put on it. It is made of a piezoceramic ring 2, in which the internal side of an elastic frictional ring 3 is fixed; this contacts axis 1, and on the outside ring 2 is wrapped by a rigid ring-like cover 4, attached to it fixedly, which in turn contacts with the wrapping flexible band. A vibrations-pressed gas film (VPGF) is produced by vibrations of the roller between the covering assembled ring-like piezoceramic element elastic frictional ring 3 and the fixed rigid axis 1.

The vibrations of the rollers in a radial direction in the loaded and unloaded functioning modes were investigated (Fig 12).

In the loaded mode, the roller is wrapped by the flexible band at angles from  $\pi/4$  to  $3/2 \pi$ . One end of the band is fixed to the rigid basis, and a weight is fixed on the other end of the band. As is obvious from the data of the performed experiment, the amplitude and resonant frequency of the roller vibrations,



Sl. 11. Vibrirajoča valja mehanizma RTM: a – pritrjeni valj (1); b – vrteči se valj (2); 1 – os, ki je trdno pritrjena na osovo; 2 – piezokeramični obroč; 3 – elastični torni obroč; 4 – tesno prilegajoči se obročasti pokrov, ki ga ovija gibki jermen

Fig. 11. RTM vibrating rollers: a – fixed (1); b – rotating (2); 1 – axis, fixedly attached to the base; 2 – piezoceramic ring; 3 – elastic frictional ring; 4 – tight ring-like cover, wrapped by a flexible band

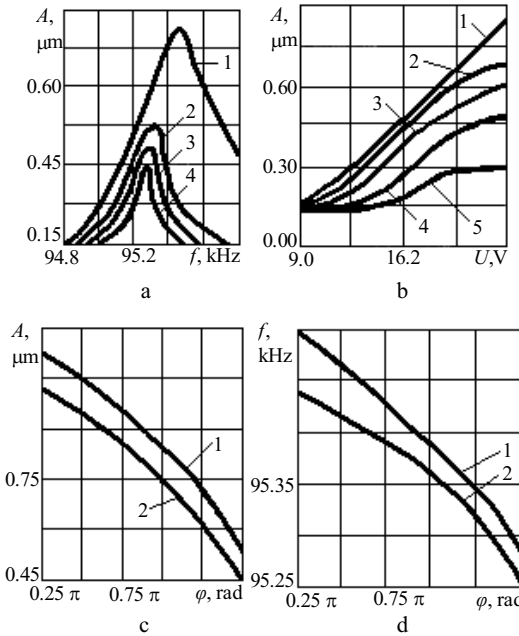
resonančna frekvenca vibracij valja ovitega z jermenom pod enakima kotoma in z različno obremenitvijo, zmanjšata s povečanjem ravnih bremena jermenja (sl. 12 a).

Ko analiziramo odvisnost amplitudne vibracije valja od električne moči z nespremenljivo resonančno frekvenco in različno stopnjo obremenitve jermenja, lahko ugotovimo, da se amplituda vibracij valja zmanjša, če se obremenitev jermenja poveča (sl. 12 b). Kadar je obremenitev jermenja majhna, je odvisnost amplitude vibracij valja skoraj linear. Če je dovedena napetost povečana, se poveča tudi amplituda vibracij.

Iz grafov (sl. 12 c in d), ki opisujeta odvisnost sprememb amplitude in frekvence vibracij valja od kota, pod katerim jermenje ovija valj pri različnih ravneh obremenitve, lahko povzamemo, da se amplituda in frekvenca zmanjšata, če se kot ovijajočega jermenja poveča.

Krivulje eksperimentalne raziskave valja št. 2 so prikazane na sliki 13.

Značilnosti frekvenčne amplitudne vibracije valja št. 2, ki se sestoji iz piezokeramičnega obroča piezokeramičnega elementa 2 z dejavočo (notranjo)



Sl. 12. Krivulje eksperimentalne raziskave vibrirajočega valja 1, ovitega s tesno prilegajočim se (obremenjenim) jermenjem

Fig. 12. The curves of an experimental research of an RTM vibrating roller 1, wrapped by a tight (loaded) band:  
 a -  $A=f(f)$ , ko/if  $U = 40 \text{ V}$ ;  $\varphi=3/2\pi$ ; P je/is: 1 - 0 N; 2 - 0,5 N; 3 - 1,0 N; 4 - 2,0 N; b -  $A=f(U)$ , ko/if  $\varphi=\pi$ ; P je/is: 1 - 0,5 N; 2 - 1,0 N; 3 - 1,5 N; 4 - 2,0 N; 5 - 2,5 N; c -  $A=f(\varphi)$ , ko/if  $U = 40 \text{ V}$ ; P je/is: 1 - 1,0 N; 2 - 2,0 N; d -  $f=f(\varphi)$ , ko/if  $U = 40 \text{ V}$ ; P je/is: 1 - 1,0 N; 2 - 2,0 N

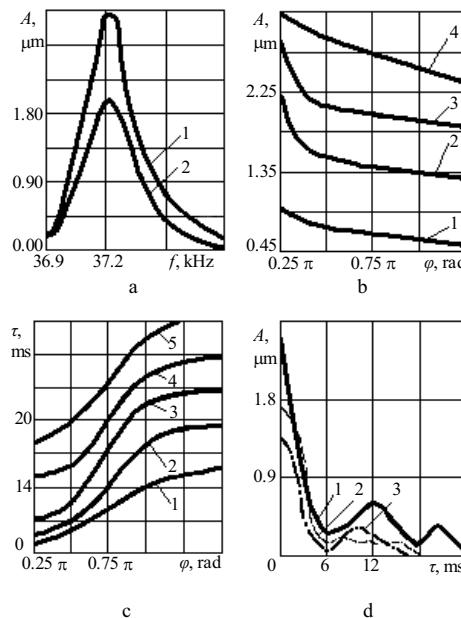
wrapped by a band at equal angles and with loads of different magnitude, diminish when increasing the level of load of the band (Fig.12 a).

When analyzing the dependence of the amplitude of the roller vibrations on the magnitude of the power-supply voltage, with a constant resonance frequency and a different level of load on the band, one can draw a conclusion, that if the load of the band is increased, the amplitude of the roller vibrations diminishes (Fig. 12 b). When the load on the band is small, the dependence of the amplitude of the roller vibrations is almost linear. If the power-supply voltage is increased, the amplitude of the roller vibrations increases as well.

From the graphs provided (Fig. 12 c and d), describing the dependence of the changes of amplitude and frequency of the roller vibrations on the angle of the roller wrapping band, with a different level of load applied, one may draw a conclusion that, if the wrapping angle of the band increases, the amplitude and frequency become reduced.

The curves of the experimental research of the RTM experimental roller No 2 are presented in Fig. 13.

The frequency amplitude vibration characteristics of the roller No 2, consisting of the piezoceramic ring of the piezoceramic ring element 2



Sl. 13. Krivulje eksperimentalne raziskave vibrirajočega valja 2, ovitega s tesno prilegajočim se (obremenjenim) jermenom: a -  $A = f(f)$  – valja za montirani piezokeramični obročasti element (sl. 2 b), ko je  $U = 60 \text{ V}$ ; 1 – velja za delovno površino piezokeramičnega obroča; 2 – velja za zunanjo površino togega obročastega pokrova 4

Fig. 13. The curves of an experimental research of RTM vibrating roller No 2, wrapped by a tight (loaded) band: a -  $A=f(f)$  for an assembled piezoceramic ring element (Fig. 2 b), when  $U = 60 \text{ V}$ ; 1 – for the working surface of the piezoceramic ring; 2 – for the outer surface of a rigid ring-like cover 4; b -  $A=f(\varphi)$ , ko/if  $P = 1,0 \text{ N}$ ;  $U$  je/is: 1 –  $10 \text{ V}$ ; 2 –  $20 \text{ V}$ ; 3 –  $30 \text{ V}$ ; 4 –  $40 \text{ V}$ ; c -  $\tau=f(\varphi)$ , ko/if  $U = 30 \text{ V}$ ;  $P$  je/is: 1 –  $0,5 \text{ N}$ ; 2 –  $1,0 \text{ N}$ ; 3 –  $1,5 \text{ N}$ ; 4 –  $2,0 \text{ N}$ ; 5 –  $3,0 \text{ N}$ ; d -  $A=f(\tau)$ , ko/if  $U = 40 \text{ V}$ ;  $\varphi=\pi$ ;  $P$  je/is: 1 –  $0 \text{ N}$ ; 2 –  $1,0 \text{ N}$ ; 3 –  $2,0 \text{ N}$

površino in togega obročastega pokrova 4 z delujočo zunanjo površino (sl. 11 b), so podane na sliki 13 a.

Iz krivulj je očitno, da je amplituda zunanja (škodljive) frekvence togega obročastega pokrova piezokeramičnega obročastega elementa 4 precej velika, če jo primerjamo z amplitudo delujoče površine piezokeramičnega obroča 2, kar pomeni, da vpliva na moč trenja med valjem 2 in ovijajočim se jermenom.

Slika 13 b kaže krivulje, ki opisujejo odvisnost amplitude montiranih piezokeramičnih obročastih elementov od kota, pod katerim gibki jermen ovija valj 2, z različno električno močjo. Iz krivulj lahko razberemo, da se s sprememboto kota ovijajočega se jermenoma od  $\pi/4$  do  $\pi/2$  amplituda frekvence znatno zmanjša. Če kot ovijajočega se jermenoma še nadalje povečamo do  $3/2 \pi$ , se amplituda frekvence, v skladu z zakonom sorazmerja, nekoliko zmanjša. Ko povečamo dovedeno električno napetost, se amplituda frekvence zveča v primeru vseh kotov, pod

working (internal) surface and a rigid ring-like cover 4 outer surface (Fig. 11 b) are given in Fig. 13 a.

It is obvious from the curves that the amplitude of the outer (parasitical) frequency of the rigid ring-like cover of the piezoceramic ring element 4 is quite high, if compared with the amplitude of the working surface of the piezoceramic ring 2, i.e., it affects the magnitude of the friction power between the roller 2 and that of the wrapping band.

Fig. 13 b displays curves describing the dependence of the amplitude of the assembled piezoceramic ring element on the angle of wrapping of the roller 2 by the flexible band with a different magnitude of power-supply voltage. One can see from the curves that as the wrapping angle changes from  $\pi/4$  to  $\pi/2$ , the amplitude of the frequency significantly reduces. When continuing to increase the wrapping angle up to  $3/2 \pi$ , the amplitude of the frequency reduces a little according to a linear law. When the power-supply voltage is increased, the amplitude of the frequency grows in all ranges of the angle of the

katerimi jermen lahko ovija valj. Ko povečamo kot obremenjenega gibkega jermenja, ki ovija valj 2, se podaljša čas nastajanja VPGF.

Do podobnega sklepa pridemo tudi v primeru, ko povečamo obremenitev jermenja in ko kot, pod katerim jermen ovija valj, ostane nespremenjen (sl. 13 c). Ko elektrodam piezokeramičnega obroča 2 ustavimo dovod energije, je trajanje dušenja VPGF odvisno od obremenitve jermenja, ki ovija valj (sl. 13 d). Bolj ko je jermen obremenjen, hitreje je udušen VPGF.

## 5 ANALIZA POJAVOV NADZORA TRENJA MED ELEMENTI MEHANIZMA RTM

Vibrirajoče elemente mehanizma RTM smo raziskali s stojalom za preizkuse, ki je bil oblikovan posebej za te raziskave. Njegova funkcija temelji na nadzoru koeficiente trenja med elementi mehanizma RTM (sl. 14).

Sila trenja  $F_{tr}$  vpliva na deformacije vzmeti 2, ko sila  $G_1$  vpliva na valja 3. Ogrodje 1 se giblje, to gibanje pa zaznata zaznavalo 8 in zapisovalna naprava 10. Ko so visokofrekvenčni električni signali poslanvi v elektrode valjev 3, ti začnejo vibrirati. Sila trenja se zmanjša za vrednost  $\Delta F_{tr}$  in pride do drsenja med valjema in jermenom (sl. 14).

Na oscilogramu 1 lahko ocenimo zmanjšanje sile trenja  $\Delta F_{tr}$ , ki ustreza gibanju ogrodja raziskovanega mehanizma RTM. Razdaljo premika  $s$  in čas gibanja  $t$  lahko ocenimo z oscilogramom 2, ki ustreza razdalji, na kateri se gibljeta valja. Očitno je, da raziskovalni preizkus (sl. 14, oscilogram 1) potrjuje pravilnost teoretičnega dela raziskave.

Analizirani so trije tipi valjev (sl. 15), od katerih dva tipa vključujeta vibrirajoče in pritrjene valje (sl. 15 a in b), tretji tip pa označuje vibrajoče in vrteče se valje (sl. 15 c).

Preizkuse smo izvedli z zveznim ter diskretnim napajanjem valjev z visokofrekvenčno napetostjo.

Preizkuse z zveznim signalom smo izvedli zato, da bi ugotovili odvisnosti sile trenja od amplitudo vibracij, od dobe dovanjanja električnih sunkov valju, od kota, pod katerim jermen ovija valj, od vlečne sile valja in od natezne sile jermenja.

Preizkuse z diskretnim krmilnim signalom pa smo izvedli zato, da bi ugotovili odvisnosti

band wrapping the roller. When increasing the angle of the loaded flexible band wrapping the roller 2, the duration of the VPGF formation increases.

A similar conclusion can be drawn when the load of the band is increased and when the wrapping angle stays the same (Fig. 13 c). When the power supply, which is connected to the electrodes of the piezoceramic ring 2, is switched off the duration of the damping of the vibrations-pressed gas film depends on the magnitude of the load of the band wrapping the roller (Fig. 13 d). The more the band is loaded, the more quickly the VPGF dampens.

## 5 RESEARCH OF THE PROCESSES OF FRICTION CONTROLLING BETWEEN THE ELEMENTS OF THE RTM

The RTM with vibrating elements was investigated with an experiment stand [8], especially designed for these investigations. Its function is based on controlling the coefficient of friction between the elements of the RTM (Fig. 14).

The friction force  $F_{tr}$  affects the deformations of the springs 2 when the force  $G_1$  influences the rollers 3. The frame 1 moves, and this movement is registered by sensor 8 and the registration device 10. When high-frequency electrical signals are sent to the electrodes of rollers 3, they start to vibrate. The frictional force decreases by the magnitude  $\Delta F_{tr}$ , and slipping between the rollers and the band appears (Fig. 14).

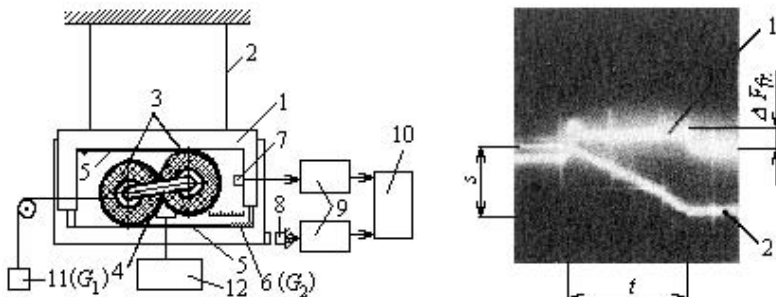
From the oscillogram 1 we can evaluate the decrease of the frictional force,  $\Delta F_{tr}$ , which conforms to the movement of the frame of the investigated RTM. The moved distance  $s$  and the movement time  $t$  can be evaluated from the oscillogram 2, which conforms to the distance of the movement of the rollers. It can be seen that experimental research (Fig. 14, oscillogram 1) confirms the correctness of the theoretical investigation.

Three types of rollers are explored (Fig. 15): two types of rollers are vibrating and fixed (Fig. 15 a and b), the rollers of the third type are vibrating and rotating (Fig. 15 c).

The experiments were performed by feeding the rollers with a high-frequency voltage in continuous and start-stop modes.

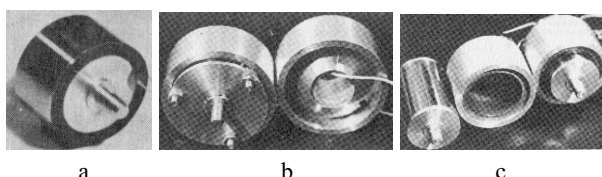
Experiments with the continuous signal mode were performed in order to find the frictional force dependencies on the amplitude of vibrations, on the period of feeding the electric impulses to the roller, on the wrapping angle of the roller by the band, on the pulling force of the roller, and on the force of stretching the band.

The start-stop experiments regulating the signal mode were carried out in order to find the dependencies of



Sl. 14. Eksperimentalno ogrodje za raziskovanje mehanizma RTM z vibrirajočima valjema (1 – ogrodje; 2 – ploska vzmjet; 3 – vibrirajoča valja; 4 – plošča; 5 – gibki jermen; 6 – utež (sila  $G_2$ ); 7,8 – elementa za zaznavanje gibanja; 9 – ojačevalnik signala; 10 – zapisovalna enota; 11 – utež (sila  $G_1$ ); 12 – visokofrekvenčni tok in značilni osciloskopogram gibanja ogrodja ter vibrirajočih valjev preučevanega mehanizma RTM

Fig. 14. The experimental stand for investigating RTM with vibrating rollers (1 – frame; 2 – flat spring; 3 – vibrating roller; 4 – plate; 5 – flexible band; 6 – weight (force  $G_2$ ); 7,8 – motion-sensing element; 9 – signal amplifier; 10 – registering unit; 11 – weight (force  $G_1$ ); 12 – high-frequency current and the characteristic oscilloscope pattern of movements of the frame and the vibrating rollers of the investigated RTM



Sl. 15. Vibrirajoči valji RTM: a - nepremični (1), glej sliko 11 a; b - nepremični (1) z valovnim vodilom; c - rotacijski (2), glej sliko 11 b

Fig. 15. RTM vibrating rollers: a – immovable (1), see Fig. 11 a; b – immovable (1) with a waveguide; c – rotary (2), see Fig. 11 b

dolžine premika  $s$  (razdalje, za katero se valj premakne v enem obdobju krmilnega sunka) od dolžine sunka  $t_{imp}$ ,  $-s = f(t_{imp})$ , od natezne sile jermenja  $G_1$ ,  $-s = f(G_1)$ , od vlečne sile valja  $G_2$ ,  $-s = f(G_2)$ , in od kota, pod katerim jermen ovija valja  $\alpha - s = f(\alpha)$ .

Iz grafa (sl. 16 a, krivulja 1) je razvidno, da je ob daljšem sunku  $t_{imp}$  daljša tudi razdalja  $s$ , ki jo naredita valja v enem obdobju krmilnega sunka.

Sila trenja  $F_r$  in čas  $t$  sta potrebna, da valja naredita razdaljo  $s$ , ko se vlečna sila jermenja  $G_2 = \text{konst.}$  zmanjšuje, če na valja vpliva večja amplituda dovedene napetosti in ju vleče večja sila  $G_1$  (sl. 16 b).

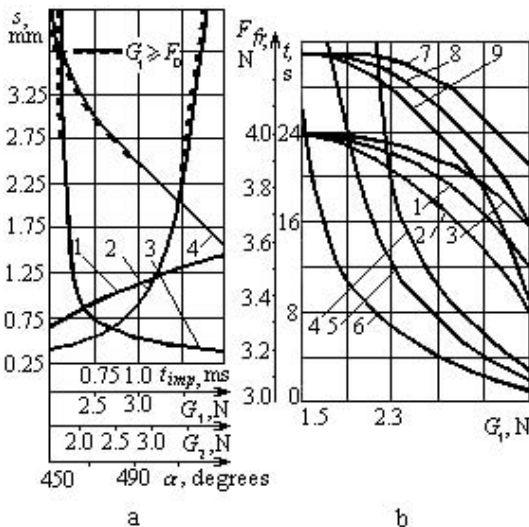
Del preizkusa smo izvedli tako, da smo vibrirajočim valjem energijo dovajali zvezno pri  $\alpha = 530^\circ$ ,  $G_2 = 2,0 \text{ N} = \text{konst.}$  Razdalja  $s$ , na kateri se premakneta valja v eni dobi krmilnega sunka, se poveča, kadar je povečana vlečna sila valja  $G_1$ . To je razvidno iz grafa (sl. 16 a, krivulja 2). Če je  $G_1 > F_0$  in je  $F_0$  zanemarljiva vrednost sile lepenja, se v primeru, ko je ta vrednost presežena, se valja začneta gibati

the roller skip length  $s$  (the distance covered by the roller in one period of regulating impulse) on impulse duration  $t_{imp}$ ,  $-s = f(t_{imp})$ , on the rollers' stretching force  $G_1$ ,  $-s = f(G_1)$ , on the band's pulling force  $G_2$ ,  $-s = f(G_2)$ , on the angle of the band wrapping the rollers  $\alpha - s = f(\alpha)$ .

As is clear from the graph (Fig. 16 a, curve 1), the longer is the duration of the impulse  $t_{imp}$ , the longer is the distance,  $s$ , that is covered by the rollers in one period of the regulating impulse.

The friction force  $F_r$  and time,  $t$ , is needed for the rollers to cover the distance  $s$ , when the pulling force  $G_2 = \text{const}$  of the band is decreasing if the rollers are influenced by a larger amplitude of feeding voltage and they are pulled by a greater force  $G_1$  (Fig. 16 b).

An experiment was made so that the vibrating rollers were fed by a continuous power-supply mode, when  $\alpha = 530^\circ$ ,  $G_2 = 2.0 \text{ N} = \text{const.}$  The distance  $s$  covered by the rollers in one period of regulating impulse increases, when increasing the force of the roller pulling  $G_1$ . This is clear from the graph (Fig. 16 a, curve 2). If  $G_1 > F_0$ , where  $F_0$  is the marginal value of the still friction force, so that when it is exceeded the rollers start moving



Sl. 16. Krivulje odvisnosti: a – pomiki valja 1 v obdobju krmilnega sunka: 1 -  $s = f(t_{imp})$ ; 2 -  $s = f(G_1)$ ; 3 -  $s = f(G_2)$ ; 4 -  $s = f(\alpha)$ ; b – odvisnosti  $F_{rr} = f(G_1)$  – 1 do 3;  $t = f(G_1)$  – 4 do 6 (za mehanizem RTM z valji 1);  $F_{rr} = f(G_1)$  – 7 do 9 (RTM z nepremičnimi valji z valovnim vodilom). Napajanje napetosti U je naslednje: 3, 4 in 7 - 10 V; 1, 5 in 8 - 20 V; 2, 6 in 9 - 30 V.

Fig. 16. Curves of dependencies: a – displacements of RTM roller 1 per one period of regulating impulse: 1 -  $s = f(t_{imp})$ ; 2 -  $s = f(G_1)$ ; 3 -  $s = f(G_2)$ ; 4 -  $s = f(\alpha)$ ; b – dependencies  $F_{rr} = f(G_1)$  – 1 to 3;  $t = f(G_1)$  – 4 to 6 (for Rolomite mechanisms with the rollers 1);  $F_{rr} = f(G_1)$  – 7 to 9 (RTM with immovable rollers with waveguides). Feeding voltage U equals: 3, 4 and 7 – 10 V; 1, 5 and 8 – 20 V; 2, 6 and 9 – 30 V.

brez stimulacije visokofrekvenčnih električnih signalov. Območje, v katerem je  $G_1 \geq F_0$ , je dodatno označeno s pikčasto črto (sl. 16 a). Dane razmere pri preizkusu so naslednje: mehanizem RTM deluje na diskretni način;  $G_2 = 2,0 \text{ N} = \text{konst.}$ ;  $\alpha = 530^\circ$ ;  $f_r = 88,5 \text{ kHz}$ ;  $U = 51 \text{ V}$ ;  $f_{imp,sek} = 5 \text{ Hz}$ ;  $t_{imp} = 1,5 \text{ ms}$ ; e -  $G_1 = 3,0 \text{ N}$ ; f -  $G_1 = 3,5 \text{ N}$ ; g -  $G_1 = 3,6 \text{ N}$ ; h -  $G_1 = 3,7 \text{ N}$ .

Razdalja  $s$ , na kateri se premakneta valja v enem obdobju krmilnega sunka, se poveča, kadar se zmanjša natezna sila jermenja (vlečna sila valja  $G_1 = \text{konst.}$ ). To je razvidno iz grafa (sl. 16 a, krivulja 3).

Kadar je sila  $G_2$  (nategnjeni jermen) zelo majhna, se valja začneta premikati brez stimulacije z visokofrekvenčnimi električnimi signali. Praznina pri preizkusu so v tem primeru naslednje: mehanizem RTM deluje na diskretni način;  $\alpha = 530^\circ$ ;  $f_r = 88,5 \text{ kHz}$ ;  $U = 51 \text{ V}$ ;  $G_1 = 3,0 \text{ N} = \text{konst.}$ ;  $f_{imp,sek} = 5 \text{ Hz}$ ;  $t_{imp} = 1,5 \text{ ms}$ ;  $G_2: j - 4,0 \text{ N}; k - 2,0 \text{ N}; l - 1,7 \text{ N}; m - 1,5 \text{ N}$ .

Razdalja  $s$ , na kateri se premakneta valja v enem obdobju krmilnega sunka, se zmanjša, kadar ta poveča kot, pod katerim jermenovi valja. To je razvidno iz grafikona (sl. 16 a, krivulja 4).

Ko je kot zavoja jermenja zelo oster,  $G_1 \geq F_0$ , se valja začneta premikati brez stimulacije z visokofrekvenčnimi električnimi signali. Razmere pri

without being influenced by the high-frequency electrical signals. The zone in which  $G_1 \geq F_0$  is additionally marked by a dotted line (Fig. 16 a). The conditions of the experiment are given as follows: RTM operating mode is start-stop;  $G_2 = 2.0 \text{ N} = \text{const.}$ ;  $\alpha = 530^\circ$ ;  $f_r = 88.5 \text{ kHz}$ ;  $U = 51 \text{ V}$ ;  $f_{imp,sek} = 5 \text{ Hz}$ ;  $t_{imp} = 1.5 \text{ ms}$ ; e -  $G_1 = 3.0 \text{ N}$ ; f -  $G_1 = 3.5 \text{ N}$ ; g -  $G_1 = 3.6 \text{ N}$ ; h -  $G_1 = 3.7 \text{ N}$ .

The distance  $s$  covered by the rollers in one period of the regulated impulse increases when this is decreasing the stretching force of band (the pulling force of roller  $G_1 = \text{const.}$ ). This is clear from the graph (Fig. 16 a, curve 3).

When the force  $G_2$  (stretching the band) is very low, the rollers start moving without being influenced by the high-frequency electrical signals. The conditions of the experiment are as follows: RTM operating mode is start-stop;  $\alpha = 530^\circ$ ;  $f_r = 88.5 \text{ kHz}$ ;  $U = 51 \text{ V}$ ;  $G_1 = 3.0 \text{ N} = \text{const.}$ ;  $f_{imp,sek} = 5 \text{ Hz}$ ;  $t_{imp} = 1.5 \text{ ms}$ ;  $G_2: j - 4.0 \text{ N}; k - 2.0 \text{ N}; l - 1.7 \text{ N}; m - 1.5 \text{ N}$ .

The distance  $s$  covered by the rollers in one period of the regulated impulse is decreasing when this is increasing the angle of the rollers' wrapping by the band. This is clear from the graphs (Fig. 16 a, curve 4).

When the wrapping angle is very low,  $G_1 \geq F_0$ , the rollers start moving without being influenced by the high-frequency electrical signals. The conditions of the

preizkusu so v tem primeru naslednje: mehanizem RTM deluje na diskretni način; za  $\alpha$  velja naslednje:  $n = 450^\circ$ ;  $\alpha = 480^\circ$ ;  $p = 500^\circ$ ;  $r = 530^\circ$ ;  $G_1 = 3,0\text{ N}$ ;  $G_2 = 2,0\text{ N}$ ;  $U = 51\text{ V}$ ;  $f_{imp,sek} = 5\text{ Hz}$ ;  $t_{imp} = 1,5\text{ ms}$ .

Nepremični vibrirajoči valji (1) z valovnim vodilom (sl. 15 b) bodo v enakih razmerah napajanja in vzbujanja, vibrirali z večjo amplitudo kakor valji 1 (brez valovnega vodila).

Odvisnosti, ki so značilne za valje z valovnim vodilom (sl. 15 b), so analogne odvisnostim valjev 1 (sl. 15 a), na primer,  $F_{tr} = f(G_1, U)$  (glej sl. 16 b, krivulje 7 do 9). Zmanjšanje  $\Delta F_{tr}$  (sila trenja) v mehanizmu valjev 1 (brez valovnega vodila) je nižje od zmanjšanja te sile v mehanizmu valjev z valovnim vodilom v enakih delovnih razmerah.

Sila trenja  $F_{tr}$  in čas  $t$ , v katerem se valja premakneta po znani razdalji  $s$ , pri  $G_1 = \text{konst.}$ , se zmanjšata, če valjema povečamo amplitudo napetosti in zmanjšamo natezno silo  $G_2$ . To je razvidno iz grafov (sl. 17 a in b). Preizkus je bil izveden ob zveznem napajanju vibrirajočih valjev pri  $\alpha = 530^\circ$ .

Sila trenja  $F_{tr}$  in čas  $t$ , v katerem se valja premakneta po razdalji  $s$ , pri  $G_1 = G_2 = \text{konst.}$ , se povečuje, ko se povečuje kot jermenovega zavoja  $\alpha$  (sl. 17 c). Ta del preizkusa je bil izveden ob zveznem napajanju vibrirajočih valjev 1.

Raba vrtečih se valjev 2 ima pri mehanizmu RTM poseben pomen (glej sl. 15 c).

Iz rezultatov eksperimentalne raziskave, prikazanih na sliki 18, je razvidno, da se sila trenja  $F_{tr}$  zmanjša, če: a) valjem dovajamo napetost z večjo amplitudo  $U$ , b) valja izpostavimo večji vlečni sili  $G_1$  (sl. 18 a), c) zmanjšamo natezno silo jermenova zavoja  $G_2$  (sl. 18 b), d) zmanjšamo kot  $\alpha$ , pod katerim jermen ovija valja (sl. 18 c).

Kakor je razvidno iz navedenih rezultatov preizkusov, ima mehanizem RTM z vrtečima in vibrirajočima valjema 2, v primerjavi z drugimi tipi, boljšo ležajno zmogljivost in je bolj občutljiv. Primerno ga je uporabljati v sklopu izjemno občutljivih sistemov. Od vibracij vsiljena plinasta plast se pri valjih 2 pojavi zelo hitro, ker je uporabljen celotna delovna površina piezokeramičnega obroča, kar pa, zaradi konstrukcije samega mehanizma RTM, ni mogoče v primeru mehanizma z valjema drugačnega tipa.

Še več, v mehanizmu RTM z vibrirajočima nepremičnima valjema (sl. 15 a in b), ki ju ovija gibki jermen, je ovira nastanku plasti vibracij med vibrirajočim valjem in jermenom v tem, da je gibki jermen relativno tanek in se hitro deformira.

experiment are as follows: RTM operating mode is start-stop;  $\alpha$  are equal:  $n = 450^\circ$ ;  $\alpha = 480^\circ$ ;  $p = 500^\circ$ ;  $r = 530^\circ$ ;  $G_1 = 3,0\text{ N}$ ;  $G_2 = 2,0\text{ N}$ ;  $U = 51\text{ V}$ ;  $f_{imp,sek} = 5\text{ Hz}$ ;  $t_{imp} = 1,5\text{ ms}$ .

The RTM's immovable (1) vibrating rollers with a waveguide (Fig. 15 b), given the same conditions of power supply and of impact on them, vibrate with a larger amplitude than rollers 1 (without the waveguides).

The dependencies characteristic of the rollers with waveguides (Fig. 15 b) are, by their type, in analogy to the dependencies of rollers 1 (Fig. 15 a), for example,  $F_{tr} = f(G_1, U)$  (see Fig. 16 b, the curves 7 to 9). The magnitude of the decreasing of  $\Delta F_{tr}$  (friction force) in the RTM with rollers 1 (without the waveguides) is lower than in the RTM with rollers with waveguides at the same working conditions.

The friction force  $F_{tr}$  and the time  $t$ , in which the rollers cover the known distance  $s$ , whereas  $G_1 = \text{const.}$ , decreases, if the rollers are provided with increased amplitude voltage and lowered band-stretching force  $G_2$ . This is evident from the graphs (Fig. 17 a and b). The experiment is carried out in continuous power-supply mode of the vibrating rollers,  $\alpha = 530^\circ$ .

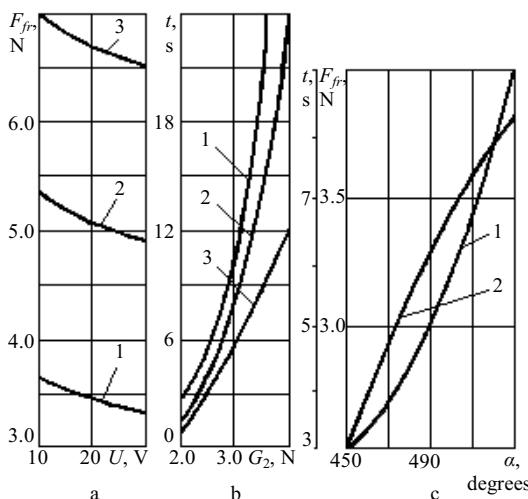
The frictional force  $F_{tr}$  and the time  $t$ , in which the rollers cover the distance  $s$ , when  $G_1 = G_2 = \text{const.}$ , is increasing when the angle of the band wrapping the rollers  $\alpha$  is increasing (Fig. 17 c). The experiment is carried out in the continuous power-supply mode of the vibrating rollers 1.

The application of the rotating rollers 2 in RTM is of a special interest (see Fig. 15 c).

From the results of the experimental research provided in Fig. 18 it is clear that the friction force  $F_{tr}$  is decreased if: a) the rollers are supplied with a higher amplitude power-supply voltage  $U$ , b) the rollers are influenced by a larger pulling force  $G_1$  (Fig. 18 a), c) the stretching force  $G_2$  of the band decreased (Fig. 18 b), d) the decreased angle  $\alpha$  of the band wrapping the rollers (Fig. 18 c).

As one can see from the results of the experiments, the RTM with the rotating vibrating rollers 2, compared with the other, has a better bearing capacity and is much more sensitive. It is advisable to use them in exceptionally sensitive systems. The vibrations-pressed gas film appears in the rollers 2 very quickly, because all the working surface of the piezoceramic ring is used, which is impossible in the RTM with rollers of another type, because of the design of the RTM itself.

Moreover, in the RTM with vibrating immovable rollers (Fig. 15 a and b), wrapped by a flexible band, the obstacle of the formation of FV between the vibrating roller and the band is that the flexible band is comparably thin and quickly deforms.



Sl. 17. Krivulje odvisnosti mehanizma RTM z valji  
Fig. 17. Dependency curves of RTM with rollers

Fig. 17. Dependency curves of RTM with rollers  
1:  $a - F_{fv} = f(U)$ , ko/if  $G_1 = 3,5 \text{ N} = \text{const}$ ;  $G_2$  je/is: 1 – 2,0 N; 2 – 3,0 N; 3 – 4,0 N; b –  $t = f(G_2)$ , ko/if  $G_1 = 3,5 \text{ N} = \text{const}$ ; U je/is: 1 – 10V; 2 – 20 V; 3 – 30 V; c –  $1 - F_{fv} = f(\alpha)$ ;  $2 - t = f(\alpha)$ , ko/if  $U = 40V$ ;  $G_1 = G_2 = 2,0 \text{ N}$

Krivulje iz teoretičnega dela raziskave smo porabili za oblikovanje vibramotorjev Rolamite.

## 6 ANALIZA DINAMIČNIH PROCESOV V VIBRAMOTORJIH ROLAMITE

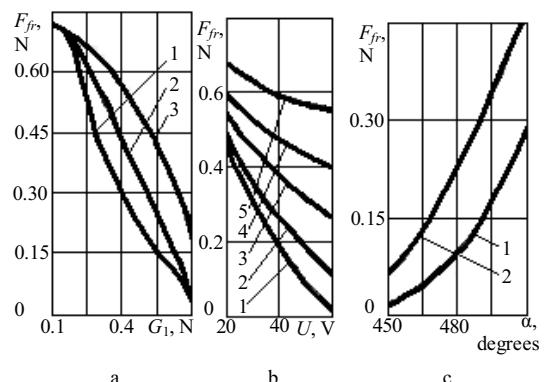
Prvi vibramotorji so izkoriščali diagonalno udarjanje piezokeramičnega pretvornika vibracij (piezokeramični elementi) ob gibljiv element, tj. ploščo ali valj [7].

Ko na elektrode pretvornika dovedemo visoko frekvenčni električni signal, se končni del piezoelektričnega pretvornika, ki ima netogi stik z rotorjem, prične eliptično gibanje in obračati rotor (sl. 19).

Določili smo najboljši kot piezokeramičnega pretvornika vibracij 2, ki udarjajo ob rotor 1, pri katerem je zagotovljeno največje število vrtljajev rotorja 1. Pri raziskovani konstrukciji vibramotorja je najboljša vrednost kota  $\alpha 125^\circ$ .

Ob konstruiranju vrtilnega vibramotorja Rolamite ter mehanizmov vlečnega jermena je bilo treba ugotoviti, kakšen vpliv ima na sinhronost vrtenja valjev uporaba načela Rolamite v mehanizmih vlečnega jermena.

Model mehanizma prenosa gibanja je bil oblikovan kot vrtilni vibramotor Rolamite (sl. 20 a), na podlagi tega pa je bilo oblikovano eksperimentalno stojalo (sl. 20 b).



Sl. 18. Mehanizem RTM z valjema 2 (glej sl. 11 b in sl. 15 c) krivulje odvisnosti

Fig. 18. RTM with rollers 2 (see Fig. 11 b and Fig. 15 c) dependency curves

a –  $F_{fv} = f(G_1)$ , ko/if  $\alpha = 500^\circ$ ;  $G_2 = 5,0 \text{ N}$ ; U je/is:  
1 – 50 V; 2 – 35 V; 3 – 20 V; b –  $F_{fv} = f(U)$ , ko/if  
 $G_1 = 0,5 \text{ N}$ ;  $\alpha = 500^\circ$ ;  $G_2$  je/is: 1 – 4,0 N;  
2 – 5,0 N; 3 – 7,0 N; 4 – 8,0 N; 5 – 9,0 N;  
c –  $F_{fv} = f(\alpha)$ ;  $G_1 = 0,5 \text{ N}$ ;  $G_2 = 5,0 \text{ N}$ ;  
U je/is: 1 – 50 V; 2 – 30 V

The curves from the theoretical research were used when designing the Rolamite vibromotors.

## 6 RESEARCH OF THE DYNAMIC PROCESSES RUNNING IN THE ROLAMITE VIBROMOTORS

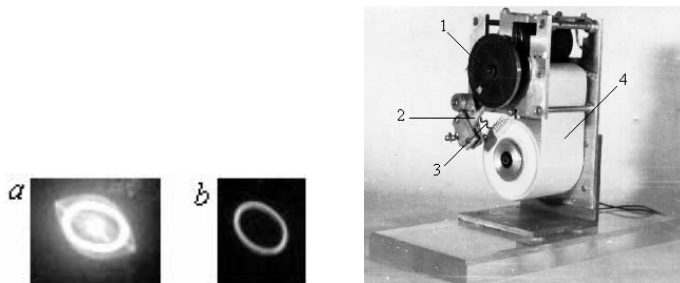
The first vibromotors used diagonal hits by the piezoelectric converter of the vibrations (piezoceramic elements) onto a movable element, i.e., a plate or a roller [7].

After providing a high-frequency electrical signal on the electrodes of the converter, the end of the piezoelectric converter, elastically connected to the rotor, starts making elliptical movements and turns the rotor (Fig. 19).

The optimal angle of the piezoelectric converter of the vibrations 2 hitting the rotor 1, at which the maximum rotations of rotor 1 are ensured, was found. The optimal value of the angle  $\alpha$  in the explored design of the vibromotor is  $125^\circ$ .

When designing the rotary RVM and the mechanisms of band pulling, it was necessary to find what impact the applying of the Rolamite principle in the mechanisms of band pulling has on the synchronicity of the rotation of the rollers.

The model of a mechanism of movement transmission was designed as a rotary Rolamite vibromotor (Fig. 20 a), and based on that an experimental stand was designed (Fig. 20 b).



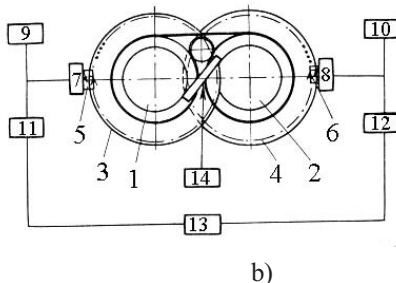
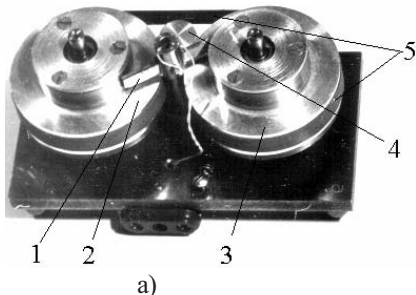
Sl. 19. Pot vrhnjega dela menjalnika (a – v trenutku, ko na elektrode pretvornika dovedemo visokofrekvenčni električni signal; b – ko se delovanje ustali) in model mehanizma z vlečnim papirnim jermenom, ki uporablja vibramotor: 1 – rotor; 2 – piezoelektrični pretvornik vibracij; 3 – žica, ki piezoelektričnemu pretvorniku vibracij dovaja visokofrekvenčno električno napetost; 4 – papirni jermen  
 Fig. 19. Path of the tip of the changer (a – at the moment of providing a high-frequency electrical signal on the electrodes of the converter; b – when the working mode has been stabilized) and a model of the mechanism of paper's band pulling, using a vibromotor: 1 – rotor; 2 – piezoelectric converter of vibrations; 3 – power supply wire of piezoelectric converter that provides a high-frequency voltage; 4 – the paper band

Pogonsko vozlišče sestoji iz piezoelektričnega pretvornika vibracij 1, ki ustvarja vrtenje valjev – rotorjev 2 in 3. Valja -rotorja 2 in 3, kakor tudi tesno prilegajoči se valj manjšega premera 4, so oviti z neskončnim jermenom 5. Valja 2 in 3 sta ovita z neskončnim jermenom 5 pod kotom, ki je večji od  $270^\circ$ , valj 4 pa je ovit pod kotom, večjim od  $180^\circ$ . Shema meritev je predstavljena na sliki 20 b.

Na gredi rotorjev 1 in 2 sta pritrjena dva enaka rastrska diska 3 in 4 z znakom, ki se odziva na svetlobni zaznavali 5 in 6. Predojačevalnika 7 in 8 sta

The drive node consists of a piezoelectric converter of the vibrations 1, which is providing a rotation of the rollers-rotors 2 and 3. The rollers-rotors 2 and 3, and also a roller of a smaller diameter 4 that is tight, are wrapped by an endless band 5. The rollers 2 and 3 are wrapped by an endless band 5 by an angle of more than  $270^\circ$ , and a roller 4 by an angle of more than  $180^\circ$ . The scheme of measurement is presented in Fig. 20 b.

On the shaft of rotors 1 and 2 two identical raster disks 3 and 4 with a raster mark that interacts with the photo sensors 5 and 6 are fixed. The former-amplifiers 7



Sl. 20. Model mehanizma prenosa gibanja kot rotacijski vibramotor Rolomite (a): 1 – piezoelektrični pretvornik vibracij; 2 in 3 – valj - rotor; 4 – valj manjšega premera; 5 – neskončni jermen in shema eksperimentalnega stojala (b): 1 in 2 - rotors; 3 in 4 – rastrska disk; 5 in 6 – svetlobni zaznavali;

7 in 8 – predojačevalnika; 9 in 10 – merilnika frekvence; 11 in 12 – razločevalnika frekvence; 13 – blok dvojnega kanala registracije; 14 – napajalnik piezoelektričnega pretvornika vibracij

Fig. 20. The model of a mechanism of movement transmission as a rotary Rolomite vibromotor (a):  
 1 – piezoelectric converter of vibrations; 2 and 3 – roller-rotor; 4 – roller of smaller diameter;  
 5 – endless band and scheme of experimental stand (b): 1 and 2 - rotors; 3 and 4 - raster disks;  
 5 and 6 - photosensors; 7 and 8 - former-amplifiers; 9 and 10 - frequency meters; 11 and 12 - frequency discriminators; 13 - block of double channels of registration; 14 - power-supply unit of piezoelectric converter of vibrations

povezana z merilnikoma frekvence 9 in 10 ter prek enakih razločevalnikov frekvence 11 in 12 tudi na blok dvojnega kanala zapisa 13. Elektrode piezoelektričnega pretvornika vibracij so priključene na napajalnik 14 in zaradi visokofrekvenčnega električnega signala, ki prihaja iz napajalnika 14, začne piezoelektrični pretvornik vibracij vibrirati in vrteći rotorja 1 in 2.

Na eksperimentalnem stojalu (sl. 20 b) smo raziskali dva rotorja RVM, katerih vrtilno gibanje je spodbudil piezoelektrični pretvornik vibracij. Nastavili smo najboljši kot ( $120^\circ$  do  $130^\circ$ ) stika pretvornika vibracij z vrtečim rotorjem. Najprej smo raziskali vibriranje dveh rotorjev vibramotorja pri prostem (neobremenjenem) teku, ko je bil pretvornik vibracij togo pritrjen na sredino vibramotorja.

Ko se amplituda dovedene električne napetosti  $U$  zveča, se poveča tudi število rotorjevih vrtljajev  $n$ , vendar pa nenatančno pritrjen piezoelektrični pretvornik povzroči nesinhrono vrtenje rotorjev (sl. 21, krivulji 1 in 2). Če sta rotorja vibramotorja ovita z neskončnim jermenom v obliki mehanizma RTM in se oboji rotorja vrtita, nesinhronost vrtenja dveh rotorjev izgine, kar pomeni, da  $\Delta n=0$  (sl. 21, krivulja 3).

Ko se poveča zunanja obremenitev enega od rotorjev, se močno poveča tudi nesinhronost vrtenja obeh rotorjev (sl. 22, krivulja 1).

Povezava dveh rotorjev z neskončnim jermenom v obliki mehanizma RTM zmanjša nesinhronost njunega vrtenja na najmanjšo vrednost (sl. 22, krivulja 3). Slike 22 tudi izhaja, da je nesinhronost vrtenja rotorjev vibramotorja Rolomite, ki sestoji iz dveh rotorjev in piezoelektričnega pretvornika vibracij, ki vrti oboji rotorja, dosti manjša od nesinhronosti vrtenja rotorjev vibramotorja Rolomite, ki sestoji iz dveh rotorjev in piezoelektričnega pretvornika vibracij, ki vrti le enega od rotorjev (sl. 22, krivulja 2).

Iz navedenega je mogoče sklepati, da največjo sinhronost vrtenja rotorjev zagotavlja vibromotor Rolomite, ki se sestoji iz dveh rotorjev in piezoelektričnega pretvornika vibracij, ki hkrati vrti oboji rotorja.

Pomanjkljivost vibromotorja, ki uporablja diagonalno udarjanje piezo električnega pretvornika vibracij (piezokeramični elementi) ob rotor, je njegova nezmožnost spremeniti smer vrtenja rotorja.

and 8 are connected to the frequency meters 9 and 10, and through identical frequency discriminators 11 and 12 to a block of double channels of registration 13. The electrodes of the piezoelectric converter of vibrations are connected to a power-supply unit 14, and during a high-frequency electrical signal from a power-supply unit 14, the piezoelectric converter of the vibrations starts to vibrate and rotates the rotors 1 and 2.

On an experimental stand (Fig. 20 b) the two RVM rotors were investigated, where the rotors rotational movement was obtained from one piezoelectric converter of vibrations. The optimal angle ( $120^\circ$  to  $130^\circ$ ) of contact for the converter of vibrations with a rotor rotated by it was used. First, the vibration mode of the two rotors, with the vibration's converter rigidly fixed to the middle of it, is investigated in the empty (unloaded) working mode.

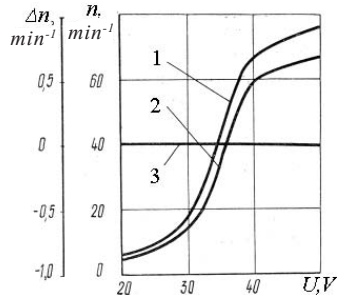
When the amplitude of the feeding voltage  $U$  is increased, then the number of turns  $n$  of rotors increases; however, inexact fastening of the piezoelectric converter leads to non-synchronous rotations of the rotors (Fig. 21, curves 1 and 2). If the two VM rotors are wrapped by an endless band in the form of RTM and both rotors are rotating, the nonsynchronicity of the rotors' rotations disappears, i.e.,  $\Delta n=0$  (Fig. 21, the curve 3).

When the external loading increases on one of the rotors, the nonsynchronicity of the rotations of both rotors sharply increases (Fig. 22, the curve 1).

The connection of the two rotors by an endless band in the form of an RTM reduces to a minimum the nonsynchronicity of their rotations (Fig. 22, the curve 3). From Fig. 22 it also follows that the magnitude of the nonsynchronicity of the rotation of the rotors of the Rolomite vibromotor of two rotors with a piezoelectric converter of vibrations, which rotates both rotors, is much less than the magnitude of the nonsynchronicity of the rotation of the rotors of the Rolomite vibromotor of two rotors with a piezoelectric converter of vibrations, which rotates only one rotor (Fig. 22, the curve 2).

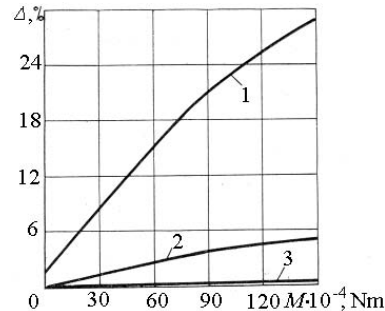
From this it is necessary to draw a conclusion that the highest synchronicity of rotation of the rotors is provided by the Rolomite vibromotor of two rotors with a piezoelectric converter of vibrations that simultaneously rotates both rotors.

A weakness of the vibromotor that used diagonal hits of the piezoelectric converter of vibrations (piezoceramic elements) onto a rotor is the impossibility of reversing the rotation of a rotor.



Sl. 21. Krivulji odvisnosti za nesinhrono vrtenje rotorjev vibramotorja pri prostem (neobremenjenem) teku: krivulji 1 in 2 - ko je  $n=f(U)$  pri dveh rotorjih, ki nista povezana z neskončnim jermenom in čigar vrtenje ustvarja splošni piezoelektrični pretvornik; krivulja 3 - ko je  $\Delta n=f(U)$  pri vibramotorju dveh rotorjev s splošnim piezoelektričnim pretvornikom vibracij potrebnim za vrtenje obeh rotorjev

Fig. 21. Dependency curves for non-synchronous rotations of rotors VM in the empty (unloaded) mode of working: curves 1 and 2 - when  $n=f(U)$  for two rotors unconnected by an endless band and getting the rotation from the general piezoelectric converter of vibrations; the curve 3 - when  $\Delta n=f(U)$  for RVM of two rotors with general piezoelectric converter of vibrations for rotating both rotors



Sl. 22. Krivulje odvisnosti vrtlne nesinhronosti rotorjev od moči zunanje obremenitve enega od rotorjev  $\Delta=f(M)$ , ko je  $U=\text{konst.}=50 \text{ V}$ : 1 - za primer dveh rotorjev, ki nista povezana z neskončnim jermenom in ju vrati splošni piezoelektrični pretvornik vibracij; 2 - za primer vibramotorja Rolomite, ki se sestoji iz dveh rotorjev in piezoelektričnega pretvornika vibracij, ki vrati le en rotor; 3 - za primer vibramotorja Rolomite, ki se sestoji iz dveh rotorjev in piezoelektričnega pretvornika vibracij, ki vrati oboje rotorja

Fig. 22. Curves of the dependencies of the rotations nonsynchronicity of the rotors on the magnitude of the external loading on one of the rotors  $\Delta=f(M)$  when  $U=\text{const}=50 \text{ V}$ : 1 - for two rotors not connected by an endless band and both getting rotation from the general piezoelectric converter of vibrations; 2 - for the Rolomite vibromotor of two rotors with a piezoelectric converter of vibrations, which rotates only one rotor; 3 - for the Rolomite vibromotor of two rotors with a piezoelectric converter of vibrations that rotates both rotors

## 7 SKLEPNE OPOMBE

S teoretičnim delom raziskave smo dokazali naslednje:

- Povečanje koeficiente suhega trenja omogoči hitrejše oblikovanje nezdrsnega območja med telesi mehanizma RTM.
- Parametri vibracij mehanizma RTM se spremeniijo takoj, ko elementi sistema RTM dosežejo nezdrsnno območje, kar pomeni, da lahko na nezdrsnno področje vplivamo z vibracijskim vzbujanjem.
- Če povečamo amplitudo vibracij, se sila trenja med telesi sistema zmanjša; če se poveča zdrsn področje med telesi sistema, se zmanjša izkoristek.

Z eksperimentalnim delom raziskave smo dokazali naslednje:

- Povečanje amplitude električne napetosti, zmanjšanje sile obremenitve gibkega jermenja in

## 7 CONCLUDING REMARKS

Theoretical research proved:

- The increasing magnitude of the dry-friction coefficient makes it faster to achieve a non-slipping zone between the bodies of the “roller-band” system of the RTM.
- From the “roller-band” system of the RTM the vibration parameters depend as quickly as bodies of the system achieve a non-slipping zone, and this means that the non-slipping zone can be operated by the excitation of vibrations.
- If the amplitude of vibrations is increasing, then the force of friction between the bodies of the system is decreasing; if the zone of slipping between the bodies of the system is increasing, the magnitude of the efficiency is decreasing.

Experimental research proved:

- The increase of the supply-voltage amplitude, the decrease of the force load magnitude of the flexible

- zmanjšanje kota, pod katerim gibki jermen ovija valj, povzročijo povečanje amplitude vibracij valja.
2. Mehanizem RTM z vrtečima se, vibrirajočima valjema, ima v primerjavi z vibrirajočima valjema drugega tipa boljšo ležajno zmogljivost in je bolj občutljiv. Zato je priporočljivo, da ga uporabljamo v izredno občutljivih sistemih.
  3. Če primerjamo vibramotor Rolomite, ki se sestoji iz dveh rotorjev in piezoelektričnega pretvornika vibracij, ki sočasno vrти oba rotorja, ter vibramotor Rolomite, ki se sestoji iz dveh rotorjev in piezoelektričnega pretvornika vibracij, ki vrти le enega od rotorjev, prva možnost omogoči večjo sinhronost vrtenja rotorjev.

band and the decrease of the angle wrapping of the roller by the flexible band cause the increase in the amplitude of the roller vibrations.

2. The RTM with rotating vibrating rollers, compared with vibrating rollers of another type, have a better bearing capacity and are much more sensitive. Therefore, it is advisable to use them in exceptionally sensitive systems.
3. If we compare the Rolomite vibromotor of two rotors with the piezoelectric converter of vibrations, which simultaneously rotates both rotors, and the Rolomite vibromotor of two rotors with a piezoelectric converter of vibrations, which rotates only one rotor, the first variant provides the highest synchronicity of the rotation of rotors.

## 8 VIRI 8 REFERENCES

- [1] Wilkes, D.F. (1967) Rolomite: A new mechanical design concept.-Research report SC-RR-67-656 A, *Sandia Laboratories*, December, 223p.
- [2] Wilkes, D.F. (1968) Rolomite: A new mechanism. *Mechanical Engineering*. April, v. 90, No 4, 11-29.
- [3] Percival, C.M., Norwood, F.R. (1969) A theoretical and experimental investigation of the dynamic response of Rolomite. *Trans. ASME, Ser.B*, v. 91, No 1, 235-239.
- [4] Ulozas, R.V. (2004) Raziskava zdrsa v mehanizmu med valjem in trakom – An investigation of slipping in Rolomite-type mechanisms. *Strojniški vestnik – Journal of Mechanical Engineering*, v.50, No 6, 302-309.
- [5] Fridman, H.D., Levesque, P. (1959) Reduction of static friction by sonic vibration.-*J. Appl. Phys.*, v. 30, No 10.
- [6] Канапенас, Р. М. (1984) Виброопоры.- Вильнюс, Мокслас, 208 с.
- [7] Бансявиčюс, Р.Ю., Рагульскис, К.М. (1981) Вибродвигатели.-Вильнюс, Мокслас, 193 с.
- [8] Invention of USSR № 609074.

Avtorjev naslov: prof. dr. Ričardas Viktoras Ulozas  
Univerza Šiauliai  
Vilniaus 141  
LT-76353 Šiauliai, Litva  
ulozas@tf.su.lt

Author's address: Prof. Dr. Ričardas Viktoras Ulozas  
Šiauliai University  
Vilniaus 141  
LT-76353 Šiauliai, Lithuania  
ulozas@tf.su.lt

Prejeto:  
Received: 17.10.2005

Sprejeto:  
Accepted: 23.2.2006

Odperto za diskusijo: 1 leto  
Open for discussion: 1 year

# Optimizacija neprekinjenega postopka sušenja v težnostnih sušilnicah

## Optimization of the Performance of the Continuous-Drying Process in Gravity Dryers

Neven Voća - Tajana Krička - Vanja Janušić  
(University of Zagreb, Croatia)

*V prihodnosti pričakujemo razvoj tehnologije in izvedbo tehničkih načrtov; seveda pa bo obseg njihove uporabe določen tudi z dejanskimi možnostmi, potrebami in delovnimi razmerami. Na vseh področjih človeške dejavnosti, tudi na področju kmetijstva, nastajajo načrti in napovedi za prihodnji razvoj. Na podlagi znanja, ki je bilo doslej uporabljeno v postopku osuševanja v gravitacijskih sušilnicah, in dosegljivih podatkov o medsebojni odvisnosti velikega števila parametrov, ta prispevek predlaga način optimizacije posameznih sklopov postopka osuševanja.*

*Celoten postopek optimizacije sušenja v gravitacijskih sušilnicah moramo razviti v posameznih stopnjah, upoštevajoč posamezne funkcionalne sklope. Vsaka stopnja vpliva na izboljšanje celotnega postopka in vse stopnje skupaj vodijo v optimizacijo delovanja sistema. Dodatna prednost predlaganega postopka je v tem, da ga lahko izvedemo postopoma. Z optimizacijo sušenja dosežemo večjo stabilnost delovanja sušilnic, zmanjšanje porabe energije in boljšo kakovost zrn.*

© 2007 Strojniški vestnik. Vse pravice pridržane.

**(Ključne besede: sušenje, optimiranje, statična lastnost, učinkovitost, mikroprocesorsko krmiljenje)**

*Technology and technological expectations are expected to develop with time; however, opportunities, needs and working conditions affect the extent of their usage. Predictions are made in all areas of human activity, and this includes the agricultural sector. Using the know-how so far applied during the drying process in gravity dryers, together with the available data on the interdependencies of a large number of parameters, this paper suggests how a system for drying could be organized by optimising the functional ensembles.*

*A comprehensive method for drying-process optimization in gravity dryers can be built in several steps from several functional ensembles. Each step improves the process, and together they represent the complete system for performance optimization. An additional property is the possibility of realizing each step. The drying-process optimization results in the stabilisation of the dryer functions, a decrease in the specific energy consumption, and better kernel quality.*

© 2007 Journal of Mechanical Engineering. All rights reserved.

**(Keywords: drying process, optimization, static properties, performance, microprocessor controller)**

### 0 UVOD

Visoke cene energije in drugi problemi, povezani z naftnim trgom, so v zadnjem desetletju spodbudili vrsto znanstvenih raziskav na področju energetike. Na primer, priča smo bili intenzivnemu raziskovanju sušenja kmetijskih pridelkov, ki je razkrilo, da je kar 40% vseh stroškov porabljenih za opravilo [1].

Vsi lahko kvarljivi pridelki morajo biti konzervirani. Konzerviranje je postopek popolne

### 0 INTRODUCTION

High energy costs and problems in the oil market have resulted in many scientific investigations in the field of energetics over the past ten years. As an example, intensive investigations have been carried out in the field of drying agricultural products, and it was determined that 40% of the overall energy costs are spent during this process [1].

All easily perishable products have to be preserved. This term refers to the final operation of com-

odstranitve prisotnih mikroorganizmov ali vsaj ustavitev njihove rasti in razmnoževanja. Ta postopek omogoči hrambo izdelka za določeno časovno obdobje, ko izdelek ostane nespremenjen, in tako omogoči njegovo uporabo ne glede na čas in kraj njegove pridelave. Namen konzerviranja je torej ohranitev primarnih značilnosti izdelka in podaljšanje njegovega roka trajanja [2].

Na podlagi doseglih podatkov o žitaricah je bilo ugotovljeno, da je osuševanje postopek, ki ga določa medsebojno vplivanje številnih parametrov. Kakovost osuševanja je odvisna od fizikalnih značilnosti ozračja, v katerem poteka osuševanje, fizičnih ter kemijskih značilnosti poljščine in debeline plasti, skozi katero prehaja voda; slednja pa je odvisna od značilnosti sušilnice. Hitrost sušenja je odvisna od vseh omenjenih dejavnikov, katerih učinke lahko opazujemo z vidika kinetike osuševalnega postopka, pa tudi s tehničnega vidika, tj. glede na kakovost osušenega pridelka [3].

Na zbirnem mestu imajo koruzna zrna delež vlage večji od ravnovesnega stanja, ki je najbolj primerno za shranjevanje. Zaradi tega je postopek osuševanja le nadaljevanje in dokončanje spontanega zorenja zrna, ki se ne more zgoditi po naravni poti. Da bi podaljšali dobo skladiščenja zrna, mora biti postopek osuševanja osredotočen na konzerviranje zrna in na ustvarjanje primernih okoliščin. Namenski osuševanja je odstranitev odvečne vsebnosti vode, tj. ohranitev le deleža vode, ki je potrebna za mirujoč obstoj [4].

Hitrost in kakovost sušenja zrna sta odvisni od postopka sušenja. Na primer, pri spontanem sušenju je temperatura zraka skoraj enaka temperaturi zrn, zaradi česar je sušenje zelo počasno. Ko pa pri postopku sušenja uporabljamo vroč zrak, se hitrost sušenja poveča. V tem primeru povečana temperatura zraka povzroči zmanjšanje vlage v zrnih in povečana razlika med vlažnostjo zrna ter vlažnostjo zraka pospeši sušenje ([5] in [6]).

Učinkovitost sušenja je odvisna od parametrov, ki se navezujejo na značilnosti zraka, tj. od toplotne intenzivnosti, hitrosti zračnega toka, relativne vlažnosti, pa tudi od načina izgradnje sušilnice ter temperature zrn. Slednja je, kot funkcija temperature zraka, najbolj pomemben in najbolj občutljiv parameter v postopku sušenja. Največje dovoljene temperature zrn, ki so odvisne od namena uporabe zrn, določajo tudi temperaturo zraka, uporabljeni v postopku sušenja. To pomeni,

pletely removing the micro-organisms that are present, or at least stopping their growth and multiplication. This process ensures the product is preserved without any changes during a specific period of time and therefore ensures that it can be used, no matter when and where it was produced. Hence, the aim of the preservation is to maintain the product's primary properties and to prolong its useful lifetime [2].

According to the available data on plants for cereal finishing, it was determined that the drying process involves the multiple interconnections of parameters. The quality of the drying process itself depends on the physical properties of the atmosphere the drying is being conducted in, on the physical and chemical properties of the product, and on the thickness of the layer the water is diffusing through. The last of these properties depends on the properties of the dryer. The velocity of the drying process depends on the above-mentioned parameters, whose effects can be observed in terms of the drying-process kinetics, and from the technological point of view, i.e., the quality of the dried product [3].

At the collection point the corn kernel has a higher moisture content than at equilibrium point, which is a desirable property for storing. This is why the drying process is only a continuation and finishing of the spontaneous ripening of the kernel, which cannot be carried out naturally. In order to store the kernel for a longer period the drying process has to be focused on kernel preservation and on providing the necessary related conditions. The aim of the drying process is to remove the redundant water content, i.e., to retain only the water content necessary for dormant life [4].

The velocity and quality of the kernel-drying process depend on the drying procedure. For instance, the air temperature during the spontaneous drying process is almost equal to the kernel temperature, which leads to a very slow drying rate. When heated air is used in the drying process, the drying rate is faster, i.e., an increased air temperature leads to a decrease in the kernel's moisture content, and so a greater difference in the moisture contents of the kernel and the air speeds up the drying process ([5] and [6]).

The drying efficiency depends on a few parameters associated with the air, i.e., its thermal intensity, flow velocity and relative humidity, as well as the dryer construction and the temperature of the kernel. The last of these is, as a function of the air temperature, the most important and the most sensitive parameter in the drying process. The maximum allowed temperatures of the kernel, which again depend on the purpose, limit the air temperatures that can be used in the drying process. This

da se zmogljivosti sušilnice na more povečati s preprostim povečanjem temperature zraka, saj bi v tem primeru sušenje zrna poškodovalo. Za postopek sušenja velja, da je osuševanje bolj izrazito pri višji temperaturi in boljšem prenosu toplotne iz zraka na sušeni pridelek. Še več, pomemben parameter sušenja je tudi hitrost prehajanja vode v razdalji med jedrom in površino pridelka ([3], [7] in [8]).

Zrna so običajno v sušilnico dostavljena z različnih krajev. Zato imajo različna zrna različne deleže vlage, pripadajo različnim sortam in hibridom, a so v sušilnici pomešana in skupaj osušena. Ker se zrna razlikujejo glede na morfološko strukturo in pripadajoča razmerja, se tudi v postopku sušenja različno obnašajo. Hitrost sprostiteve odvečne vode, ki ustvari higroskopično ravnovesje, se spreminja glede na vrsto hibrida (v primeru koruznih zrn znaša 14%). Glede na prehajanje vode skozi zrna je najbolj problematičen semenski mešiček in Katić [9] je ugotovil, da je debelina semenskega mešička obratno sorazmerna ( $r=0,83$ ) s hitrostjo sušenja. Razmerja v zrnih vplivajo na postopek sušenja tudi z ustvarjanjem odpornosti proti zračnemu toku. Sušenje lahko zmanjša prostornino zrn za 40%, zaradi česar se spremeni poroznost kupa zrn v sušilnici, kar še dodatno poveča odpornost proti zračnemu toku [9].

Ob izhodu iz sušilnice imajo zato zrna različne deleže vlage. V preteklih desetih letih so se razlike med vlogo osušenih zrn še dodatno povečale zaradi slabih gradenj sušilnic, tako da se je razpon deleža vode lahko povečal tudi do 11 %. V takšni situaciji je skoraj nemogoče organizirati dolgotrajno skladiščenje zrn, zato je treba uvesti nove tehnologije osuševanja.

Ko govorimo o postopku sušenja, je poleg dejavnikov, kakor sta kakovost zrn in zmogljivost sušilnice pomemben tudi dejavnik porabe energije na kilogram vode, ki izhlapi iz zrn. Teoretično je energija potrebna za izparevanje vode enaka specifični entalpiji nasičene pare pri tlaku, ki ustreza temperaturi izparevanja ([11] do [13]).

Namen tega prispevka je, na podlagi najnovejšega znanja in sodobnih tehnik, predlagati nov način organizacije sistema neprekinjenega sušenja v navpičnih gravitacijskih sušilnicah.

## 1 RAZISKOVALNA METODOLOGIJA

Za potrebe nadzora neprekinjenega sušenja zrna smo upoštevali le posamezne odvisnosti med

means that the capacity of the dryer cannot be increased simply by increasing the air temperature, because this would lead to a drying process that has detrimental effects on the dried kernel. For the drying regime, the higher the temperature and the better the air-to-product heat transfer, the more intensive is the resulting drying process. Moreover, an important parameter in the drying process is the rate of water fluctuation from the centre of the product to its surface ([3], [7] and [8]).

The kernels that are dried in a dryer are usually being supplied from different places. Consequently, these kernels have different moisture contents and are of different varieties and hybrids, which are then mixed and dried when entering the dryer. Because the kernels differ in morphological structure and proportions, they behave differently in the drying process. The rate of release of the redundant water content until the hygroscopic equilibrium is achieved differs depending on the hybrid (for the corn kernel this means 14%). The pericarp is the major problem in terms of the water flow through the kernel, and Katić (1985) established that its thickness is inversely related ( $r=0.83$ ) to the velocity of the drying process. Kernel proportions also affect the drying process by providing a resistance to the air flow. The drying process can decrease the kernel's volume by 40%, which changes the pile porosity in the dryer and subsequently leads to a greater resistance to the flow of air [9].

Accordingly, these exceptional kernels have a different moisture content when exiting the dryer. In the past ten years the differences in kernel moisture after the drying process were even more obvious because of poor dryer constructions, which caused variations in the water content of up to 11% [10]. The long-term storage of such kernels is almost impossible to achieve, so there is a need for the introduction of new drying technologies.

When speaking of the drying process, besides parameters such as kernel quality and dryer capacity, the specific energy consumption per kilogramme of water evaporated from the kernel is also an important parameter. Theoretically, the energy that is necessary for the evaporation of the water is equal to the specific enthalpy of saturated steam at the pressure that corresponds to the evaporation temperature ([11] to [13]).

The aim of this paper is to propose a new way of organising a system of continuous drying in vertical gravity dryers, based on the latest knowledge and modern techniques.

## 1 RESEARCH METHODOLOGY

For the purposes of monitoring the continuous kernel drying, single dependencies

dvema ali tremi spremenljivkami, drugim pa smo določili stalne vrednosti in tako preprečili njihovo učinkovanje.

Kakovostni nadzor parametrov postopka sušenja zrn je osnova za zadovoljivo neprekinjeno sušenje, saj omogoča potrebno kakovost zrn ob izhodu iz sušilnice. Za sušenje množice zrn je potrebno, da spremenimo nekatere dejavnike, npr. temperaturo osuševalnega zraka ali hitrost prezračevanja. V gravitacijskih sušilnicah so zrna izpostavljena enakim razmeram, zato so na svoji poti proti izhodu iz sušilnice lahko izpostavljena načrtovanim parametrom. Če spremenimo enega izmed dejavnikov in pri tem želimo, da rezultat osuševalnega postopka ostane nespremenjen, moramo spremeniti tudi preostale dejavnike. To je osnovno vodilo optimizacije sušenja, s katerim želimo dosegči:

- najboljšo mogočo kakovost zrn,
- najmanjši čas sušenja ali največjo zmogljivost sušilnice,
- najamanjšo porabo energije.

Doseganje največje zmogljivosti sušilnice in najmanjše porabe energije je težava naloga. Za doseganje najboljše mogoče kakovosti zrn pa je potrebno temeljito poznavanje obnašanja zrn v različnih razmerah. Poznati moramo vse dejavnike, ki vplivajo na kakovost zrn. Te dejavnike lahko izrazimo v obliki:

- preglednic ali diagramov ustaljenih odvisnosti med spremenljivkami;
- krivulj dejavnikov, ki kažejo ustaljene odvisnosti;
- matematičnih izrazov, s katerimi dobimo približne vrednosti odvisnosti spremenljivk;
- preglednic in diagramov, ki kažejo odvisnosti spremenljivk od časa;
- diferencialnih enačb sistemov, posebej tistih, ki izrazijo približne vrednosti odvisnosti določenih spremenljivk od časa ter drugih spremenljivk.

Zaradi velikega števila podatkov je treba voditi njihovo klasifikacijo glede na tip in potencialno rabo podatkov. Sam postopek osuševanja pa lahko opazujemo z uporabo ustaljenih ali dinamičnih značilnosti, odvisno od tega, ali čas definiramo kot dejavnik naše raziskave.

## 1.1 Ustaljene lastnosti

Naši predlogi za izboljšano gradnjo gravitacijskih sušilnic se nanašajo tudi na določitev številnih meril, potrebnih za boljše delovanje

between two to three variables were taken into consideration, while others were kept at constant values and their effects were eliminated.

Qualitative monitoring of the parameters of the kernel-drying process is the basis for satisfactory continuous drying because it ensures the required quality of the kernel when it exits the dryer. The batch-drying process requires the parameters, e.g., the drying-air temperature or the ventilation speed, to be changed. In gravity dryers the kernel is exposed to the same conditions in order to be exposed to the programmed parameters on its journey to the dryer's exit. If one of the parameters is being modified, and the result of the drying process is expected to remain unchanged, the other parameters need to be modified, too. This is the basis for the drying-process optimization, in order to achieve:

- the best kernel quality,
- the minimum drying period or maximum dryer capacity,
- the minimum energy consumption.

Achieving the maximum dryer capacity and the minimum energy consumption is a difficult problem. However, obtaining the best kernel quality requires a comprehensive knowledge of kernel behaviour in different conditions. All the parameters that affect the kernel quality need to be known. These parameters are expressed in the form of:

- tables or diagrams of the static dependencies between variables,
- parameter curves showing static dependencies,
- mathematical expressions, used for an approximation of the variables' dependencies,
- tables or diagrams expressing the variables' dependence on time,
- differential equations of the systems, especially those which approximate a particular variable's dependence on time and other variables.

Because of the large amount of data it is necessary to carry out their classification from the data-type and the potential-application points of view. The drying process itself can be observed by using either static or dynamic properties, depending on whether time is taken into consideration as a parameter.

## 1.1 Static properties

The present proposals for improving the gravity dryers' construction also refer to establishing numerous criteria for better operation of the dryer,

sušilnice, kar pa je spet povezano s kakovostjo izdelka, najmanjšimi stroški izdelave sušilnice in njenimi tehničnimi rešitvami, ki naj omogočijo najmanjšo porabo energije in časa. Razpon spremenljivk postopka in "delovno polje" določimo z izbiro določenega tipa konstrukcije in zmogljivosti sušilnice, v kateri je večina postopkov optimiziranih. Diagrami odvisnosti določenih spremenljivk znotraj določenih delovnih polj kažejo ustaljene lastnosti. Izbiro avtomatičnega upravljanja ali avtomatiziranega vodenja temelji na teh lastnostih. Poleg tega so pogosto določeni tudi pomembni podatki o vrednostih tretje spremenljivke. V primeru večje vrednosti določene spremenljivke ali parametra je ustaljena lastnost izražena kot krivulja parametra. Ko v izračunih uporabljamo ustaljene lastnosti, je koristno, da odvisnosti med spremenljivkami pokažemo z matematičnimi izrazi.

## 1.2. Dinamične lastnosti

Dinamične lastnosti določijo obnašanje spremenljivk v času. Ko govorimo o sušilnicah, je primerno, da določimo njihovo dinamično obnašanje in ga predstavimo v obliki prehodnih lastnosti ali kot odziv na skočno funkcijo. Tovrstni časovni diagrami kažejo potencialne pojave odziva neke spremenljivke v času, ko druga spremenljivka skokovito spremeni svojo vrednost. Te podatke uporabimo, ko določamo čas in način obnašanja določene spremenljivke, ki smo jo spremenili zato, da bi lahko predvideli obnašanje druge spremenljivke.

Dinamično obnašanje izrazimo matematično v obliki diferencialnih enačb. Vendar pa moramo, pred določitvijo postopka z uporabo diferencialnih enačb, nastaviti toliko enačb, kolikor je spremenljivk. Da bi lahko uporabljali te enačbe na določenih predmetih, morajo koeficienti enačb ustrezati izbranemu predmetu. V našem primeru morajo ustrezati sušilnici.

Pregled rezultatov osuševanja je prikazan z dvema diferencialnima enačbama. V praksi smo enačbi preizkusili z uporabo določenega osušitvenega modela, ki smo ga kasneje uporabili tudi za določitev koeficientov enačb. Numerične rešitve teh enačb, in posledično tudi vrednosti spremenljivk, se niso znatno spremenjale. Vendar se je ta sistem diferencialnih enačb nanašal na zelo preprost model in veliko parametrov ter podmen smo zanemarili. Zato lahko ta pregled osuševalnega postopka uporabljamo le v nekaterih splošnih

which again refer to the quality of the existing product, to the minimum dryer-production costs and to the plant's technical solutions with a minimum energy and time consumption. The range of the process variables and the "working field" are determined by choosing the dryer's construction and capacity type, in which the majority of processes are optimal. Diagrams showing the dependence of particular variables within estimated working fields are known as static properties. The selection of automatic manipulation or automatic conduction is based upon these properties. In addition to that, important data regarding the values of the third variable are often specified. In the case of a higher value of a particular variable or parameter, the static property is expressed as parameter curves. When using static properties in calculations it is useful to express dependencies between variables with mathematical expressions.

## 1.2. Dynamic properties

The dynamic properties define the behaviour of the variables with time. When speaking of dryer-type plants it is convenient to determine the dynamic behaviour and to present it in the form of transitive properties or as a response to the leap. Time diagrams of this kind indicate the potential occurrence of one variable's response when the other variable changes its value by leaps. This data is used when determining the time and conduction modus of particular variables, which were changed in order to predict the behaviour of the latter.

The dynamic behaviour is mathematically expressed in the form of differential equations. However, before determining a process using differential equations it is necessary to set up as many equations as there are variables. In order to use these equations on a specific object, the equation coefficients have to correspond with this object. In this case they have to correspond to the dryer.

An overview of the drying-process results is presented with two differential equations. In practise they were tested by using a certain drying model, which was again used to determine the equation coefficients. Numerical solutions of these equations, and consequently the variables' values, did not differ significantly. However, this system of differential equations was related to a very simple model and a lot of parameters and hypotheses were omitted. Accordingly, this drying process overview can be

analizah, ne moremo pa ga uporabljati za potrebe delovanja določene sušilnice.

## 2 REZULTATI IN RAZPRAVA

Iz izkušenj upravljanja osuševalnega postopka v težnostnih sušilnicah in ob upoštevanju medsebojnih vplivov velikega števila spremenljivk v prispevku predlagamo optimizacijo sistema znotraj posameznih funkcionalnih enot, ki vključujejo meritve in signalizacijo, upravljanje, avtomatsko krmiljenje, ustavitevne ukrepe in vodenje.

### 2.1 Meritve in signalizacija

Meritve določenih spremenljivk ponujajo vpogled v način poteka postopka. Tako sledimo stalno spremenljivkam pa tudi mejnim in kritičnim spremenljivkam.

Prve se nanašajo na vlago v vstopnih zrnih, temperaturo vročega zraka po končanem segrevanju, temperature posameznih predelov osuševalnega zraka, hitrost zračnega toka ali znižanje zračnega tlaka v sušilnici, temperaturo zraka v sušilnici in v hladilniku, temperaturo zrn ob izpustu iz sušilnice, fluktuacijo zrn v sušilnici, porabo goriva, temperaturo in vlažnost okolja ter vlažnost izhodnega zraka.

Mejne in kritične spremenljivke se nanašajo na zasedenosť sušilnice, dovod vlažnih zrn, najvišjo temperaturo v sušilnici, stanje motornih naprav itn.

### 2.2 Upravljanje

Sklop upravljalnih naprav omogoči neposredno ali posredno vplivanje na osnovne spremenljivke postopka in s tem popravke postopka. Upravljanje izvajamo na tri načine: ročno, ročno na daljavo in avtomatsko. Spremenljivke, ki jih upravljamo, vključujejo mešanje vročega in zunanjega zraka, mešanje vročega in povratnega zraka, delovanje ventilacije (hitrost osuševalnega zraka in delovanje zapore za zrna) in hitrost zrn, ki potujejo skozi sušilnico.

### 2.3 Avtomatsko krmiljenje

Z združitvijo meritvenih in upravljalskih funkcij z učinkovito negativno povratno zvezo je mogoče ustvariti krmilne zanke, ki pomagajo ohraniti

used in some analyses, but it is not applicable when operating a specific dryer.

## 2 RESULTS AND DISCUSSION

Using the experience of managing the drying process in gravity dryers, and based on the interdependencies of a great number of variables, this paper suggests organising the system for the purpose of its optimization through functional units, which include measurement and signalization, managing, automatic control, blocking effects and conduction.

### 2.1 Measurement and signalization

The measurement of particular variables gives an insight into the way the process is being run. The continuously changeable variables, the borderline and the critical variables are monitored.

The first relates to the moisture of the entering kernel, the hot-air temperature after the heating process, the section drying-air temperatures, the air-flow velocity or the air-pressure decrease in the dryer, the air temperature in the dryer and the cooler, the temperature of the exiting kernel, the kernel fluctuation in the dryer, the fuel consumption, the environmental temperature and the humidity, and the exiting air's humidity.

The borderline and critical variables relate to the dryer's occupancy, the delivery of humid kernels, the maximum air temperature in the dryer, the condition of the motor device, etc.

### 2.2 Managing

The group of managing devices enables a direct or indirect effect on the fundamental process variables and therefore ensures the process corrections. It is carried out in three steps, i.e., manually, remote manually, and automatically. The variables that are being managed include the hot- and outer-air mixing, the hot- and recurrent-air mixing, the ventilator operation (the velocity of the drying air, and the working of the kernel excluder) and the kernel velocity when passing through the dryer.

### 2.3 Automatic control

By integrating the measuring and managing functions with a meaningful negative recurrent conjunction it is possible to deliver controlling circuits

vrednosti spremenljivk v določenih mejah. S tem preprečimo motnje, ki bi jih lahko povzročile nenadzorovane spremembe omenjenih spremenljivk, kar pomeni, da z omenjenim postopkom zmanjšamo število spremenljivk, ki bi lahko povzročile prekinitev osuševalnega postopka. Krmilne funkcije izvajamo z naslednjimi sklopi opreme:

- posameznimi krmilnimi zankami s stabilnimi vrednostmi;
- posameznimi krmilnimi zankami z nastavljenimi vrednostmi;
- industrijskim krmilnikom, ki združuje vse merjene in krmilne spremenljivke in vodi postopek.

## 2.4 Ustavitevni ukrepi

Ko se sprožijo signali, ki opozarjajo na mejne in kritične vrednosti, se sprožijo določeni ustavitevni ukrepi za postopek. Ti so prilagojeni dogodkom v sušilnici in v sosednjih prostorih: povečanje temperature v sušilnici nad predpisano, premajhen dotok vlažnih zrn, motnje v postopku ogrevanja ali prekinitev delovanja katerikoli bistvenih rabljenih naprav.

## 2.5 Vodenje

Postopek vodenja vključuje ustaljeno in dinamično sinhronizacijo spremenljivk ali parametrov, tako da lahko kljub nekaterim nenadzorovanim spremembam ohranimo nespremenjene rezultate postopka in stalno kakovost pridelka.

Ta postopek nadzoruje inteligentni industrijski krmilnik, čigar nastavitev moramo prilagoditi tovrstnemu opravilu (upoštevati moramo odvisnosti med spremenljivkami ter tehnološke in ekonomske kriterije). Krmilnik mora biti zmožen sprejeti več tipov podatkov, ki v obliki preglednic in diagramov izražajo ustaljene in dinamične lastnosti. Krmilnik izvaja tudi obdelavo podatkov, tako da podatke lahko prepozna kot matematične funkcije, ki jih nato preoblikuje v enačbe. Drugi tip podatkov so matematični izrazi. Tretji tip podatkov so posamezni podatki, ki določajo parametre postopka kakor na primer vrsta sušenega blaga, cena goriva itn. Nazadnje mora krmilnik sprejeti še podatke o določenem postopku, pridobljene od naprav za merjenje in signaliziranje, hkrati s podatki o vrednostih in spremembah nenadzorovanih spremenljivk.

Ob uporabi vseh navedenih podatkov, krmilnik nenehno izvaja izračune, ki pomenijo temelj

that can help in maintaining the variables' values within set margins. This ensures the elimination of interferences caused by uncontrolled changes to these values, i.e., this leads to a decrease in the number of variables that can cause an interception of the drying process. The control functions are accomplished through a few levels of plant equipping:

- single control circuits with stable values,
- single control circuits with externally set values,
- an industrial controller that unites all the measured and controlling variables and operates the process.

## 2.4 Blocking effects

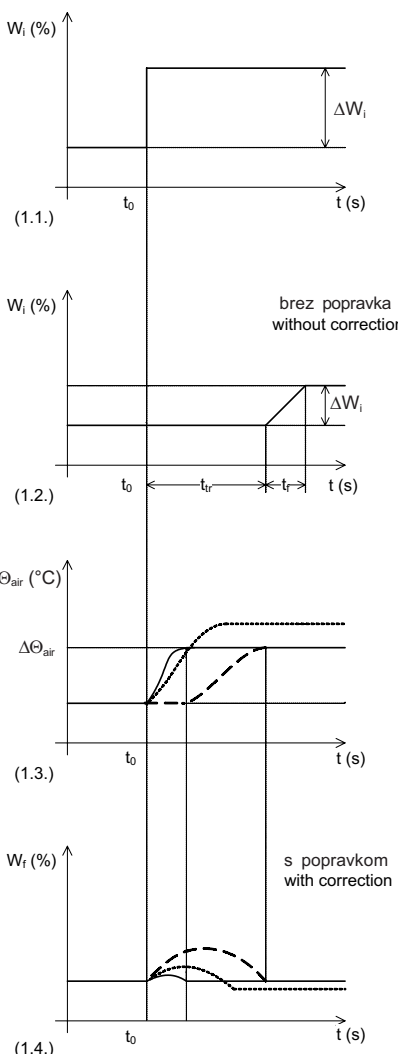
When borderline and critical values are being signalled, the critical values activate certain blocking effects in the process. They are specified by the dryer's and attached buildings' solutions: exceeding the prescribed dryer temperature, the shortage of humid kernel inflow, the interferences with the burner functions and the ending of the vital device functions in the plant.

## 2.5 Conduction

The conduction procedure involves the static and dynamic synchronization of process variables or parameters, so that constant process results and constant product quality are preserved in spite of uncontrolled changes.

This procedure is supervised by an intelligent industrial controller, which needs to be set up for this kind of operation (i.e., the dependencies between the variables and the technological and economic criteria need to be entered). The controller has to be able to accept a few types of data that contain the static and dynamic properties in the form of tables and diagrams. Data processing is also conducted by the controller so it can recognize them as mathematical functions, which are then transformed into equations. The second types of data are previously arranged mathematical expressions. The third forms are single data, which specify the process parameters such as the type of the drying material, the fuel price, etc. Finally, the controller has to accept the actual process data that are obtained from the measuring and signalling equipment, together with data relating to the values and changes of unmonitored variables.

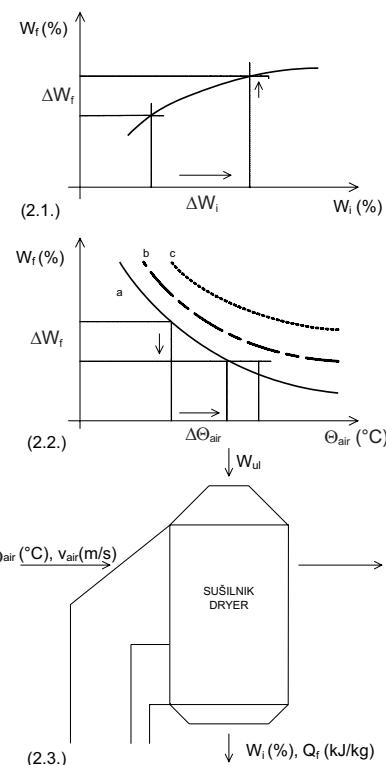
Using all the above-mentioned data, the controller continuously performs calculations, which



Sl. 1. Dinamične lastnosti  
Fig. 1. Dynamic properties

za nadzor spremenljivk in njihovo spremenjanje glede na vrednosti in čas. Še več, izračuni vsebujejo merila za optimalno krmiljenje postopka, ki pa jih lahko tudi sprememimo in jih prilagodimo želeni odvisnosti med kakovostjo osušenega pridelka, zmogljivostjo in porabo energije.

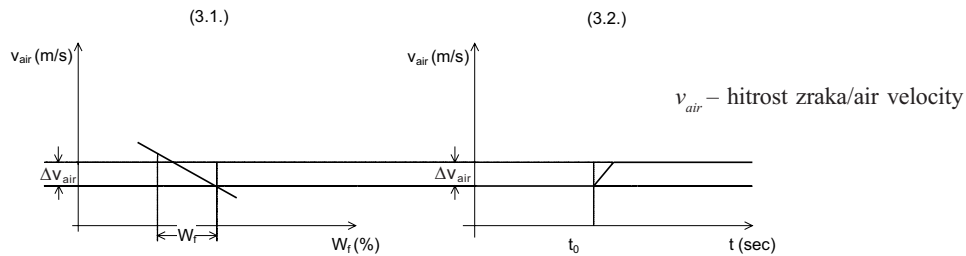
Slike 1, 2 in 3 prikazujejo delovanje krmilnika. Glede na sliko 1.1 se v primeru, ko se začetni delež vlage v zrnih ( $w_i$ ) poveča med postopkom stabilnega sušenja, drugi parametri pa ohranijo nespremenjene vrednosti, končni delež vlage v zrnih ( $w_f$ ) poveča po preteklu določenega časa prenosa ( $t_{tr}$ ) (sl. 2.3). To povečanje se pokaže postopoma (sl. 1.2) in z določeno časovno stalnicijo,  $t_f$ . Končna sprememba končnega deleža vlage bo



Sl. 2. Ustaljene lastnosti  
Fig. 2. Static properties

represent the basis for variables' monitoring and their variation with value and time. Furthermore, the calculations include the conduction criteria for an optimal process, which can then be altered and consequently balanced to a desired dependence between the dried material's quality, capacity and energy consumption.

Figures 1, 2 and 3 show a controller-functioning system. According to Figure 1.1., if the initial kernel moisture content ( $w_i$ ) is increased during a stabilized drying process, while other parameters retain the same values, the final kernel moisture content ( $w_f$ ) will be increased after a certain transport period ( $t_{tr}$ ) (Fig. 2.3). This increase will manifest itself gradually (Fig. 1.2) with a particular time constant,  $t_f$ . The final change of the final moisture content will be equal to the static



Sl. 3. Ustaljene in dinamične lastnosti hitrosti osuševalnega zraka  
Fig. 3. Static and dynamic properties of the velocity of the drying air

enaka ustaljeni lastnosti s slike 2.1. Popravki delovanja sušilnice, ki so zasnovani na podatkih o spremembji končnega deleža vlage, kažejo, da mora skozi sušilnico iti vsaj en tovor zrn z nezaželenim končnim deležem vlage.

Za potrebe pridobitve primerno osušenih zrn lahko, po opravljenih meritvah začetnega deleža vlage v zrnih, vplivamo na več parametrov. Gre za naslednje mogoče spremembe:

- povečanje temperature osuševalnega zraka,
- povečanje hitrosti toka osuševalnega zraka,
- podaljšanje časa sušenja.

Glede na sliko 1 lahko odstranitev začetnega deleža vlage v zrnu,  $w_i$ , dosežemo s povečanjem temperature osuševalnega zraka za vredno st.  $\Theta_{air}$ , ki jo za določen osuševani pridelek izračunamo z ustaljenimi lastnostmi s slike 2.2. Polna črta na sliki 1.3 kaže spremembo temperature osuševalnega zraka, ki je potrebna za doseganje kar najbolj učinkovite poprave končnega deleža vlage v zrnih. Po popravku bomo dobili končni delež vlage zrn, ki jo prikazuje polna črta na sliki 1.4. Če do temperaturnih sprememb pride kasneje, kakor to prikazuje prekinjena črta na sliki 1.3, bo končni delež vlage v zrnih vsebovala večjo napako, ki bo trajala dlje časa kakor napaka iz prvega primera (prekinjena črta na sl. 1.4.). Do nezadovoljivega rezultata bo prišlo tudi v primeru, ko se temperatura premočno poveča. V tem primeru bo imela napaka končnega deleža vlage v zrnih nasprotni predznak (pikčasti črti v sl. 1.3 in 1.4.). Če predpostavimo, da je povečanje hitrosti toka osuševalnega zraka kompenzacijsko spremenljivka, lahko ustaljeno lastnost (sl. 3.1) uporabimo v izračunih, ki posledično vplivajo na spremembo hitrosti zraka za vrednost  $\Delta v_{air}$ . Zdaj tudi ugotovimo, da imajo dinamične lastnosti temperaturne spremembe in hitrosti spremembe zračnega toka podobne časovne stalnice. To pomeni, da bo končno delovanje podobno, takšno, kakršnega prikazuje polna krivulja na sliki 1.4.

property shown in Figure 2.1. The correction of the dryer functions, based on the data regarding the modification of the final moisture content suggests that at least one filling with an undesired final moisture content has to be passed through.

By measuring the initial moisture content of the kernel for the purpose of obtaining qualitatively dried kernels, several parameters can be affected on time. They are:

- an increase in the drying-air temperature,
- an increase in the drying-air velocity flow,
- a prolongation of the drying period.

According to Figure 1, removing the initial moisture content of the kernel,  $w_i$ , can be accomplished by increasing the drying-air temperature by  $\Theta_{air}$ , which is calculated using the static properties shown in Figure 2.2 for a specific material that is being dried. The solid line shown in Figure 1.3 shows the change in the drying-air temperature that is required to achieve the most efficient correction of the final moisture content of the kernel. This will lead to the final moisture content of the kernel shown with the solid line in Figure 1.4. If the temperature changes begin later, as shown with the dashed line in Figure 1.3, the final moisture content of the kernel will have a greater error and will exist for longer than in the first case (the dashed line in Fig. 1.4.). An unsatisfactory result will also be achieved if there is a large effect on the temperature increase. In this case the final moisture content of the kernel will take an error of the opposite sign (the dotted lines shown in Figs. 1.3. and 1.4.). If an increase in the velocity of the drying air flow is considered as a compensating variable, then the static property (Fig. 3.1.) can be used in calculations, which subsequently affects the change in the air velocity by  $\Delta v_{air}$ . Furthermore, it is clear that the dynamic properties of the temperature change and the velocity of the air-flow change have similar time constants. This means that the final functioning will be similar, as shown in the solid curve in Figure 1.4.

Merila za odločitev med tema dvema funkcijama so tehnološka in ekonomska. Krmilnik izvaja izračune, s katerimi ugotavlja, katera možnost je optimalna. Še več, krmilnik ima že nastavljena tehnološka merila, po katerih najvišja temperatura osuševalnega zraka ne sme biti presežena, povečanje hitrosti zračnega toka pa ne sme povzročiti utekočinjenja.

Če zgoraj opisani primeri vsebujejo kakršnakoli tveganja, jih lahko preprečimo z ukrepi, kot npr. upočasnitve gibanja zrn skozi sušilnico s podaljšanjem osuševalnega časa ali z zmanjšanjem zmogljivosti sušilnice.

V praksi manjšanje zmogljivosti sušilnice sicer ni običajno; kljub temu pa v primeru, ko ima sušilnica neprimerno zmogljivost, ki ne ustrezajo naravnim razmeram osuševanja zrna, lahko pride do povečane rabe energije, velikih razlik v deležu vlage v zrnih, tveganega skladiščenja in celo nevarnosti požara.

### 3 SKLEP

Ne glede na finančne možnosti lastnikov sušilnic in njihovo opremljenost predmeti, izbrani za nadzor, upravljanje in vodenje osuševalnega postopka, žal ne ustrezajo trenutnim zahtevam v Republiki Hrvaški ali v tujini. Ne le, da niti najbolj moderno opremljene sušilnice niso optimalno izkoriščene, njihovo delovanje ustvarja velike stroške in daje nezanesljive rezultate. Na podlagi raziskovalnih poročil in poznavanja moderne mikroprocesorske tehnologije lahko priporočimo rabo zgoraj opisane rešitve, tj. namestitev krmilnikov, ki bodo krožno izvajali potrebne izračune. Ti izračuni so temelj za upravljanje s spremenljivkami, ki se v določenem obdobju spremenijo, kar vodi v optimizacijo osuševalnega postopka v gravitacijskih sušilnicah.

Dodatna prednost opisanega predloga je v tem, da je mogoče tehnična dela in finančne vložke investitorja izvesti postopno. Rezultati predlagane rešitve so izboljšano in poenoteno delovanje sušilnice, manjša poraba energije in boljša kakovost osušenih zrn.

The criteria for choosing between these two functions are technological and economic. The controller performs calculations to determine which of them is optimal. Moreover, it has already set technological criteria, i.e., that the maximum drying-air temperature cannot be exceeded, and that the increase in the velocity of the air flow must not cause a fluidization process.

If there is any hazard in the above-mentioned situations, there are some measures that need to be taken, such as slowing down the kernel's movement through the dryer by prolonging the drying period or by decreasing its capacity.

In practice it is not common to decrease the capacity of a dryer; however, if the dryer has an inadequate capacity, which does not match the kernel's natural conditions, i.e., its drying possibilities, this leads to an increase in energy consumption, large differences in the kernel's moisture content, unsafe storage and a possible fire hazard.

### 3 CONCLUSION

Plants designated for process monitoring, managing and conducting, unfortunately, do not meet the present solutions in the Republic of Croatia nor abroad, no matter what the financial potentials of the dryer's owner are or what equipment is available. Indeed, even the most modern equipped dryers are not only non-optimised, but in fact represent high costs and unreliable results. Based on such reports and knowledge regarding the modern achievements of microprocessor technology, it is advisable to introduce the above given solution, i.e., to introduce controllers that will perform calculations cyclically. These are a basis for managing the variables, so that they are modified by their value during a certain period, which consequently leads to optimization of the drying process in gravity dryers.

An additional property of the proposed solution is the possibility to realize in phases the technical equipment and the financial possibilities of the investor. The results are better and uniform dryer functions with lower energy consumption and a better kernel quality.

### 4 LITERATURA 4 REFERENCES

- [1] Putier, F. (1993) Product quality and thermal treatment. *Feed mix.* 1(2), 34-37.

- [2] Brooker D. B., F. W. Bakker-Arkema, C. W. Hall (1992). Drying and storage of grain and oilseeds. *Van Nostrand Reinhold*. New York, USA.
- [3] Mujumdar, A.S. (2000) Drying technology in agriculture science. *Science Publisher*, Enfield, USA
- [4] Krička, T., N. Voća, Ž. Jukić, D. Kiš, S. Voća (2005) Motnje v postopku hlejanja koruznega zrnja v vertikalnih gravitacijskih sušilnicah. *Strojniški vestnik – Journal of Mechanical Engineering*. 51(4), 204-216.
- [5] Li, H., R.V. Morey (1989) Thin-layer drying of yellow dent corn. *Transactions of the American Society of Agricultural Engineers*. 27(2), 581-585.
- [6] Doyomaz, I., M. Pala (2003) The thin-layer drying characteristics of corn. *Journal of Food Engineering*. 60, 125-130
- [7] Soponronnarit, S., A. Pongtornkulpanich, S. Prachayawarakorn (1997) Corn quality after drying fluidization technique at high temperature. *Drying Technology*. 15(10), 2577-2586
- [8] Nedeljkov, M. I., M. P. Stakić (1987) Prikaz eksperimentalnog postrojenja i rezultata ispitivanja kinetike konvektivnog sušenja zrnatih kultura. *Symposium proceedings. XV International Symposium of Technologists for Drying and Storing*, Stubičke Toplice. 36-58.
- [9] Katić, Z. (1985) Istodobno sušenje kukuruznog zrna raznih sorata i hibrida različite vlage na početku sušenja. *Symposium proceedings. I International Symposium of Technologists for Drying and Storing*. Stubičke Toplice, 86-104.
- [10] Bratko, J. (1990) Neujednačenost vlage zrna kukuruza na izlazu iz sušare. *Symposium Proceedings. VI International Symposium of technologists for drying and storing*. Tuheljske Toplice. 108-116.
- [11] Katić, Z., S. Pliestić, T. Krička, N. Kerep (1989) Utjecaj visokotemperaturnog predsušenja na energetsku i materijalnu bilancu sušenja kukuruza *Symposium Proceedings. V International Symposium of Technologists for Drying and Storing*, Stubičke Toplice. 1-13.
- [12] Miketinac, M. J., S. Sokansanj, Z. Tutek (1992) Određivanje koeficijenta prijenosa mase i topline u isušivanju sloja. *Symposium Proceedings. XV International Symposium of Technologists for Drying and Storing*, Tuheljske Toplice. 14-23.
- [13] Katić, Z. (1997) Sušenje i sušare u poljoprivredi, *Multigraf doo*. Zagreb.

Naslov avtorjev: mag. Neven Voća

prof. dr. Tajana Krička  
Vanja Janušić  
Univerza v Zagrebu  
Fakulteta za kmetijstvo  
Svetosimunska 25  
10 000 Zagreb, Hrvatska  
nvoca@agr.hr

Authors' Address: Mag. Neven Voća

Prof. Dr. Tajana Krička  
Vanja Janušić  
University of Zagreb  
Faculty of Agriculture  
Svetosimunska 25  
10 000 Zagreb, Croatia  
nvoca@agr.hr

Prejeto: 13.3.2006  
Received:

Sprejeto:  
Accepted: 22.6.2006

Odperto za diskusijo: 1 leto  
Open for discussion: 1 year

## Osebne vesti - Personal Events

### Prešernove nagrade za študente Fakultete za strojništvo v Ljubljani - Students' Prešeren Awards of the Faculty of Mechanical Engineering in Ljubljana

#### JANEZ GARVAS

Naslov: Študija izvedljivosti proizvodnje bioplina 400 GVŽ za soproizvodnjo toplotne in električne energije  
Mentor: izr. prof. dr. Vincenc Butala

Janez Garvas je bil rojen 24. avgusta 1981 v Ljubljani. Osnovno šolo je obiskoval v domačem kraju na Škofljici. Srednješolsko izobrazbo si je pridobil na Gimnaziji Ledina in uspešno maturiral leta 2000. Oktobra istega leta se je vpisal na Fakulteto za strojništvo v Ljubljani in septembra 2005 diplomiral na visokošolskem strokovnem študiju, smer energetsko in procesno strojništvo. V času študija je opravljal in sodeloval pri različnih projektih na področjih energetskega in procesnega strojništva. Oktobra istega leta se je vpisal na Fakulteti za strojništvo v program za pridobitev univerzitetne izobrazbe.

V okviru Laboratorija za ogrevalno, sanitarno in solarno tehniko na Fakulteti za strojništvo je kandidiral na razpisano temo za Prešernovo nagrado in izvedel delo z naslovom: "Študija izvedljivosti pridobivanja bioplina 400 GVŽ za soproizvodnjo toplotne in električne energije". V omenjenem delu je obravnavana problematika soproizvodnje toplotne in električne energije iz ostankov, ki nastajajo pri vzreji govedi. Študija je izvedena s tehnično-procesnega in tudi ekonomskega vidika.

#### ALEŠ BIZJAK

Naslov: Optomehatronski sistem za rastrsko vodenje žarka pri laserskem označevanju  
Mentor: izr. prof. dr. Janez Diaci

Aleš Bizjak je bil rojen 3. junija 1981 v Novem mestu. Osnovno šolo je obiskoval v Leskovcu pri Krškem, gimnazijo pa v Brežicah. Po maturi leta 2000 se je odločil za študij strojništva v Ljubljani. V tretjem letniku se je usmeril v študij mehatronike in ga junija 2006 tudi uspešno končal z zagovorom diplomske naloge "Krmilnik sistema za rastrsko vodenje žarka pri laserskem označevanju". Decembra 2006 se je zaposlil v podjetju I.H.S. d.o.o. v Krškem kot mladi

raziskovalec.

Nagrajenec je v okviru raziskave preučil izvedljivost in uporabnost rastrskega vodenja žarka pri laserskem označevanju. V ta namen je samostojno zasnoval in razvil izviren odklonski sistem na osnovi vrtljivega poligonskega zrcala in lečja, ki omogoča vodenje laserskega žarka po vrstici na tak način, da je gorišče žarka ves čas na površini obdelovanca. Delovanje sistema za rastrsko vodenje žarka je preizkusil in opredelil na laboratorijskem laserskem označevalnem sistemu. Pri tem je prikazal, da je sistem zlasti primeren za izdelavo večjih in/ali preprostejših označb na obdelovancih, ki se pomikajo po tekočem traku. V takšnih primerih je rastrski sistem tudi bistveno cenejši in hitrejši od sedanjih vektorskih.

#### ALJAŽ OSTERMAN

Naslov: Termični efekti kavitacije  
Mentor: prof. dr. Brane Širok

Aljaž Osterman je bil rojen 20. decembra 1982 v Ljubljani. Po končani osnovni šoli je postal Zoisov štipendist, šolanje pa je nadaljeval na Gimnaziji Bežigrad, kjer je leta 2001 z odliko maturiral. V šolskem letu 2001/02 se je vpisal na Fakulteto za strojništvo v Ljubljani, kjer je v tretjem letniku izbral usmeritev Toplotni stroji in naprave na energetski smeri. Med študijem je bil večkrat nagrajen za najboljšega študenta v letniku. Dodiplomski študij je sklenil z zagovorom diplome v jeseni 2006. Sedaj je zaposlen na Fakulteti za strojništvo kot mladi raziskovalec, ukvarja pa se predvsem s kavitacijo.

V nalogi je kandidat Aljaž Osterman predstavil nov - izviren postopek vrednotenja kavitacije s pomočjo računalniško podprtne infrardeče termografije. V prvem delu naloge opiše eksperimentalno raziskavo kavitacije na osnovni (fenomenološki) ravni. V osrednjem delu naloge predstavi eksperimentalno metodo zaznavanja temperaturnih učinkov kavitacije. Postopek omogoča detekcijo temperaturnih polj neposredno na površini germanijevega stekla v stiku s kapljevinou. Časovno in krajevno spremenjanje temperaturnih polj v mejni plastki kapljevine opazuje kot posledico propada

kavitacijskih mehurčkov, ki so nastali z ultrazvočnim vzbujanjem. Iz oblike in kinematike širjenja temperaturnih polj sklepa o intenzivnosti kavitacije. Na fenomenološki ravni oblikuje medsebojno povezavo med kavitacijo in termičnimi učinki kavitacije.

Osnovni prispevek dela je novo razvita infrardeča termovizijska metoda merjenja kavitacijskih učinkov. Metoda bo uporabljena v nadaljnjih raziskavah temeljnih mehanizmov kavitacije, odpirajo pa se tudi možnosti razvoja eksperimentalne metode za diagnostiko kavitacije in erozijskih posledic. Delo je podano pregledno z jasnim opisom izhodišč naloge, dobljenimi rezultati in pogledom v prihodnje dejavnosti.

### **URBAN MOHAR in JURIJ FERFOLJA**

Naslov: Analiza vpliva strukture (morfologije) na časovno odvisno vedenje polimerov

Mentor: prof. dr. Igor Emri

Urban Mohar je bil rojen 16. februarja 1981 v Ljubljani. Osnovno šolo je končal na Vrhniku in šolanje nadaljeval na Gimnaziji Ledina v Ljubljani. Leta 2000 se je vpisal na visokošolski študijski program Fakultete za strojništvo v Ljubljani. Dejaven je v Klubu vrhniških študentov. Trenutno je zaposlen v podjetju Ydria Motors.

Jurij Ferfolja je bil rojen 1. februarja 1981 v Šempetru pri Gorici. Po končani osnovni šoli v Novi Gorici se je leta 1996 vpisal na Srednjo strojno tehnično šolo na Tehničnem šolskem centru Nova Gorica. V tem času se je dejavno ukvarjal s cestnim kolesarstvom, bil reden član mladinske kolesarske reprezentance v letih 1998 in 1999, nastopil na svetovnem mladinskem prvenstvu leta 1998 ter osvojil več medalj na mladinskih državnih prvenstvih. Leta 2002 se je vpisal na visokošolski študijski program Fakultete za strojništvo v Ljubljani. V študijskem letu 2004/05 je bil v sklopu študijske izmenjave na programu Erasmus Socrates 10 mesecev na Universitat Politecnica de Catalunya v Barceloni. V prostem času dela kot sommelier za Slovensko turistično organizacijo, kjer skrbi za promocijo slovenskih vin na svetovnih turističnih borzah. Trenutno opravlja pripravnštvo v razvojnem oddelku podjetja ITW Metalflex iz Tolmina in pripravlja diplomo.

Delo obravnava nove možnosti spreminjanja funkcionalnosti polimernega izdelka s pomočjo

spreminjanja strukture materiala v fazi predelovanja in posledično njegovega časovno odvisnega vedenja, ki opredeljuje trajnost končnega izdelka. Predstavljena raziskava išče odgovore na dvoje vprašanj: (i) ali je mogoče s sedanjim opremo za procesiranje polimerov v industrijskem okolju (npr. ekstrudiranje) ustvariti razmere, pri katerih se pojavijo nelinearni postopki med oblikovanjem strukture materiala, in (ii) kolikšne spremembe strukture in posledično mehanske in druge lastnosti končnega polimernega izdelka lahko dosežemo v industrijskem okolju s spremembami v tehnologiji (t.j., s spremembami parametrov postopkov).

Rezultati predstavljene analize kažejo, da je mogoče tehnološke razmere v območju temperatur in tlakov, tipičnih za iztiskovanje polimerov v industrijskih razmerah, spremeniti tako, da pomembno vplivamo na oblikovanje strukture in posledično na časovno odvisne mehanske lastnosti materiala in s tem na funkcionalnost končnega izdelka. Avtorja raziskave pokažeta, da je s spremembami postopkovnih parametrov v območju industrijskih razmer mogoče izboljšati trajnost za več velikostnih razredov. To odpira nove možnosti na področju spreminjanja funkcionalnosti polimernih izdelkov in s tem povečevanje njihove konkurenčne zmožnosti na svetovnem trgu.

### **JAN ČERNETIČ**

Naslov: Aktivno dušenje hrupa na primeru prezračevalnega kanala

Mentor: prof. dr. Mirko Čudina

Jan Černetič je bil rojen 11. junija 1982 v Ljubljani. Osnovno šolo je obiskoval v Logu pri Brezovici, leta 1997 se je vpisal na Gimnazijo Jožeta Plečnika. Po maturi leta 2001 se je vpisal na univerzitetni študij Fakultete za strojništvo v Ljubljani in se usmeril v energetsko strojništvo. I. del strokovne prakse je opravil leta 2002 v Laboratoriju za eksperimentalno mehaniko, II. del pa leta 2005 v podjetju IMS Industrijski meritni sistemi na področju merjenja in vrednotenja hrupa. Leta 2006 je z odliko diplomiral na področju aktivnega dušenja hrupa. Istega leta je kandidiral za mesto mladega raziskovalca na Fakulteti za strojništvo in bil tudi sprejet.

V času študija je dejavno sodeloval z laboratorijem za delovne stroje in tehnično akustiko v okviru katerega je izdelal nalogu z naslovom "Aktivno dušenje hrupa na primeru prezračevalnega kanala". Kandidat je v delu podrobnejše predstavil zančno

strukturo pri dejavnem dušenju hrupa. Opravil je tudi številne preizkuse z namenom izdelati čim bolj preprost in učinkovit analogni sistem dejavnega dušenja hrupa v prezračevalnem kanalu. Namen je bil prikazati, da je učinkovit sistem mogoče narediti tudi brez uporabe elektronskih ali analognih filtrov ter krmilnikov. V ožjem frekvenčnem pasu je dosegel zmanjšanje hrupa za 18 dB(A), največja raven dušenja pa je znašala 22 dB(A).

### MITJA MAZEJ

Naslov: Polje koncentracij primesi pri lokalni klimatizaciji  
Mentor: izr. prof. dr. Vincenc Butala

Mitja Mazej je bil rojen 21. maja 1982 v Celju, kjer je obiskoval osnovno šolo in gimnazijo. Po

uspešno opravljeni maturi leta 2001 se je vpisal na Fakulteto za strojništvo Univerze v Ljubljani, kjer je 30. junija 2006 diplomiral na smeri Energetsko in procesno strojništvo, usmeritev topotna tehnika - procesno strojništvo. Za Prešernovo nagrado je kandidiral z razpisano temo "Polje koncentracij primesi pri lokalni klimatizaciji". V delu je bilo analizirano delovanje sistema za lokalno klimatizacijo delovnega mesta na podlagi opravljenih meritev hitrosti zraka in koncentracij slednega plina z uporabo metode zmanjševanja

Tako po diplomiranju se je za krajši čas zaposlil v zasebnem podjetju v Celju, od 1. novembra 2006 dalje pa je zaposlen na Fakulteti za strojništvo Univerze v Ljubljani kot mladi raziskovalec na področju energetike v Laboratoriju za ogrevalno, sanitarno in solarno tehniko.

## Doktorati, magisterija in diplome - Doctor's, Master's and Diploma Degrees

### DOKTORATI

Na Fakulteti za strojništvo Univerze v Ljubljani so z uspehom zagovarjali svoje doktorske disertacije:

dne 5. decembra 2006: **Boštjan Drobnič**, z naslovom: "Tokovne in temperaturne razmere v rotacijskem regenerativnem prenosniku toplotne" (mentorja: prof. dr. Janez Oman in prof. dr. Matija Tuma);

dne 8. decembra 2006: **Tadej Kokalj**, z naslovom: "Modeliranje in optimizacija laserskega tvorjenja kapljic iz kovinske žice" (mentorja: prof. dr. Edvard Govekar in prof. dr. Igor Grabec);

dne 22. decembra 2006: **Boštjan Černe**, z naslovom: "Vpliv večdimenzijskega prenosa toplotne na toplotni odziv lahkih gradbenih elementov" (mentor: prof. dr. Sašo Medved) in **Nikola Holeček**, z naslovom: "Modeliranje aerodinamičnih lastnosti kondenzatorjev sušilnih strojev nove generacije" (mentorji: prof. dr. Brane Širok, prof. dr. Mirko Čudina in prof. dr. Rudolf Podgornik).

Na Fakulteti za strojništvo Univerze v Mariboru sta z uspehom zagovarjala svoje doktorske disertacije:

dne 15. decembra 2006: **mag. Andrej Godina**, z naslovom: "Merilna negotovost pri kalibraciji merilnih kladic iz različnih materialov po postopku mehanske primerjave" (mentor: prof. dr. Janko Drnovšek);

dne 18. decembra 2006: **mag. Matejka Turel**, z naslovom: "Razvoj novih optičnih

senzorskih sistemov za spremljanje anorganskih parametrov odpadne vode" (mentorja: prof. dr. Aleksandra Lobnik in prof. dr. Otto S. Wolfbeis);

S tem so navedeni kandidati dosegli akademsko stopnjo doktora znanosti.

### MAGISTERIJA

Na Fakulteti za strojništvo Univerze v Ljubljani je z uspehom zagovarjal svoje magistrske delo:

dne 21. decembra 2006: **Martin Mele**, z naslovom: "Spajanje aluminija z gnetenjem" (mentor: prof. dr. Janez Tušek).

Na Fakulteti za strojništvo Univerze v Mariboru je z uspehom zagovarjala svoje magistrske delo:

dne 13. decembra 2006: **Marija Pintar**, z naslovom: "Industrijski tekstilni odpadki v Sloveniji in njihovo recikliranje" (mentorja: prof. dr. Bojana Vončina in prof. dr. Niko Samec).

S tem sta navedena kandidata dosegla akademsko stopnjo magistra znanosti.

### DIPLOMIRALISO

Na Fakulteti za strojništvo Univerze v Ljubljani sta pridobila naziv univerzitetni diplomirani

inženir strojništva:

dne 27. decembra 2006: Metod IVANČIČ,  
Tomaž OŠTIR.

Na Fakulteti za strojništvo Univerze v  
Mariboru sta pridobila naziv univerzitetni diplomirani  
inženir strojništva:

dne 21. decembra 2006: Peter GROBELNIK,  
Teo VIDA.

\*

Na Fakulteti za strojništvo Univerze v  
Ljubljani so pridobili naziv diplomirani inženir

strojništva:

dne 14. decembra 2006: Matej DURIČ,  
Kristijan KRAJNIK, Aleš KUŽNIK, Luka LEVSTEK,  
Andrej MEDVEDEC, Matej MOŽINA, Primož  
TEKAVEC, Jernej VUGA;

dne 18. decembra 2006: Vojko LAJOVEC,  
Gregor KLINC, Matjaž RUPNIK, Aleksandar ILIĆ.

Na Fakulteti za strojništvo Univerze v  
Mariboru so pridobili naziv diplomirani inženir  
strojništva:

dne 4. decembra 2006: Marko MALAVAŠIČ;

dne 21. decembra 2006: Igor KAPITAN,  
Martin PETRIČ, Miran POPIČ, Roman ŠUŠTARŠIČ.

## Navodila avtorjem - Instructions for Authors

Članki morajo vsebovati:

- naslov, povzetek, besedilo članka in podnaslove slik v slovenskem in angleškem jeziku,
- dvojezične preglednice in slike (diagrami, risbe ali fotografije),
- seznam literature in
- podatke o avtorjih.

Strojniški vestnik izhaja od leta 1992 v dveh jezikih, tj. v slovenščini in angleščini, zato je obvezen prevod v angleščino. Obe besedili morata biti strokovno in jezikovno med seboj usklajeni. Članki naj bodo kratki in naj obsegajo približno 8 strani. Izjemoma so strokovni članki, na željo avtorja, lahko tudi samo v slovenščini, vsebovati pa morajo angleški povzetek.

Za članke iz tujine (v primeru, da so vsi avtorji tujci) morajo prevod v slovenščino priskrbeti avtorji. Prevajanje lahko proti plačilu organizira uredništvo. Če je članek ocenjen kot znanstveni, je lahko objavljen tudi samo v angleščini s slovenskim povzetkom, ki ga pripravi uredništvo.

### VSEBINA ČLANKA

Članek naj bo napisan v naslednji obliki:

- Naslov, ki primerno opisuje vsebino članka.
- Povzetek, ki naj bo skrajšana oblika članka in naj ne presega 250 besed. Povzetek mora vsebovati osnove, jedro in cilje raziskave, uporabljeno metodologijo dela, povzetek rezultatov in osnovne sklepe.
- Uvod, v katerem naj bo pregled novejšega stanja in zadostne informacije za razumevanje ter pregled rezultatov dela, predstavljenih v članku.
- Teorija.
- Eksperimentalni del, ki naj vsebuje podatke o postaviti preskusa in metode, uporabljeni pri pridobitvi rezultatov.
- Rezultati, ki naj bodo jasno prikazani, po potrebi v obliki slik in preglednic.
- Razprava, v kateri naj bodo prikazane povezave in poslopišitve, uporabljeni za pridobitev rezultatov. Prikazana naj bo tudi pomembnost rezultatov in primerjava s poprej objavljenimi deli. (Zaradi narave posameznih raziskav so lahko rezultati in razprava, za jasnost in preprostješje bralčevu razumevanje, združeni v eno poglavje.)
- Sklepi, v katerih naj bo prikazan en ali več sklepov, ki izhajajo iz rezultatov in razprave.
- Literatura, ki mora biti v besedilu oštevilčena zaporedno in označena z oglatimi oklepaji [1] ter na koncu članka zbrana v seznamu literature. Vse opombe naj bodo označene z uporabo dvignjene številke<sup>1</sup>.

### OBLIKA ČLANKA

Besedilo članka naj bo pripravljeno v urejevalniku Microsoft Word. Članek nam dostavite v elektronski obliki.

Ne uporabljajte urejevalnika LaTeX, saj program, s katerim pripravljamo Strojniški vestnik, ne uporablja njegovega formata.

Enačbe naj bodo v besedilu postavljene v ločene vrstice in na desnem robu označene s tekočo številko v okroglih oklepajih

Papers submitted for publication should comprise:

- Title, Abstract, Main Body of Text and Figure Captions in Slovene and English,
- Bilingual Tables and Figures (graphs, drawings or photographs),
- List of references and
- Information about the authors.

Since 1992, the Journal of Mechanical Engineering has been published bilingually, in Slovenian and English. The two texts must be compatible both in terms of technical content and language. Papers should be as short as possible and should on average comprise 8 pages. In exceptional cases, at the request of the authors, speciality papers may be written only in Slovene, but must include an English abstract.

For papers from abroad (in case that none of authors is Slovene) authors should provide Slovenian translation. Translation could be organised by editorial, but the authors have to pay for it. If the paper is reviewed as scientific, it can be published only in English language with Slovenian abstract, that is prepared by the editorial board.

### THE FORMAT OF THE PAPER

The paper should be written in the following format:

- A Title, which adequately describes the content of the paper.
- An Abstract, which should be viewed as a mini version of the paper and should not exceed 250 words. The Abstract should state the principal objectives and the scope of the investigation, the methodology employed, summarize the results and state the principal conclusions.
- An Introduction, which should provide a review of recent literature and sufficient background information to allow the results of the paper to be understood and evaluated.
- A Theory
- An Experimental section, which should provide details of the experimental set-up and the methods used for obtaining the results.
- A Results section, which should clearly and concisely present the data using figures and tables where appropriate.
- A Discussion section, which should describe the relationships and generalisations shown by the results and discuss the significance of the results making comparisons with previously published work. (Because of the nature of some studies it may be appropriate to combine the Results and Discussion sections into a single section to improve the clarity and make it easier for the reader.)
- Conclusions, which should present one or more conclusions that have been drawn from the results and subsequent discussion.
- References, which must be numbered consecutively in the text using square brackets [1] and collected together in a reference list at the end of the paper. Any footnotes should be indicated by the use of a superscript<sup>1</sup>.

### THE LAYOUT OF THE TEXT

Texts should be written in Microsoft Word format. Paper must be submitted in electronic version.

Do not use a LaTeX text editor, since this is not compatible with the publishing procedure of the Journal of Mechanical Engineering.

Equations should be on a separate line in the main body of the text and marked on the right-hand side of the page with numbers in round brackets.

## Enote in okrajšave

V besedilu, preglednicah in slikah uporabljajte le standardne označbe in okrajšave SI. Simbole fizikalnih veličin v besedilu pišite poševno (kurzivno), (npr. *v*, *T*, *n* itn.). Simbole enot, ki sestojijo iz črk, pa pokončno (npr.  $\text{ms}^{-1}$ , K, min, mm itn.).

Vse okrajšave naj bodo, ko se prvič pojavitjo, napisane v celoti v slovenskem jeziku, npr. časovno spremenljiva geometrija (ČSG).

## Slike

Slike morajo biti zaporedno oštevilčene in označene, v besedilu in podnaslovu, kot sl. 1, sl. 2 itn. Posnete naj bodo v ločljivosti, primerni za tisk, v kateremkoli od razširjenih formatov, npr. BMP, JPG, GIF. Diagrami in risbe morajo biti pripravljeni v vektorskem formatu, npr. CDR, AI.

Pri označevanju osi v diagramih, kadar je le mogoče, uporabite označbe veličin (npr. *t*, *v*, *m* itn.), da ni potrebno dvojezično označevanje. V diagramih z več krivuljami, mora biti vsaka krivulja označena. Pomen označke mora biti pojasnjен v podnapisu slike.

Vse označbe na slikah morajo biti dvojezične.

## Preglednice

Preglednice morajo biti zaporedno oštevilčene in označene, v besedilu in podnaslovu, kot preglednica 1, preglednica 2 itn. V preglednicah ne uporabljajte izpisanih imen veličin, ampak samo ustrezne simbole, da se izognemo dvojezični podvajitvi imen. K fizikalnim veličinam, npr. *t* (pisano poševno), pripisite enote (pisano pokončno) v novo vrsto brez oklepajev.

Vsi podnaslovi preglednic morajo biti dvojezični.

## Seznam literature

- Vsa literatura mora biti navedena v seznamu na koncu članka v prikazani obliki po vrsti za revije, zbornike in knjige:
- [1] A. Wagner, I. Bajšić, M. Fajdiga (2004) Measurement of the surface-temperature field in a fog lamp using resistance-based temperature detectors, *Stroj. vestn.* 2(2004), pp. 72-79.
  - [2] Vesenjak, M., Ren Z. (2003) Dinamična simulacija deformiranja cestne varnostne ograje pri naletu vozila. *Kuhljevi dnevi '03*, Zreče, 25.-26. september 2003.
  - [3] Muhs, D. et al. (2003) Roloff/Matek Maschinenelemente – Tabellen, 16. Auflage. *Vieweg Verlag*, Wiesbaden.

## SPREJEM ČLANKOV IN AVTORSKE PRAVICE

Uredništvo Strojniškega vestnika si pridržuje pravico do odločanja o sprejemu članka za objavo, strokovno oceno recenzentov in morebitnem predlogu za krajšanje ali izpopolnitve ter terminološke in jekovne korekturje.

Avtor mora predložiti pisno izjavo, da je besedilo njegovo izvirno delo in ni bilo v dani obliki še nikjer objavljeno. Z objavo preidejo avtorske pravice na Strojniški vestnik. Pri morebitnih kasnejših objavah mora biti SV naveden kot vir.

## PLAČILO OBJAVE

Avtorji vseh prispevkov morajo za objavo plačati prispevek v višini 20,00 EUR na stiskano stran prispevka. Prispevek se zaračuna po sprejemu članka za objavo na seji Uredniškega odbora.

## Units and abbreviations

Only standard SI symbols and abbreviations should be used in the text, tables and figures. Symbols for physical quantities in the text should be written in italics (e.g. *v*, *T*, *n*, etc.). Symbols for units that consist of letters should be in plain text (e.g.  $\text{ms}^{-1}$ , K, min, mm, etc.).

All abbreviations should be spelt out in full on first appearance, e.g., variable time geometry (VTG).

## Figures

Figures must be cited in consecutive numerical order in the text and referred to in both the text and the caption as Fig. 1, Fig. 2, etc. Pictures may be saved in resolution good enough for printing in any common format, e.g. BMP, GIF, JPG. However, graphs and line drawings should be prepared as vector images, e.g. CDR, AI.

When labelling axes, physical quantities, e.g. *t*, *v*, *m*, etc. should be used whenever possible to minimise the need to label the axes in two languages. Multi-curve graphs should have individual curves marked with a symbol, the meaning of the symbol should be explained in the figure caption.

All figure captions must be bilingual.

## Tables

Tables must be cited in consecutive numerical order in the text and referred to in both the text and the caption as Table 1, Table 2, etc. The use of names for quantities in tables should be avoided if possible: corresponding symbols are preferred to minimise the need to use both Slovenian and English names. In addition to the physical quantity, e.g. *t* (in italics), units (normal text), should be added in new line without brackets.

All table captions must be bilingual.

## The list of references

References should be collected at the end of the paper in the following styles for journals, proceedings and books, respectively:

- [1] A. Wagner, I. Bajšić, M. Fajdiga (2004) Measurement of the surface-temperature field in a fog lamp using resistance-based temperature detectors, *Stroj. vestn.* 2(2004), pp. 72-79.
- [2] Vesenjak, M., Ren Z. (2003) Dinamična simulacija deformiranja cestne varnostne ograje pri naletu vozila. *Kuhljevi dnevi '03*, Zreče, 25.-26. september 2003.
- [3] Muhs, D. et al. (2003) Roloff/Matek Maschinenelemente – Tabellen, 16. Auflage. *Vieweg Verlag*, Wiesbaden.

## ACCEPTANCE OF PAPERS AND COPYRIGHT

The Editorial Committee of the Journal of Mechanical Engineering reserves the right to decide whether a paper is acceptable for publication, obtain professional reviews for submitted papers, and if necessary, require changes to the content, length or language.

Authors must also enclose a written statement that the paper is original unpublished work, and not under consideration for publication elsewhere. On publication, copyright for the paper shall pass to the Journal of Mechanical Engineering. The JME must be stated as a source in all later publications.

## PUBLICATION FEE

For all papers authors will be asked to pay a publication fee prior to the paper appearing in the journal. However, this fee only needs to be paid after the paper is accepted by the Editorial Board. The fee is €20.00 per printed paper page.